LBL-14842
Excerpt

Lawrence Berkeley Laboratory
UNIVERSITY OF CALIFORNIA

EARTH SCIENCES DIVISION

Chapter 7. Dissolution Rate of Solid Radioactive Waste

Excerpt from Volume II of

Analytical Performance Models for Geologic Repositories

RECEIVED
LAWRENCE
BERKELEY LABORATORY

AUG 31 1988

LIBRARY AND
DOCUMENTS SECTION

P.L. Chambré, T.H. Pigford, A. Fujita, T. Kanki,
A. Kobayashi, H. Lung, D. Ting, Y. Sato, and S.J. Zavoshy

October 1982

LBL-14842 c.2

Prepared for the U.S. Department of Energy under Contract Number DE-AC03-76SF00098.

DISCLAIMER

This document was prepared as an account of work sponsored by the United States Government. While this document is believed to contain correct information, neither the United States Government nor any agency thereof, nor the Regents of the University of California, nor any of their employees, makes any warranty, express or implied, or assumes any legal responsibility for the accuracy, completeness, or usefulness of any information, apparatus, product, or process disclosed, or represents that its use would not infringe privately owned rights. Reference herein to any specific commercial product, process, or service by its trade name, trademark, manufacturer, or otherwise, does not necessarily constitute or imply its endorsement, recommendation, or favoring by the United States Government or any agency thereof, or the Regents of the University of California. The views and opinions of authors expressed herein do not necessarily state or reflect those of the United States Government or any agency thereof or the Regents of the University of California.

LBL-14842
Excerpt

Chapter 7. Dissolution Rate of Solid Radioactive Waste

Excerpt from Volume II of

Analytical Performance Models for Geologic Repositories

P.L. Chambré, T.H. Pigford, A. Fujita, T. Kanki,
A. Kobayashi, H. Lung, D. Ting, Y. Sato, and S.J. Zavoshy

October 1982

Earth Sciences Division
Lawrence Berkeley Laboratory
University of California
Berkeley, California 94720

* Prepared for the U.S. Department of Energy under Contract Number DE-AC03-76SF00098 administered by the Office of Nuclear Waste Isolation, Battelle Memorial Institute under MPO E511-05200.

7.1 Mass Transfer From a Fuel Canister by Diffusion

Paul L. Chambré

Consider a cylinder of finite length imbedded in a porous medium. The cylinder matrix contains a diffusing specie such as $Si(OH)_x$ or UO_2 which is set free at the surface of the cylinder at the solubility limit $\hat{c}_s$ of this specie in water and then diffuses into the exterior unbounded space. The diffusion coefficient is assumed constant. The governing equation for the conservation of mass of the diffusing species outside the cylinder in absence of any losses is

$$K \frac{\partial \hat{c}}{\partial t} = D_f \nabla^2 \hat{c} \tag{7.1.1a}$$

Here D_f is the diffusion coefficient of the species in water and K its retardation coefficient.

The boundary conditions are respectively

$$\hat{c} = \hat{c}_s \tag{7.1.1b}$$

on the surface of the cylinder and

$$\hat{c} = 0 \tag{7.1.1c}$$

on an infinite <u>spherical</u> surface enclosing the cylinder. If the concentration at infinity is non-zero, a change in the reference datum of $\hat{c}$ reduces that problem to the above formulation. Prior to the time t = 0 the diffusing nuclide has zero concentration in the exterior (porous) medium.

For a cylinder of finite length, the Laplace operator in eq. (7.1.1a) has the form

$$\nabla^2(\ ) = \frac{\partial^2(\ )}{\partial r^2} + \frac{1}{r}\frac{\partial(\ )}{\partial r} + \frac{1}{r^2}\frac{\partial^2(\ )}{\partial \theta^2} + \frac{\partial^2(\ )}{\partial z^2} \tag{7.1.2}$$

where r, θ, z are cylindrical coordinates. For the exterior diffusion problem which we wish to solve, compact analytical solutions of eqs. (7.1.1) and (7.1.2) are not possible because the interior bounding surface is a cylinder and the exterior surface is a sphere. This of course does not mean that the posed problem does not possess a solution. Indeed one can obtain it in numerical form or by analytical approximations. Since we wish to retain a compact analytical solution to this problem, a suitable approximation is made for the shape of the cylinder. The finite cylinder shape is approximated by a slender prolate spheriod which is generated by rotating a family of confocal ellipses about their major axis. This family generates not only the replacement for the finite cylinder, but produces also the outer spherical boundary which is a member of this family.

One might consider also other forms for the approximation. Suppose the inner surface of the domain is maintained in the exact form of a finite cylinder and the outer boundary is now a cylinder, but of infinite extent. For simplicity, consider furthermore that a steady state prevails so that one deals with the solution of Laplaces equation in the exterior field. Subject to the boundary condition (7.1.1b) the solution sought is mathematically equivalent to the problem of determining the capicitance of a cylinder in an infinite cylindrical box. It is well known that this problem does not possess an exact closed form solution although it can be readily shown that such a solution exists and is unique and can be approximated by various means. With these comments in mind, we reiterate that the interior cylinder surface will be approximated by a slender prolate spheroid which is described by the prolate spheroidal coordinates (α,β,ψ). Since the reader may not be familiar with this coordinate system,

we review and summarize in the following its main characteristics.

The relationship between prolate spheroidal coordinates (α,β,ψ) and the common rectangular coordinates (x,y,z) are given by

$$\begin{aligned} x &= f \sinh\alpha \sin\beta \cos\psi \\ y &= f \sinh\alpha \sin\beta \sin\psi \\ z &= f \cosh\alpha \cos\beta \end{aligned} \tag{7.1.3}$$

where f is the focal distance of the prolate spheroid measured from the coordinate origin, see Fig. 7.1.1. To exhibit the geometric significance of α, take α to be constant and let

$$a = f \cosh\alpha, \quad b = f \sinh\alpha \tag{7.1.4}$$

in eq. (7.1.3). If these three equations are squared and added, there results

$$\left(\frac{x}{b}\right)^2 + \left(\frac{y}{b}\right)^2 + \left(\frac{z}{a}\right)^2 = 1 \tag{7.1.5}$$

Since α and hence a and b are constants, this represents a prolate spheroid in the x,y,z coordinate system (see Fig. (7.1.1)). One observes from (7.1.4) that as α becomes small, the prolate spheroid tends to a small diameter "cylinder". This "cylinder" has a radius b and a length given by (7.1.5) as 2a. In the following, we shall approximate the cylinder by small positive values of α. On the other hand, as α becomes very large, so do both a and b and (7.1.5) tends to the description of a sphere of large radius. The entire α range generates a family of prolate ellipsoids.

In order to exhibit the geometric significance of β, take β to be a constant and let

$$\bar{a} = f \cos\beta, \quad \bar{b} = f \sin\beta \tag{7.1.6}$$

Again square the equations in (7.1.3) and add so that

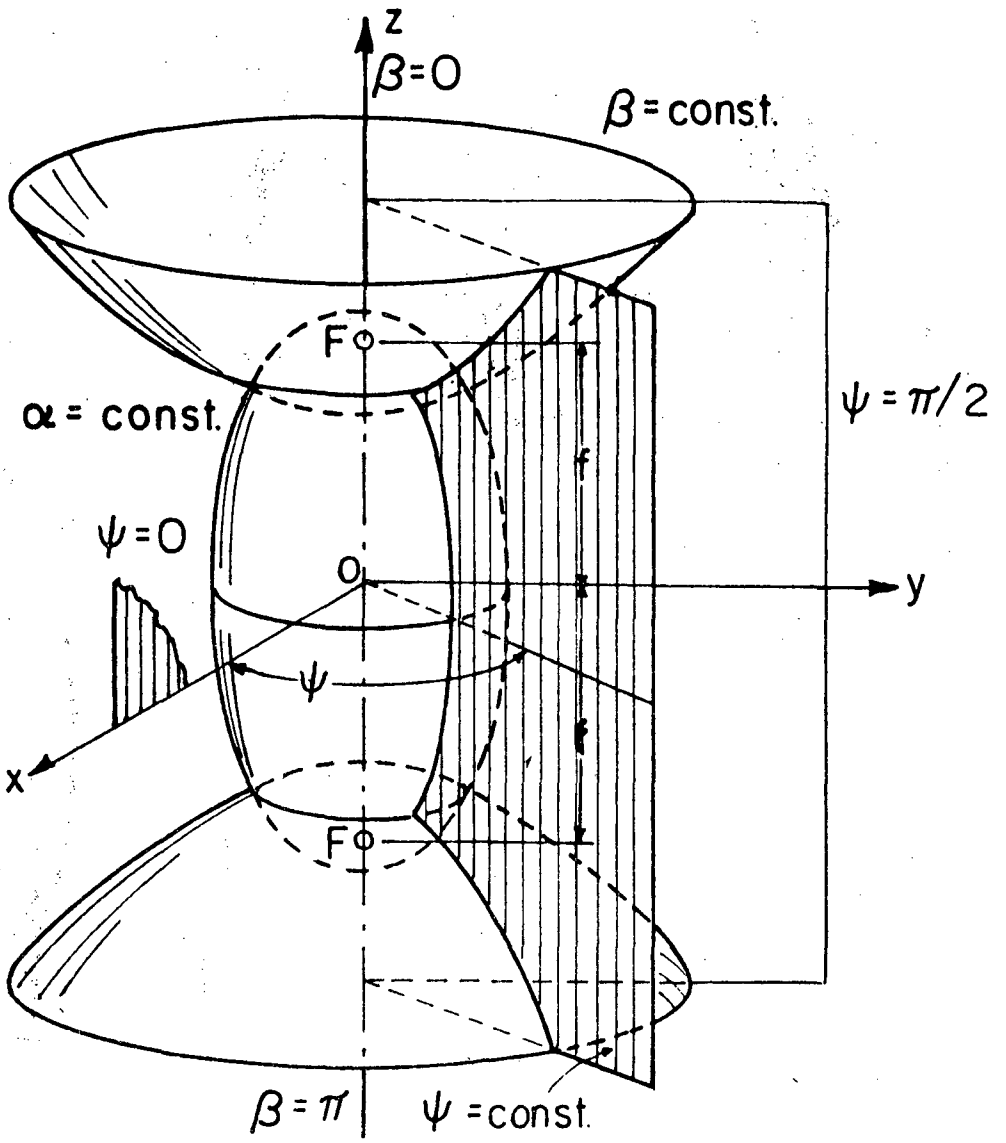

XBL 828-6304

Fig. 7.1.1. Prolate spheroidal coordinates (α,β,ψ). Coordinate surfaces are prolate spheroids (α = const), hyperboloids of revolution (β = const), and half-planes (ψ = const).

$$-\left(\frac{x^2 + y^2}{\bar{b}^2}\right) + \left(\frac{z}{\bar{a}}\right)^2 = 1 \tag{7.1.7}$$

Hence for β constant and thus $\bar{a}$ and $\bar{b}$ constant, this equation represents a family of hyperboloids of two sheets with foci at $\pm$ f as shown in Fig. (7.1.1). When $\beta = 0$, $\bar{a} = f$ and $\bar{b} = 0$, while when $\beta = \pi$, $\bar{a} = -f$ and $\bar{b} = 0$. For either of these cases (7.1.7) reduces in the limit to the collapsed hyperboloid, i.e., the positive and negative z axis from f to ∞ and -f to $-\infty$ respectively. When $\beta = \frac{\pi}{2}$, $\bar{a} = 0$, $\bar{b} = f$ for which (7.1.7) reduces in the limit to z = 0, i.e., the x-y plane. Finally, as can be seen from Fig. (7.1.1), the family of half planes ψ = constant with $o \leq \psi \leq 2\pi$ forms the third member of orthogonal coordinate system α, β, ψ which has the range

$$o \leq \alpha \leq \infty \; ; \; o \leq \beta \leq \pi \; ; \; o \leq \psi \leq 2\pi \tag{7.1.8}$$

In this coordinate system the square of the element of arc length is given with help of (7.1.3) by

$$(ds)^2 = f^2 \; (\sinh^2\alpha + \sin^2\beta) \left[(d\alpha)^2 + (d\beta)^2\right] + \\ + f^2 \sinh^2\alpha \, \sin^2\beta (d\psi)^2 \tag{7.1.9}$$

From this one obtains the metric coefficients of this coordinate system as

$$h_\alpha = h_\beta = f \, (\sinh^2\alpha + \sin^2\beta)^{1/2} ; \; h_\psi = f \sinh\alpha \, \sin\beta \tag{7.1.10}$$

Now the form of the governing eq. (7.1.1a) in this curvilinear orthogonal coordinate system is

$$K \frac{\partial \hat{c}}{\partial t} = D_f \left[\frac{1}{h_\alpha h_\beta h_\psi} \left\{\frac{\partial}{\partial\alpha}\left(\frac{h_\beta h_\psi}{h_\alpha} \frac{\partial \hat{c}}{\partial\alpha}\right) + \frac{\partial}{\partial\beta}\left(\frac{h_\alpha h_\psi}{h_\beta} \frac{\partial \hat{c}}{\partial\beta}\right) + \right.\right. \\ \left.\left. \frac{\partial}{\partial\psi}\left(\frac{h_\alpha h_\beta}{h_\psi} \frac{\partial \hat{c}}{\partial\psi}\right)\right\}\right] \tag{7.1.11}$$

which reduces with help of (7.1.10) to

$$K \frac{\partial \hat{c}}{\partial t} = D_f \left[\frac{1}{f^2(\sinh^2\alpha + \sin^2\beta)} \left\{ \frac{1}{\sinh\alpha} \frac{\partial}{\partial\alpha} \left(\sinh\alpha \frac{\partial \hat{c}}{\partial\alpha} \right) + \right.\right.$$

$$\left.\left. + \frac{1}{\sin\beta} \frac{\partial}{\partial\beta} \left(\sin\beta \frac{\partial \hat{c}}{\partial\beta} \right) + \left(\frac{1}{\sinh^2\alpha} + \frac{1}{\sin^2\beta} \right) \frac{\partial^2 \hat{c}}{\partial\psi^2} \right\} \right] \tag{7.1.12}$$

$$\alpha_s < \alpha < \infty, \; o < \beta \leqslant \pi, \; o < \psi \leqslant 2\pi$$

An alternate form of this equation is useful. Let

$$\zeta = \cosh\alpha, \; \mu = \cos\beta, \; \psi = \psi \tag{7.1.13}$$

then (7.1.11) transforms into

$$K \frac{\partial \hat{c}}{\partial t} = \frac{D_f}{f^2\left(\zeta^2-\mu^2\right)} \left\{ \frac{\partial}{\partial\zeta} \left[(\zeta^2-1) \frac{\partial \hat{c}}{\partial\zeta} \right] + \frac{\partial}{\partial\mu} \left[(1-\mu^2) \frac{\partial \hat{c}}{\partial\mu} \right] + \right.$$

$$\left. + \frac{\zeta^2-\mu^2}{(\zeta^2-1)(1-\mu^2)} \frac{\partial^2 \hat{c}}{\partial\psi^2} \right\} \tag{7.1.14}$$

$$\zeta_s < \zeta < \infty, \; -1 \leqslant \mu \leqslant 1, \; o < \psi \leqslant 2\pi$$

as one can readily show. In (7.1.12) and (7.1.14) α_s and ζ_s describe the cylinder (prolate spheroid) surface. Particular solutions to this equation can be constructed by separation of variables. With

$$\hat{c}(\zeta,\mu,\psi,t) = e^{-s^2 t} \; \phi(\zeta,\mu,\psi) \tag{7.1.15}$$

ϕ satisfies the Helmholtz equation in prolate spheroidal coordinates

$$\frac{\partial}{\partial\zeta}\left[(\zeta^2-1)\frac{\partial\phi}{\partial\zeta}\right] + \frac{\partial}{\partial\mu}\left[(1-\mu^2)\frac{\partial\phi}{\partial\mu}\right] + \frac{\zeta^2-\mu^2}{\left(\zeta^2-1\right)\left(1-\mu^2\right)}\frac{\partial^2\phi}{\partial\psi^2} +$$

$$+ k^2\left(\zeta^2-\mu^2\right)\phi = 0, \quad \text{where } k^2 = \frac{(sf)^2K}{D_f} \tag{7.1.16}$$

This equation can be separated again with

$$\phi(\zeta,\mu,\psi) = R_{mn}(k,\zeta)\, S_{mn}(k,\mu) \begin{matrix}\cos\\ \sin\end{matrix}(m\psi) \tag{7.1.17}$$

Here the radial function $R_{mn}(k,\zeta)$ and the angular function $S_{mn}(k,\mu)$ satisfy the differential equations

$$\frac{d}{d\zeta}\left[(\zeta^2-1)\frac{d}{d\zeta}R_{mn}(k,\zeta)\right] - \left(\kappa_{mn} - k^2\zeta^2 + \frac{m^2}{\zeta^2-1}\right)R_{mn}(k,\zeta) = 0$$

$$\frac{d}{d\mu}\left[\left(1-\mu^2\right)\frac{d}{d\mu}S_{mn}(k,\mu)\right] + \left(\kappa_{mn}-k^2\mu^2 - \frac{m^2}{1-\mu^2}\right)S_{mn}(k,\mu) = 0 \tag{7.1.18}$$

The separation constants k^2 and κ_{mn}, which are eigenvalues in our problem, would be determined by boundary conditions imposed on R_{mn} and S_{mn}. This method of solution is not pursued in the following since the determination of the spheriodal eigenfunctions and eigenvalues for the exterior problem are mathematically quite involved. We will instead obtain the necessary information about the solution by application of Laplace transform techniques.

Before proceeding with this, we make the simplication that the concentration of the diffusing element on the cylinder surface is independent of

the angle ψ and constant over the entire surface so that $c(\zeta,\mu,\tau)$ obeys, see eq. (7.1.14).

$$\frac{\partial c}{\partial \tau} = \frac{1}{\left(\zeta^2-\mu^2\right)}\left\{\frac{\partial}{\partial \zeta}\left[(\zeta^2-1)\frac{\partial c}{\partial \zeta}\right] + \frac{\partial}{\partial \mu}\left[(1-\mu^2)\frac{\partial c}{\partial \mu}\right]\right\} ,$$

$$\zeta_s < \zeta < \infty, \ -1 \leqslant \mu \leqslant 1 \tag{7.1.19}$$

$$c(\zeta,\mu,o) = 0, \ \zeta_s \leqslant \zeta < \infty , \ -1 \leqslant \mu \leqslant 1 \tag{7.1.20}$$

$$c(\zeta_s,\mu,\tau) = 1, \ -1 \leqslant \mu \leqslant 1, \ \tau > 0 \tag{7.1.21}$$

$$c(\infty,\mu,\tau) = 0 \quad -1 \leqslant \mu \leqslant 1, \ \tau \geqslant 0 \tag{7.1.22}$$

$$\frac{\partial c(\zeta,o,\tau)}{\partial \mu} = 0 \quad \zeta_s \leqslant \zeta < \infty , \ \tau \geqslant 0 \tag{7.1.23}$$

where

$$c(\zeta,\mu,\tau) = \frac{\hat{c}(\zeta,\mu,\tau)}{\hat{c}_s} \ ; \ \tau = \frac{D_f t}{Kf^2} \tag{7.1.24}$$

The initial condition is given by (7.1.20). The boundary conditions on the surface of the cylinder and on the spherical surface at the point at infinity are given by (7.1.21) and (7.1.22) respectively. Eq. (7.1.23) describes the symmetry of c about the midplane $\mu = 0$ of the cylinder. We now develop the steady solution as well as the early time and large time (approach to the equilibrium) behavior of this solution.

The Steady State Solution

For this case the governing equation for $c(\zeta)$ and its side conditions reduce to

$$\frac{d}{d\zeta}\left[(\zeta^2-1)\frac{dc}{d\zeta}\right] = 0 , \quad \zeta_s \leqslant \zeta < \infty \tag{7.1.25}$$

$$c(\zeta_s) = 1 \tag{7.1.26}$$

$$c(\infty) = 0 \tag{7.1.27}$$

If the concentration at infinity is non-zero, a change in the reference datum ($\hat{c}$) reduces that problem to the above formulation. Here c has no μ dependence because the boundary conditions (7.1.21) to (7.1.23) can be met in the indicated way. The solution to this problem is elementary and is given by

$$c(\zeta) = \frac{Q_o(\zeta)}{Q_o(\zeta_s)} \qquad \zeta_s \leqslant \zeta < \infty \tag{7.1.28}$$

where

$$Q_o(\zeta) = \frac{1}{2} \log \frac{\zeta+1}{\zeta-1} \tag{7.1.29}$$

is the Legendre function of the second kind and zero order. In view of

$$\frac{\zeta+1}{\zeta-1} = \frac{\cosh\alpha + 1}{\cosh\alpha - 1} = \coth^2 \frac{\alpha}{2} \tag{7.1.30}$$

Eq. (7.1.28) yields

$$c(\alpha) = \frac{\log \coth \frac{\alpha}{2}}{\log \coth \frac{\alpha_s}{2}}, \quad \alpha_s \leqslant \alpha < \infty \tag{7.1.31}$$

The diffusion flux is then given by

$$\vec{J} = -D_e \hat{c}_s \text{ grad } c$$

$$= \frac{-D_e \hat{c}_s}{h_\alpha} \frac{dc}{d\alpha} \tag{7.1.32}$$

Here $D_e = \varepsilon D_f$ is the effective diffusion coefficient of the species in the water saturated porous medium, and ε is the porosity of the medium. Eq.(7.1.32) with the help of (7.1.10), yields the diffusion flux from the surface of the prolate spheroid

$$\vec{J}_s = \left(\frac{D_e \hat{c}_s}{f}\right) \frac{1}{(\sinh^2\alpha_s + \sin^2\beta)^{1/2} \log(\coth \frac{\alpha_s}{2}) \sinh \alpha_s} \tag{7.1.33}$$

One observes that although the concentration is uniformly distributed over the surface $\alpha = \alpha_s$, the surface flux is a function of position β. The flux is largest over the top and bottom caps of the cylinder where β is close to o and π as shown in Fig. (7.1.1). The expression (7.1.33) is typical of the surface flux from an arbitrarily shaped body, in a diffusion field governed by Laplace's equation, subject to boundary conditions of type (7.1.26), (7.1.27). Dimensional analysis shows that

$$\vec{j}_s = \left(\frac{D_e \hat{c}_s}{\ell}\right) \text{function of body geometry}$$

where ℓ is some characteristic body dimension, which in the present case can be readily identified from (7.1.33). In order to obtain the total rate of mass transport from the cylinder, one must integrate $\vec{j}_s$ over the surface S of the prolate spheroid

$$\dot{m} = \int_S |\vec{j}_s| \; dS \tag{7.1.34}$$

Since $dS = h_\beta h_\psi \, d\beta d\psi$ one obtains with (7.1.10) and (7.1.33) the formula for the total rate of mass transport from a prolate spheroid

$$\dot{m} = \frac{4\pi D_e \hat{c}_s f}{\log(\coth \frac{\alpha_s}{2})} \quad . \tag{7.1.35}$$

For a slender prolate spheroid which is to approximate a cylinder of length to radius ratio $\frac{L}{b} \geq 10$, $\alpha_s << 1$. Hence one can approximate

$$\coth\left(\frac{\alpha_s}{2}\right) \simeq \frac{2}{\alpha_s} \; , \; b \simeq f\,\alpha_s \text{ by using (7.1.4) and } f \simeq \frac{L}{2}$$

thus,

$$b = \frac{L}{2}\alpha_s \text{ or } \frac{2}{\alpha_s} = \frac{L}{b} \quad .$$

With this (7.1.35) yields

$$\dot{m} = \frac{2\pi D_e \hat{c}_s L}{\log\left(\frac{L}{b}\right)} \tag{7.1.36}$$

an approximation for the total rate of mass transport from a slender cylinder of length L and radius b.

The principal physical feature of this formula is that $\dot{m}$ diminishes with decreasing radius b (L being held constant) but for a fixed radius $\dot{m}$ increases with L. These formulas and the equation for the fractional dissolution rate will be illustrated in section 7.5.

We consider next the question of the length of time required to establish the steady state solution.

The Transient Solution

The analysis is conducted in two parts, the early time behavior and the large time behavior of the solution to equations (7.1.19-23), since the complete solution to these equations is difficult to obtain. The large time behavior is of greatest interest since it gives an indication of the time span necessary to establish the steady state. We will compute only the dominant leading term of the solutions since it will furnish the desired information.

The Large Time Behavior

The governing equation (7.1.19) and its side conditions are subjected to a Laplace transform with respect to the variable τ and a Legendre transform with respect to the variable μ. $c(\zeta,\mu,\tau)$ thereby changes in succession into

$$c(\zeta,\mu,p) = \int_0^\infty e^{-p\tau}\, c(\zeta,\mu,\tau)\, d\tau \tag{7.1.37}$$

$$c(\zeta,2n,p) = \int_0^1 c(\zeta,\mu,p)\, P_{2n}(\mu)d\mu \tag{7.1.38}$$

where the $P_{2n}(\mu)$ are the Legendre polynomials of even order. Only even members of the set are required on account of the symmetry condition (7.1.23). We have shown that for the leading term of the solution, only $P_o(\mu) = 1$ and thus $c(\zeta,o,p)$ are required. The details are omitted.

Applying (7.1.37) to (7.1.19) yields with help of (7.1.20).

$$\frac{\partial}{\partial\zeta}\left[(\zeta^2-1)\frac{\partial c(\zeta,\mu,p)}{\partial\zeta}\right] + \frac{\partial}{\partial\mu}\left[(1-\mu^2)\frac{\partial c(\zeta,\mu,p)}{\partial\mu}\right] = p(\zeta^2-\mu^2)c(\zeta,\mu,p) \tag{7.1.39}$$

Then applying (7.1.38) gives with n = o,

$$\frac{d}{d\zeta}\left[(\zeta^2-1)\frac{dc(\zeta,o,p)}{d\zeta}\right] + (1-\mu^2)\frac{\partial c(\zeta,\mu,p)}{\partial\mu}\Bigg|_0^1 = p\int_0^1 (\zeta^2-\mu^2).$$

$$.c(\zeta,\mu,p)\, d\mu \tag{7.1.40}$$

One observes, having first Laplace transformed equations (7.1.19) - (7.1.23), that the second (integrated) term in (7.1.40) vanishes by (7.1.23). The integral on the right hand side of (7.1.40) has the form

$$\int_0^1 (\zeta^2-\mu^2)\, c(\zeta,\mu,p)d\mu = \left(\zeta^2 - \frac{1}{3}\right)c(\zeta,o,p) - \frac{2}{3}\int_0^1 c(\zeta,\mu,p)P_2(\mu)d\mu \tag{7.1.41}$$

The last integral can be shown to have no contribution to the leading term, so there results for $c(\zeta,o,p) \equiv c(\zeta,p)$

$$\frac{d}{d\zeta}\left[(\zeta^2-1)\frac{dc}{d\zeta}\right] = p\left(\zeta^2 - \frac{1}{3}\right)c,\ \zeta_s < \zeta < \infty \tag{7.1.42}$$

with the boundary conditions

$$c(\zeta_s,p) = \frac{1}{p}\ ;\ c(\infty,p) = 0 \tag{7.1.43}$$

We propose a solution to (7.1.42) of the form

$$c(\zeta,q) = \phi(\zeta,q)e^{-q(\zeta-\zeta_s)} \quad , \; q = \sqrt{p} \tag{7.1.44}$$

where $\phi(\zeta,q)$ is to be determined by substitution into (7.1.42). There results

$$\frac{d}{d\zeta}\left[(\zeta^2-1)\frac{d\phi}{d\zeta}\right] = R(\phi,q) \tag{7.1.44a}$$

where

$$R(\phi,q) \equiv 2q\left[(\zeta^2-1)\frac{d\phi}{d\zeta} + \zeta\phi\right] + \frac{2}{3}\; q^2\phi \tag{7.1.44b}$$

In view of eq. (7.1.43) we take the boundary conditions on $\phi(\zeta,q)$ to be

$$\phi(\zeta_s,q) = \frac{1}{q^2} \tag{7.1.45}$$

$$\phi(\infty,q) = 0$$

We now define the Green's function $G(\zeta,\xi)$ for the differential operator in (7.1.44a) in order to solve that equation. Let

$$\frac{d}{d\zeta}\left[(\zeta^2-1)\;\frac{dG(\zeta,\xi)}{d\zeta}\right] = -\delta(\zeta-\xi) \tag{7.1.46}$$

$$G(\zeta_s,\xi) = G(\infty,\xi) = 0$$

Then with $F(a,b) = \displaystyle\int_a^b \frac{d\zeta}{(\zeta^2-1)}$ (7.1.47)

we have

$$(\zeta^2-1)\frac{dG}{d\zeta} = A \text{ or } G(\zeta,\xi) = AF(\zeta_s,\xi) \;,\; \zeta_s < \zeta < \xi \tag{7.1.48}$$

$$(\zeta^2-1)\frac{dG}{d\zeta} = -B \text{ or } G(\zeta,\xi) = -BF(\xi,\infty) \;,\; \xi < \zeta < \infty$$

The continuity of $G(\zeta,\xi)$ and the unit jump discontinuity of $(\zeta^2-1)\dfrac{dG}{d\zeta}$ at $\zeta = \xi$.

determines

$$A = D^{-1}F(\xi,\infty) \ , \ B = D^{-1}F(\zeta_s,\xi) \ ; \ D = F(\zeta_s,\infty) \tag{7.1.49}$$

so that

$$G(\zeta,\xi) = \begin{cases} \left[D^{-1}F(\xi,\infty)\right] \ F(\zeta_s,\zeta) \ , \ \zeta_s \leqslant \zeta \leqslant \xi \\ \\ \left[D^{-1}F(\zeta_s,\xi)\right] \ F(\zeta,\infty) \quad \xi \leqslant \zeta < \infty \end{cases} \tag{7.1.50}$$

On evaluating D and F there results

$$G(\zeta,\xi) = \begin{cases} \dfrac{Q_0(\xi)}{Q_0(\zeta_s)} \quad \left[Q_0(\zeta) - Q_0(\zeta_s)\right] \ , \ \zeta_s \leqslant \zeta < \xi \\ \\ \dfrac{Q_0(\zeta)}{Q_0(\zeta_s)} \quad \left[Q_0(\xi) - Q_0(\zeta_s)\right] \ , \ \xi \leqslant \zeta < \infty \end{cases} \tag{7.1.51}$$

Returning now to the solution of eq. (7.1.44) we consider as our starting point Green's theorem

$$\int_{\zeta_s}^{\infty} \left\{ G \frac{d}{d\zeta} \left[(\zeta^2-1) \frac{d\phi}{d\zeta}\right] - \phi \frac{d}{d\zeta} \left[(\zeta^2-1) \frac{dG}{d\zeta}\right] \right\} d\zeta =$$

$$= \left\{ (\zeta^2-1) \left[G \frac{d\phi}{d\zeta} - \phi \frac{dG}{d\zeta}\right] \right\} \Bigg|_{\zeta_s}^{\infty} \tag{7.1.52}$$

One substitutes for the differential operators under the integral sign the equations (7.1.44a) and (7.1.46), then one makes use of the integral property of the delta function and applies the boundary conditions (re-stated)

$$G(\infty,\xi) = \phi(\infty,\xi) = 0; \ G(\zeta_s,\xi) = 0, \ \phi(\zeta_s,q) = \frac{1}{q^2} \tag{7.1.53}$$

There results

$$\phi(\xi,q) = (\zeta_s^{\,2}-1)\,\frac{dG(\zeta_s,\xi)}{d\zeta}\,\frac{1}{p} - \int_{\zeta_s}^{\infty} G(\zeta,\xi)\,R\,(\phi(\zeta),q)\,d\zeta \tag{7.1.54}$$

But by (7.1.48)

$$(\zeta_s^{\,2}-1)\,\frac{dG(\zeta_s,\xi)}{d\zeta} = A \tag{7.1.55}$$

where A is given by (7.1.49). If one evaluates the integrals, substitutes the result into (7.1.54) and interchanges the labels ξ and ζ, there results the Fredholm integral equation

$$\phi(\zeta,q) = \frac{Q_o(\zeta)}{Q_o(\zeta_s)}\,\frac{1}{q^2} - \int_{\zeta_s}^{\infty} G(\xi,\zeta)\,R\,(\phi(\xi),q)\,d\xi \tag{7.1.56}$$

The large time behavior of the solution is determined by the "small p" behavior of its transform. For this reason, one usually expands the transform of the solution ϕ in powers of p or q. This amounts to the iterative solution of the integral equation in form of a Neuman series. For our purpose (7.1.56) shows that the leading term in such a series is the first (integrated) term on the right hand side, i.e.,

$$\phi^o(\zeta,q) = \frac{Q_o(\zeta)}{Q_o(\zeta_s)}\,\frac{1}{q^2} \tag{7.1.57}$$

Higher approximations can be computed by substituting this into (7.1.44b) and then evaluating the integral (7.1.56) provided that this is done to the correct order of the dismissed μ terms. In the present, we restrict ourselves to the zeroth, i.e., the leading approximation to $c(\zeta,q)$ which is a combination of eqs. (7.1.44) and (7.1.57)

$$c(\zeta,q) = \frac{Q_o(\zeta)}{Q_o(\zeta_s)}\,\frac{e^{-q(\zeta-\zeta_s)}}{q^2} \tag{7.1.58}$$

The Laplace and Legendre inversions produce then the desired approximation for the large time solution

$$c(\zeta,\mu,\tau) = \frac{Q_o(\zeta)}{Q_o(\zeta_s)} \operatorname{erfc}\left(\frac{\zeta-\zeta_s}{2\tau^{1/2}}\right) \tag{7.1.59}$$

As $\tau \to \infty$, the complementary error function tends towards unity so that this expression agrees with the steady solution given by Eq.(7.1.28).

The diffusion flux from the surface of the prolate spheroid is given in the ζ coordinate system by

$$\vec{j} = -\frac{D_e \hat{c}_s}{h_\zeta} \frac{\partial c}{\partial \zeta}\Bigg|_{\zeta = \zeta_s} \quad \text{where } h_\zeta = f\sqrt{\frac{\zeta^2-\mu^2}{\zeta^2-1}}$$

$$\vec{j} = -\frac{D_e \hat{c}_s}{h_{\zeta_s}} \left\{ \frac{Q_o'(\zeta_s)}{Q_o(\zeta_s)} - \frac{1}{\sqrt{\pi\tau}} \right\} \tag{7.1.60}$$

The time span necessary to establish the steady state to 1% requires that

$$\frac{1}{\sqrt{\pi\tau}} = 10^{-2} \left| \frac{Q_o'(\zeta_s)}{Q_o(\zeta_s)} \right| \tag{7.1.61}$$

With $(L/_b) = 20$, $\left| \frac{Q_o'(\zeta_s)}{Q_o(\zeta_s)} \right| \simeq \frac{1}{4} \frac{(20)^2}{\log(20)} = 33.5$ $D_f = 5\text{x}10^{-5} \frac{\text{cm}^2}{\text{sec}}$, K=100

and f = 150 cm, eq (7.1.24) yields

$$t_{\text{steady state}} = \frac{10^4 \text{ x } 2.25 \text{ x } 10^4 \text{ x}10^2}{3.14 \text{ x } 5 \text{ x } 10^{-5} \text{x } (33.5)^2} = 1.28 \text{ x } 10^{11} \text{ sec}$$

$$= 4000 \text{ yrs} \tag{7.1.62}$$

This is an appreciably long time period and its consequence in establishing the steady state in laboratory experiments must be appreciated. For increased retardation this time span increases.

It is within the context of such experiments that the early time behavior of the solution is of interest. We turn next to the analysis of

The Early Time Behavior

In contrast to the large time behavior which is characterized by small values of the Laplace transform parameter p, we are now interested in the large valued parameter case as $p \to \infty$.

The starting point of the analysis is eq. (7.1.42) for $c(\zeta,p)$

$$\frac{d}{d\zeta}\left[(\zeta^2-1)\ \frac{dc}{d\zeta}\right] = p\ (\zeta^2 - \frac{1}{3})\ c\ ,\ \zeta_s < \zeta < \infty \tag{7.1.63}$$

with the boundary conditions (7.1.43)

$$c(\zeta_s,p) = \frac{1}{p}\ ;\quad c(\infty,p) = 0 \tag{7.1.64}$$

One of the most useful techniques for obtaining the asymptotic solution of (7.1.63) for $p \to \infty$ is with help of the Liouville approximation. For this introduce the new independent variable

$$\eta = \int_{\zeta_s}^{\zeta} \left(\frac{(\zeta')^2 - \frac{1}{3}}{(\zeta')^2 - 1}\right)^{1/2} d\zeta' \tag{7.1.65}$$

and the new dependent variable

$$N = \left(\left[\zeta^2-1\right]\ \left[\zeta^2 - \frac{1}{3}\right]\right)^{1/4} c \tag{7.1.66}$$

There results the greatly simplified equation

$$\frac{d^2N}{d\eta^2} = \left[p + g\ (\eta)\right]\ N \tag{7.1.67}$$

for which

$$N(\infty,p) = 0 \tag{7.1.68}$$

Since one treats $p \to \infty$, the function $g(\eta)$ is as usual treated as a negligible contribution and its specific form is of no further interest in the following except for the fact that it is a continuous and bounded function.

The dominant solution of (7.1.67) which satisfies (7.1.68) is

$$N(\eta,p) = Ae^{-p^{1/2}\eta} \tag{7.1.69}$$

If this is substituted into (7.1.66) and the boundary condition (7.1.64) is applied there results

$$c(\zeta,p) = \left(\frac{\left[\zeta_s{}^2-1\right]\left[\zeta_s{}^2-\frac{1}{3}\right]}{\left[\zeta^2-1\right]\left[\zeta^2-\frac{1}{3}\right]}\right)^{1/4} \frac{e}{p}^{-p^{1/2}\eta} \tag{7.1.70}$$

On inversion there results

$$c(\zeta,\mu,\tau) = \left(\frac{\left[\zeta_s{}^2-1\right]\left[\zeta_s{}^2-\frac{1}{3}\right]}{\left[\zeta^2-1\right]\left[\zeta^2-\frac{1}{3}\right]}\right)^{1/4} \operatorname{erfc}\left(\frac{\eta}{2\tau^{1/2}}\right) \tag{7.1.71}$$

where $\eta(\zeta)$ is given by (7.1.65). The early time surface diffusion flux can be determined from this equation and it exhibits, analogous to the second term in eq. (7.1.60), a $\tau^{-1/2}$ behavior, but with a different numerical coefficient.

7.2 Mass Transfer From a Fuel Canister by Diffusion and Forced Convection

Paul L. Chambré

Consider a cylinder of infinite length imbedded in a porous medium through which water is flowing steadily in accordance with Darcy's law. The cylinder matrix contains a diffusing nuclide which is set free at the surface of the cylinder at the solubility limit of the species in water and then diffuses into the exterior unbounded space. All material properties are assumed constant. The flow is taken normal to the axis of the cylinder, but inclined flows can also be treated by the analysis given below. The governing equation for the conservation of mass of the diffusing species from a cylinder of radius r_o in the presence of radioactive decay is

$$K \frac{\partial \hat{c}}{\partial t} + u(\hat{r},\theta) \frac{\partial \hat{c}}{\partial \hat{r}} + \frac{v(\hat{r},\theta)}{\hat{r}} \frac{\partial \hat{c}}{\partial \theta} = D_f \left(\frac{\partial^2 \hat{c}}{\partial \hat{r}^2} + \frac{1}{\hat{r}} \frac{\partial \hat{c}}{\partial \hat{r}} + \frac{1}{\hat{r}^2} \frac{\partial^2 \hat{c}}{\partial \theta^2} \right) - \lambda K \hat{c} ,$$

$$r_o < \hat{r} < \infty , \; o \leqslant \theta \leqslant 2\pi, \; t > 0 \qquad (7.2.1)$$

Here

$$u(r,\theta) = -U \left(1 - \frac{r_o^2}{\hat{r}^2} \right) \cos\theta ; \; v(\hat{r},\theta) = U \left(1 + \frac{r_o^2}{\hat{r}^2} \right) \sin\theta \qquad (7.2.2)$$

are the radial and tangential pore velocity components derived from D'Arcy's potential flow in the porous medium with U the free stream pore velocity far away from the cylinder. $\hat{r}$ is the radial distance from the center of the cylinder and θ the angle measured in the tangential flow direction from the frontal stagnation point at the cylinder surface. K is the retardation coefficient and D_f is the diffusion coefficient of the species in the liquid.

Prior to the time t = 0, the diffusing nuclide has zero concentration

in the porous medium. At time t = 0 the concentration at the surface of the cylinder is changed to a constant value c_s

$$\hat{c}(r_o,\theta,t) = c_s,\ o \leqslant \theta \leqslant 2\pi,\ t \geqslant 0 \tag{7.2.3}$$

and maintained at this surface concentration c_s subsequently. The boundary condition far from the cylinder is held at zero concentration

$$\hat{c}(\infty,\theta,t) = 0\ ,\ o \leqslant \theta \leqslant 2\pi,\ t \geqslant 0 \tag{7.2.4}$$

It is convenient to introduce non-dimensional variables with

$$\tau = \frac{Ut}{Kr_o},\ r = \frac{\hat{r}}{r_o}\ ,\ c(r,\theta,\tau) = \frac{\hat{c}(\hat{r},\theta,t)}{c_s}\ e^{\lambda t}$$

$$Pe = \frac{Ur_o}{D_f}\ ,\ \text{the Peclet number} \tag{7.2.5}$$

$$Da = \frac{K\lambda r_o}{U},\ \text{the Damkohler number for convective mass transport.}$$

Then the governing equations for $c(r,\theta,\tau)$ transform to

$$\frac{\partial c}{\partial \tau} - \left(1 - \frac{1}{r^2}\right) \cos\theta\ \frac{\partial c}{\partial r} + \left(1 + \frac{1}{r^2}\right) \frac{\sin\theta}{r}\ \frac{\partial c}{\partial \theta} = \frac{1}{Pe}\left(\frac{\partial^2 c}{\partial r^2} + \frac{1}{r}\frac{\partial c}{\partial r} + \frac{1}{r^2}\frac{\partial^2 c}{\partial \theta^2}\right)$$

$$1 < r < \infty,\ o \leqslant \theta \leqslant 2\pi\ \tau > o \tag{7.2.6}$$

$$c(1,\theta,\tau) = e^{Da\tau}\ ,\ o \leqslant \theta \leqslant 2\pi,\ \tau \geqslant o \tag{7.2.7}$$

$$c(\infty,\theta,\tau) = 0,\ o \leqslant \theta \leqslant 2\pi,\ \tau \geqslant o \tag{7.2.8}$$

with the initial condition that $c(r,\theta,0) = 0$.

For typical porous media flows the Peclet number Pe may be large. Typically, with U=2 m/yr, r_o = 0.15 m, and $D_f = 1\times10^{-5}$ cm^2/sec will yield a Peclet number of 10.

This suggests an asymptotic solution of the equation system for large Peclet numbers. In this case the principal resistance to mass transfer from the cylinder surface is in a direction normal to the fluid layer surrounding the cylinder, i.e., in the r direction. The diffusion transport tangential to the surface, i.e., the term $\frac{1}{r^2}\frac{\partial^2 c}{\partial\theta^2}$, can then be neglected as will be shown below. To obtain the asymptotic form of the equations, introduce the new independent variable R in place of r

$$r = 1 + \frac{R}{\sqrt{Pe}} \quad , \tag{7.2.9}$$

then eq. (7.2.6) takes on the form

$$\frac{\partial c}{\partial\tau} - 2R\cos\theta\,\frac{\partial c}{\partial R} + 2\sin\theta\,\frac{\partial c}{\partial\theta} = \frac{\partial^2 c}{\partial R^2} + 0\left(Pe^{-1/2}\right) \tag{7.2.10}$$

This is to be solved for $c(R,\theta,\tau)$ subject to, see (7.2.7), (7.2.8)

$$c(o,\theta,\tau) = e^{Da\tau} \;,\; o \leqslant \theta \leqslant 2\pi,\; \tau \geqslant o \tag{7.2.11}$$

$$c(\infty,\theta,\tau) = 0,\; o \leqslant \theta \leqslant 2\pi,\; \tau \geqslant o \tag{7.2.12}$$

with zero initial condition.

For large Pe numbers the last term in eq. (7.2.10) is neglected. By an additional change of the independent variables, one can reduce the time dependent diffusion and convection equation (7.2.10) to a simpler time dependent diffusion problem without convection. New independent variables $\eta(R,\theta)$, $\zeta(\tau,\theta)$ are introduced which transform $c(R,\theta,\tau)$ into $\bar{c}(\eta,\zeta)$

$$\text{i.e.,}\quad \bar{c}(\eta,\zeta) = c(R,\theta,\tau) \tag{7.2.13}$$

These variables are given by

$$\zeta(\tau,\theta) = -\frac{1}{2}\cos\theta + \frac{1}{2}\left\{\frac{1-f(\tau,\theta)}{1+f(\tau,\theta)}\right\} \tag{7.2.14a}$$

where $f(\tau,\theta) = e^{-4\tau}\,\frac{a(\theta)}{b(\theta)}$ with $a(\theta) = \left(\frac{2}{1+\cos\theta}\right)$, $b(\theta) = \left(\frac{2}{1-\cos\theta}\right)$

and

$$\eta(R,\theta) = R\sin\theta\ . \tag{7.2.14b}$$

As the reader can readily verify, these transformations, which are deduced by group-theoretical considerations, change eq. (7.2.10) to a very simple equation for $\bar{c}(\eta,\zeta)$, i.e.,

$$\frac{\partial\bar{c}}{\partial\zeta} = \frac{\partial^2\bar{c}}{\partial\eta^2}\ ,\ \eta > o,\ \zeta > o \tag{7.2.15}$$

subject to the side conditions

$$\bar{c}(o,\zeta) = 1\ ,\ \zeta \geqslant o \tag{7.2.16}$$

$$\bar{c}(\infty,\zeta) = o,\ \zeta \geqslant o \tag{7.2.17}$$

with the condition that $\bar{c}(\eta,o) = 0$.

The solution to this problem is

$$\bar{c}(\eta,\zeta) = \operatorname{erfc}\left(\frac{\eta}{2\sqrt{\zeta}}\right) \tag{7.2.18}$$

The solution in R,θ,τ variables is obtained by substituting $\eta(R,\theta)$, and $\zeta(\theta,\tau)$ in (7.2.18). One obtains after some simplifications that:

$$c(R,\theta,\tau) = \operatorname{erfc}\left(R\sqrt{\frac{\coth 2\tau + \cos\theta}{2}}\right) \tag{7.2.19}$$

This solution satisfies (7.2.10) with side condition (7.2.11) replaced by unity. To obtain the τ dependent boundary condition given

by (7.2.11) we use Duhamel's integral, i.e.,

$$c(R,\theta,\tau) = \int_0^\tau c(o,\theta,\tau') \frac{\partial}{\partial\tau}\left[\operatorname{erfc}\left(R\sqrt{\frac{\coth 2(\tau-\tau') + \cos\theta}{2}}\right)\right]d\tau' \qquad (7.2.20)$$

Integrating by parts and transforming back to the original variable $\hat{c}$ one obtains

$$\hat{c}(\hat{r},Pe,Da,t,\theta) = c_s \exp\left(-\frac{Da\ Ut}{Kr_o}\right) \operatorname{erfc}\left[\left(\frac{\hat{r}}{r_o} - 1\right)\sqrt{\frac{Pe}{2}\left(\coth\frac{2Ut}{Kr_o} + \cos\theta\right)}\right] +$$

$$+ c_s\ Da \int_0^{\frac{Ut}{Kr_o}} e^{-Da\tau} \operatorname{erfc}\left[\left(\frac{\hat{r}}{r_o} - 1\right)\sqrt{\frac{Pe}{2}\left(\coth 2\tau + \cos\theta\right)}\right] d\tau \qquad (7.2.21)$$

This solution (7.2.21) describes the time dependent concentration field in the presence of radioactive decay in a Darcy flow about a cylinder.

The surface mass flux for a diffusing nuclide is

$$\vec{j}(Pe,Da,t,\theta) = -D_e \left.\frac{\partial\hat{c}}{\partial\hat{r}}\right|_{\hat{r}=r_o}$$

$$= \frac{D_e c_s}{r_o}\sqrt{\frac{2Pe}{\pi}}\left[\exp\left(-\frac{Da\ Ut}{Kr_o}\right)\sqrt{\coth\frac{2Ut}{Kr_o} + \cos\theta} +\right.$$

$$\left. + Da\int_0^{\frac{Ut}{Kr_o}} e^{-Da\tau}\sqrt{\coth 2\tau + \cos\theta}\ d\tau\right] \qquad (7.2.22)$$

where $D_e = \varepsilon\ D_f$ in the effective diffusion coefficient of the diffusing nuclide and ε the porosity of the medium.

The surface mass flux, according to (7.2.22) depends on time and the angular position. The angular dependence is removed by averaging the surface mass flux over the cylinder perimeter. On the account of symmetry we have

$$\vec{J}_{av}\ (Pe,Da,t) = \frac{1}{\pi}\int_0^{\pi} \vec{j}\ (Pe,Da,t,\theta)\ d\theta$$

$$= \frac{D_e c_s}{\pi r_o}\sqrt{\frac{2Pe}{\pi}}\left[\exp\left(-\frac{Da\ Ut}{Kr_o}\right)\ I\left(\frac{Ut}{Kr_o}\right) + Da\int_0^{\frac{Ut}{Kr_o}} e^{-Da\tau}\ I(\tau)\ d\tau\right]$$

(7.2.23)

where

$$I(\tau) \equiv \int_0^{\pi} (\coth 2\tau + \cos\theta)^{1/2}\ d\theta$$

To evaluate $I(\tau)$ we proceed as follows

$$I(\tau) = \int_0^{\pi}\left(-1 + \frac{2e^{2\tau}}{e^{2\tau}-e^{-2\tau}} + \cos\theta\right)^{1/2} d\theta$$

$$= 2\int_0^{\pi/2}\left(\frac{2}{1-e^{-4\tau}} - 2\sin^2\phi\right)^{1/2} d\phi$$

$$= \frac{2\sqrt{2}}{m(\tau)}\ E\ [m^2(\tau)] \qquad (7.2.24)$$

where $m(\tau) \equiv (1-e^{-4\tau})^{1/2}$ and $E[x]$ is the complete elliptic integral of the second kind. Substituting for $I(\tau)$ in (7.2.23) one obtains

$$\vec{J}_{av}(Pe,Da,t) = \frac{4D_e c_s}{\pi r_o}\sqrt{\frac{Pe}{\pi}}\left\{\frac{\exp\left(-\frac{Da\ Ut}{Kr_o}\right)E\left[m^2\left(\frac{Ut}{Kr_o}\right)\right]}{m\left(\frac{Ut}{Kr_o}\right)} + Da\int_0^{\frac{Ut}{Kr_o}} e^{-Da\tau}\ \frac{E[m^2(\tau)]}{m(\tau)}d\tau\right\}$$

(7.2.25)

In absence of radioactive decay (λ=Da=0) there results

$$\vec{j}_{av}(Pe,o,t) = \frac{4D_e c_s}{\pi r_o} \sqrt{\frac{Pe}{\pi}} \quad \frac{E[m^2(\frac{Ut}{Kr_o})]}{m(\frac{Ut}{Kr_o})} \tag{7.2.26}$$

For application in section (7.5), we require the steady state, average surface mass flux in absence of radioactive decay. Hence, (7.2.26) yields as $t \to \infty$, with $m(\infty) = 1$ and $E[1] = 1$, that

$$\vec{j}_{av} = \frac{4D_e c_s}{\pi r_o} \sqrt{\frac{Pe}{\pi}} \tag{7.2.27}$$

The mass transfer per unit length of cylinder under steady state condition is then given by

$$\dot{m} = \vec{j}_{av} \times 2\pi r_o = 4.5135\ D_e c_s \sqrt{Pe} \tag{7.2.28}$$

a result well known in heat and mass transfer studies where it is shown to be valid for a range of Pe>4 (K2),(L1).

From (7.2.26) one can estimate the time necessary to establish the surface mass flux to 99% of the steady state mass flux. From table of complete elliptic integral of the second kind one obtains that the criteria is given by

$$\frac{Ut}{Kr_o} = 1.2 \tag{7.2.29}$$

For a flow of U = 1 m/yr, r_o = 0.15 m, and K = 100, t = 18 years, a relatively short time for the establishment of a steady state when compared with the case of pure diffusion. There t = 4000 years was obtained (see 7.1.62).

The analysis leading to the solution (7.2.21) for the time independent boundary condition is readily generalized to a time dependent boundary condition. The starting point for this analysis is Eq.(7.2.20). If in (7.2.3), c_s is replaced by $c_s\ \phi(t)$, one must change $c(o,\theta,\tau')$ in (7.2.20) to $e^{Da\tau'}\ \phi\left(\frac{\tau' Kr_o}{U}\right)$

As an illustration consider the radioactive decay of the surface concentration according to

$$\hat{c}(r_o,\theta,t) = c_s\, e^{-\lambda t} \qquad o<\theta \leq 2\pi, \quad t \geq o \tag{7.2.30}$$

in place of Eq.(7.2.3). Here $\phi(t) \equiv e^{-\lambda t}$. Hence, we have

$$c(o,\theta,\tau') = e^{Da\tau'}\, e^{\frac{-\lambda\tau' K r_o}{U}} = 1 \tag{7.2.31}$$

After substitution of $c(o,\theta,\tau')$ into (7.2.20) one can perform the integration analytically. Transforming back to the $\hat{c}$ and evaluating surface mass flux one obtains

$$\vec{j}\,(Pe,Da,\theta,t) = \frac{D_e c_s}{r_o} \exp\left(-\frac{Da\ Ut}{Kr_o}\right) \sqrt{\frac{2P_e}{\pi}\left[\coth\left(\frac{2Ut}{Kr_o}\right) + \cos\theta\right]}\ . \tag{7.2.32}$$

This shows that the surface mass flux no longer reaches a steady state but tends toward zero as $t \to \infty$.

For a flow parallel to the cylinder axis the mass transfer can be approximated as follows. The lateral cylinder surface is unwrapped into a flat plate of length L and width $2\pi r_o$, and subjected to a flow in the direction of the plate length. The steady mass transfer from a flat plate of width $2\pi r_o$ and length L under longitudinal flow is given by

$$\dot{M}_{long} = 2.257\ D_e c_s \left(\frac{UL}{D_f}\right)^{1/2} 2\pi r_o\ , \tag{7.2.33}$$

while the mass transfer from a cylinder of length L with the flow normal to the cylinder axis is in view of (7.2.25)

$$\dot{M}_{norm} = 4.513\ D_e c_s \left(\frac{Ur_o}{D_f}\right)^{1/2} L \tag{7.2.34}$$

Hence

$$\frac{\dot{M}_{norm}}{\dot{M}_{long}} = \frac{4.513}{(2.257)\sqrt{2\,\pi}} \left(\frac{L}{2r_o}\right)^{1/2}$$

For a canister, with an aspect ratio $\frac{L}{2r_o} = 13.2$

$$\frac{\dot{M}_{norm}}{\dot{M}_{long}} \simeq 1.63$$

This indicates that for flow parallel to the cylinder axis, the mass transfer is decreased by about 63% compared to that due to the flow normal to the cylinder axis because the thickness of the diffusion boundary layer is greater for $\dot{M}_{long}$ than for $\dot{M}_{norm}$.

Finally we note that the large Peclet number approximation made in the analysis prevents one from letting the free stream Darcy velocity U become small. If $U \to o$, in eq. (7.2.1), the convection terms drop out and the equation describes then a temporal balance between the effects of diffusion and radioactive decay. For a constant surface concentration, given by eq. (7.2.3), the modified eq. (7.2.1) generates then a steady state solution as $t \to \infty$. Since the θ dependence is no longer needed, the governing equation is

$$\frac{\partial^2 \hat{c}}{\partial r^2} + \frac{1}{r}\frac{\partial \hat{c}}{\partial r} - \beta^2 \hat{c} = 0, \; r > 1$$

where

$$\beta^2 = \frac{r_o^2 \lambda K}{D_f}, \; r = \frac{\hat{r}}{r_o}, \tag{7.2.35}$$

with the boundary conditions

$$\hat{c}(1) = c_s, \; \hat{c}(\infty) = 0. \tag{7.2.36}$$

The solution is given by

$$\hat{c}(r) = c_s \frac{K_o(\beta r)}{K_o(\beta)} \ , \ r > 1 \tag{7.2.37}$$

so that the surface mass flux is

$$\vec{j}(r_o) = \frac{D_e c_s}{r_o} \left\{ \beta \frac{K_1(\beta)}{K_o(\beta)} \right\} \tag{7.2.38}$$

Here $K_o(\eta)$, $K_1(\eta)$ are the modified Bessel functions of zero and first order respectively.

A detailed numerical evaluation of the mass transfer without radioactive decay, i.e., eq. (7.2.28), as well as the fractional dissolution rate are given in section 7.5. The other formulae derived above including their dependence on radioactive decay will be investigated in the future.

7.3 Mass Transfer From a Fuel Canister by Diffusion and Free Convection

Paul L. Chambré

The problem concerns the mass transfer from a heated vertical cylinder which is imbedded in a water saturated porous medium. The temperature of the cylinder exceeds that of the surrounding with the result that a free convection pattern develops which drives the fluid along the cylinder surface. This induced velocity affects the mass transport of a diffusing species from the cylinder surface into the surrounding medium. It is thought that the effects of free convection might be important during that time when the fuel canister generates a sufficiently large amount of decay heat to maintain a temperature difference of about 50°C (or more) between the canister surface and the surrounding medium. The aim of the analysis is to determine the velocity, temperature and concentration fields and to develop a formula for the surface mass flux.

The following assumptions are made:

a) A steady state description is adopted.

b) The vertical cylinder surface is replaced by a flat plate surface having the same length as the cylinder and a width equal to the cylinder circumference.

c) The pore water is assumed to have temperature independent properties except for its density. The water flow obeys Darcy's law. The fluid filling the porous medium is assumed to be a single phase.

d) Boundary layer theory simplifications are assumed valid, see eq. (7.3.14) below.

The governing equations are:

<u>Conservation of Mass</u>

$$\frac{\partial u}{\partial x} + \frac{\partial v}{\partial y} = 0 \qquad (7.3.1)$$

Conservation of Momentum (Darcy's Law)

$$u = -\frac{k}{\mu}\left(\frac{\partial p}{\partial x} + \rho g\right) \tag{7.3.2}$$

$$v = -\frac{k}{\mu}\frac{\partial p}{\partial y} \tag{7.3.3}$$

Conservation of Energy

$$u\frac{\partial T}{\partial x} + v\frac{\partial T}{\partial y} = \alpha_e \nabla^2 T \quad , \alpha_e \equiv \frac{\lambda_e}{\rho c_p} \tag{7.3.4}$$

Conservation of Species

$$u\frac{\partial \hat{c}}{\partial x} + v\frac{\partial \hat{c}}{\partial y} = \varepsilon D_f \nabla^2 \hat{c} \tag{7.3.5}$$

Equation of State of Liquid

$$\rho = \rho_\infty \left\{1 - \beta\,(T - T_\infty)\right\} \tag{7.3.6}$$

where

$$\nabla^2 \equiv \frac{\partial^2}{\partial x^2} + \frac{\partial^2}{\partial y^2} \tag{7.3.7}$$

The coordinate system is shown in Fig. (7.3.1). The velocity components u,v point respectively into the x and y direction. In the above equations p, T, ρ, c_p are the pressure, temperature, density and heat capacity of the liquid and ρ_∞ its density far away from the plate. k is the permeability of the porous medium. λ_e is the effective thermal conduction of water saturated porous medium as measured in the laboratory. μ and β are dynamic viscosity and coefficient of thermal expansion of the liquid in the porous medium respectively. D_f is the diffusion coefficient of the diffusing species in the liquid.

The boundary conditions for our problem are

$$v(x,o) = o,\ T(x,o) = T_w;\ \hat{c}(x,o) = c_s,\ \text{for } x>o \tag{7.3.8}$$

$$u(x,\infty) = v(x,\infty) = 0;\ T(x,\ ) = T_\infty;\ \hat{c}(x,\infty) = 0,\ \text{for } x>o \tag{7.3.9}$$

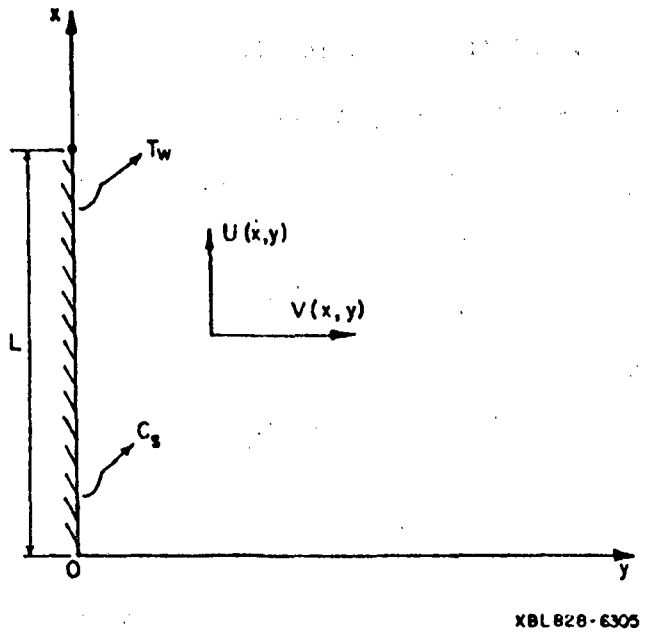

Fig. 7.3.1. Co-ordinate system used in the free convection model.

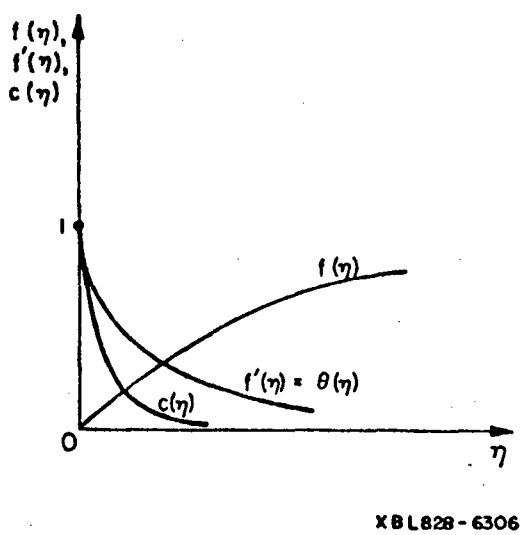

Fig. 7.3.2. Qualitative shape of f(η), f'(η) and c(η) for large Lewis number.

There will be a "slip" condition for the u component of the velocity at the plate surface which is as yet unknown. Furthermore, the temperature difference $(T_w - T_\infty)$ which depends among other parameters on the heat release from the cylinder is also determined subsequently.

Eq. (7.3.1) can be satisfied in the usual way by introducing the stream function $\psi(x,y)$ with

$$u(x,y) = \frac{\partial\psi}{\partial y} \; ; \; v(x,y) = -\frac{\partial\psi}{\partial x} \tag{7.3.10}$$

If one differentiates (7.3.2) with respect to y, (7.3.3) with respect to x and then algebraically adds the resulting equations, one obtains with help of (7.3.6) and (7.3.10),

$$\left(\frac{k}{\mu}\,\rho_\infty\,\beta g\right)\frac{\partial T}{\partial y} = \nabla^2\psi \tag{7.3.11}$$

On the other hand (7.3.4) and (7.3.5), expressed with (7.3.10), give

$$\frac{\partial\psi}{\partial y}\,\frac{\partial T}{\partial x} - \frac{\partial\psi}{\partial x}\,\frac{\partial T}{\partial y} = \alpha_e\nabla^2 T \tag{7.3.12}$$

$$\frac{\partial\psi}{\partial y}\,\frac{\partial\hat{c}}{\partial x} - \frac{\partial\psi}{\partial x}\,\frac{\partial\hat{c}}{\partial y} = \varepsilon D_f\nabla^2\hat{c} \tag{7.3.13}$$

One has thus these three governing equations for the determination of the unknown functions ψ,T and $\hat{c}$. For the purpose of establishing the main physical features of the solution, it is convenient to utilize the boundary layer simplifications. These imply that the transport of mass, energy and concentration in the major flow direction (i.e., u) is small compared to that normal to the plate. With

$$\frac{\partial^2\psi}{\partial x^2} \ll \frac{\partial^2\psi}{\partial y^2}\;,\;\; \frac{\partial^2 T}{\partial x^2} \ll \frac{\partial^2 T}{\partial y^2}\;,\;\; \frac{\partial^2\hat{c}}{\partial x^2} \ll \frac{\partial^2\hat{c}}{\partial y^2} \tag{7.3.14}$$

Equations 7.3.11-13 result in,

$$(\rho_\infty \frac{k}{\mu} \beta g) \frac{\partial T}{\partial y} = \frac{\partial^2 \psi}{\partial y^2} \tag{7.3.15}$$

$$\frac{\partial \psi}{\partial y} \frac{\partial T}{\partial x} - \frac{\partial \psi}{\partial x} \frac{\partial T}{\partial y} = \alpha_e \frac{\partial^2 T}{\partial y^2} \tag{7.3.16}$$

$$\frac{\partial \psi}{\partial y} \frac{\partial \hat{c}}{\partial x} - \frac{\partial \psi}{\partial x} \frac{\partial \hat{c}}{\partial y} = \varepsilon D_f \frac{\partial^2 \hat{c}}{\partial y^2} \tag{7.3.17}$$

These equations are subject to the boundary conditions, (see (7.3.8), (7.3.9) and (7.3.10))

$$\frac{\partial \psi(x,o)}{\partial x} = 0, \; T(x,o) = T_w \; ; \; \hat{c}(x,o) = c_s \tag{7.3.18}$$

$$\frac{\partial \psi(x,\infty)}{\partial x} = \frac{\partial \psi(x,\infty)}{\partial y} = 0 \; , \; T(x,\infty) = T_\infty \; ; \; \hat{c}(x,\infty) = 0 \tag{7.3.19}$$

valid for x>o.

Equations (7.3.15) and 7.3.16), which are coupled equations for T and ψ, are solved first. One determines thereby the temperature induced stream function $\psi(x,y)$ which describes the free convection flow pattern. With knowledge of ψ, one can then solve for the concentration $\hat{c}(x,y)$ separately. For this reason we concentrate first on the solution of (7.3.15) and (7.3.16). These partial differential equations are reduced to ordinary differential equation by the introduction of the similarity variables

$$\eta = Ra^{1/2} \, (y/\sqrt{xL}) \tag{7.3.20}$$

$$\psi = \alpha_e \, (Ra)^{1/2} \, (\frac{x}{L})^{1/2} \, f(\eta) \tag{7.3.21}$$

$$\theta(\eta) = \frac{T-T_\infty}{T_w-T_\infty} \tag{7.3.22}$$

$$c(\eta) = \frac{\hat{c}}{c_s} \tag{7.3.23}$$

where

$$Ra = \frac{\rho_\infty g}{\alpha_e} \left(\frac{k}{\mu}\right) \beta \, (T_w-T_\infty)L \tag{7.3.24}$$

Here L is the length of the plate and Ra the Rayleigh number of the liquid saturated porous medium. With these variables the governing equations reduce to

$$f'' \ (\eta) - \theta' \ (\eta) = 0 \tag{7.3.25}$$

$$\theta'' \ (\eta) + \frac{1}{2} f \ (\eta) \ \theta' \ (\eta) = 0 \tag{7.3.26}$$

$$\Lambda^{-1} c'' \ (\eta) + \frac{1}{2} f \ (\eta) \ c' \ (\eta) = 0 \tag{7.3.27}$$

where

$$\Lambda = \frac{\alpha_e}{\varepsilon D_f} = Le \tag{7.3.28}$$

is the Lewis number. The boundary conditions transform to

$$f(o) = 0 \ ; \ \theta(o) = 1 \ ; \ c(o) = 1 \tag{7.3.29}$$

$$f'(\infty) = 0 \ ; \ \theta(\infty) = 0 \ ; \ c(\infty) = 0 \tag{7.3.30}$$

as can be seen by introducing the new variables into (7.3.18) and (7.3.19).

A final integral of eq. (7.3.25), which satisfies the boundary conditions (7.3.30) for f' and θ at $\eta = \infty$, is given by

$$f' \ (\eta) = \theta(\eta) \tag{7.3.31}$$

Since the x component of the free convection velocity is determined by

$$u = \frac{\partial\psi}{\partial y} = \left(\frac{\alpha_e}{L}\,\mathrm{Ra}\right) f'(\eta) \tag{7.3.32}$$

one observes that the normalized vertical velocity $\dfrac{u(\eta)}{\left(\frac{\alpha_e}{L}\,\mathrm{Ra}\right)}$ and the temperature distribution $\theta(\eta)$ are, according to (7.3.31), of the same form. Thus, the determination of the function $f(\eta)$ is of central importance. To obtain an equation for $f(\eta)$, eliminate θ between equations (7.3.25), (7.3.26) and (7.3.31), with the result that

$$\frac{d^3f}{d\eta^3} + \frac{1}{2} f \frac{d^2f}{d\eta^2} = 0 \tag{7.3.33}$$

Exactly the same differential equation arises in the problem of the boundary layer flow of a viscous fluid over a flat plate, the famous Blasius problem (B2). But in contrast to the boundary conditions $f(o) = f'(o) = 0$, $f'(\infty) = 1$ in that problem, the conditions for the present case read

$$f(o) = 0 \;;\; f'(o) = 1 \;;\; f'(\infty) = 0 \tag{7.3.34}$$

The qualitative shape of the solution $f(\eta)$ of (7.3.33), (7.3.34) and that of its derivative $f'(\eta)$ are shown in Fig. (7.3.2). As already stated, the free convection induced vertical velocity component and the temperature distribution normal to the plate are both characterized by the shape of the $f'(\eta)$ function.

Next we determine the mass transfer from the vertical surface. For this one requires the normal derivative $\left.\frac{\partial\hat{c}}{\partial y}\right|_{y=0}$ which in turn involves $\left.\frac{\partial c}{\partial\eta}\right|_{\eta=0}$. But η contains Ra and in this Rayleigh number there occurs the as yet unknown temperature difference (T_w-T_∞). (T_w-T_∞) is determined by the heat flux through the canister surface and the convective and conductive heat

transport into the porous medium. So one must first find $(T_w - T_\infty)$. The local heat transfer from the surface of the plate is defined by

$$q'' = -\lambda_e \left.\frac{\partial T}{\partial y}\right|_{y=0}$$

which with (7.3.20) and (7.3.22) yields

$$q'' = -\lambda_e (T_w - T_\infty)^{3/2} \left(\frac{k}{\mu}\frac{\rho_\infty \beta g}{\alpha_e}\right)^{1/2} x^{-1/2}\, \theta'(o) \qquad (7.3.35)$$

where λ_e is the effective thermal conductive of the saturated porous medium. The total rate of heat transfer from a plate of length and width W is then

$$Q = W \int_0^L q''(x)\, dx$$

$$= -W \lambda_e (T_w - T_\infty)^{3/2} \left(\frac{k}{\mu}\frac{\rho_\infty \beta g}{\alpha_e}\right)^{1/2} 2L^{1/2}\, \theta'(o) \qquad (7.3.36)$$

Fig. (7.3.3) shows the variation of spent fuel heat generation with time. We now define the magnitude of the average heat flux from the entire plate as

$$\bar{q}'' \equiv \frac{|Q|}{WL}$$

$$= \lambda_e (T_w - T_\infty)^{3/2} \left(4\frac{k}{\mu}\frac{\rho_\infty \beta g}{L\alpha_e}\right)^{1/2} |\theta'(o)| \qquad (7.3.37)$$

Hence the desired temperature difference between plate surface and the porous media is given by

$$(T_w - T_\infty) = \left\{\frac{(\bar{q}'')^2}{4\lambda_e^2 \frac{k}{\mu}\frac{\rho_\infty \beta g}{L\alpha_e}\left[\theta'(o)\right]^2}\right\}^{1/3} \qquad (7.3.38)$$

$(T_w - T_\infty)$ is seen to be a function of the average heat flux issuing from the fuel canister and the properties of the porous medium. The assumption

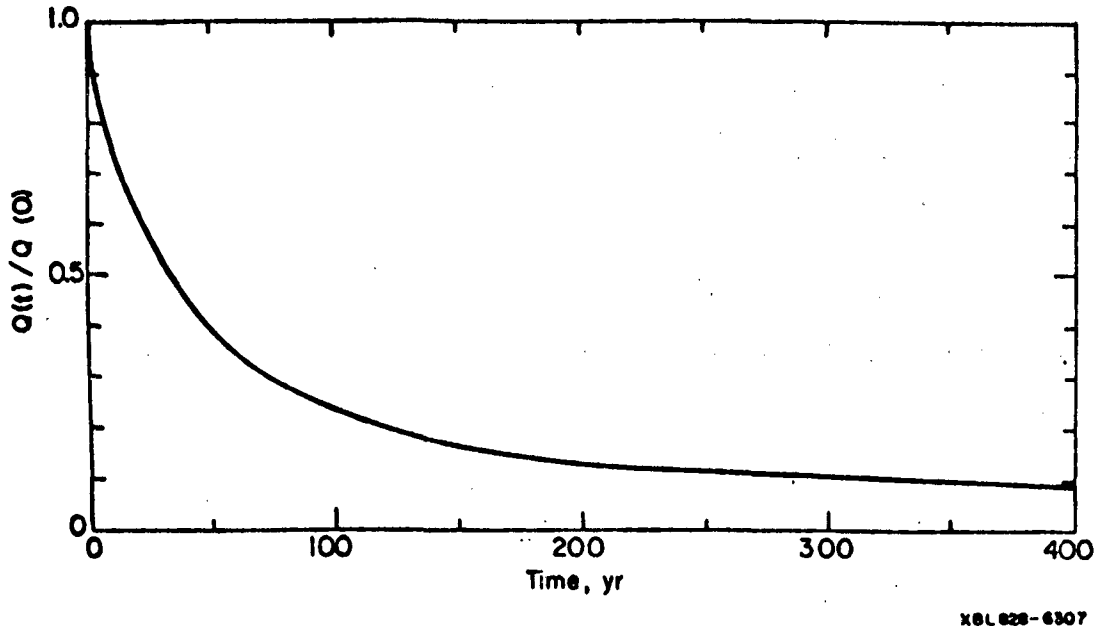

Fig. 7.3.3. Variation of normalized decay heat generation of a spent fuel with time Q (0) is the initial decay heat generation and is equal to 0.55 Kw.

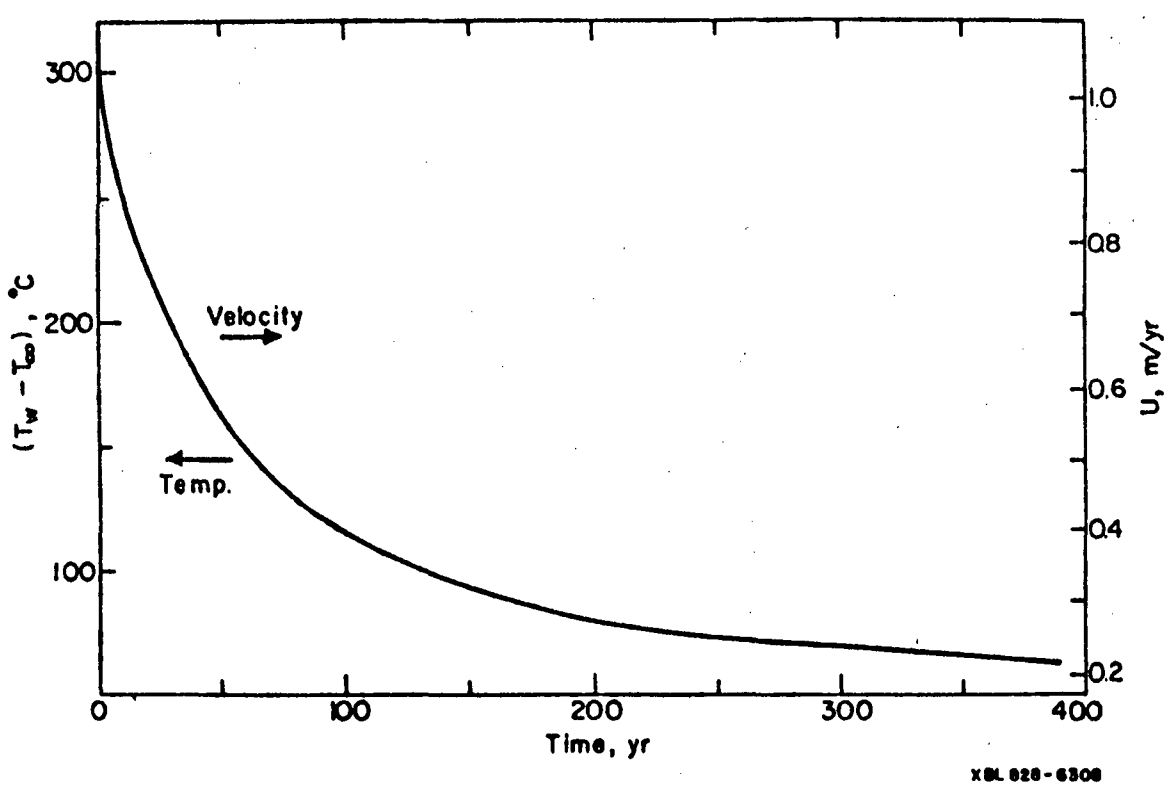

Fig. 7.3.4. Variation of temperature difference $(T_w - T_\infty)$ and free convection velocity with time for a spent fuel canister.

is made that the average heat flux varies so slowly with time so that (7.3.38) can be applied to a quasi-steady state. Fig. (7.3.4) shows a typical trend for this temperature difference as a function of time for a given $\bar{q}''$ (t) descriptive of a spent fuel. The temperature difference drops to 100°C in about 130 years. The calculation is based on the following parameters values

$\lambda = 2.894$ w/m °K	(1)	$\beta = 2.07 \times 10^{-4}$ 1/°K	
$k = 2.96 \times 10^{-14}$ m^2	(1)	$L = 4.7$ m	(2)
$\mu = 5.5 \times 10^{-4}$ kg/m sec		$r = 1.78 \times 10^{-1}$ m	(2)
$\rho_\infty = 10^3$ kg/m^3		$Q(o) = 5.5 \times 10^2$ w	(2)
$c_p = 4.184 \times 10^3$ J/kg °K		$\theta'(o) = \frac{-1}{\pi}$	

Before proceeding with the mass transfer analysis we estimate next the magnitude of the vertical slip velocity component u for the above data. From (7.3.32) and (7.3.34) the free convection velocity component along the plate surface is given by

$$u = \left(\frac{\alpha_e Ra}{L}\right)$$

$$= \rho_\infty \beta g \, (T_w - T_\infty) \, \frac{k}{\mu} \qquad (7.3.39)$$

For a temperature difference of 100°C one computes u = 0.34 m/yr. This is competitive with commonly assumed groundwater flows of 0.1 to 1 m/yr which are used in the far-field calculations. Fig. (7.3.4) gives the magnitude of the free convection velocity as a function of time.

The local mass transfer rate from the plate is now computed from the solution of (7.3.27) subject to the boundary conditions (7.3.29) and

(7.3.30) for $c(\eta)$. The desired solution is

$$c(\eta) = 1 - \frac{\int_0^{\eta} \exp\left(-\frac{\Lambda}{2}\int_0^{\eta'} f(s)ds\right) d\eta'}{\int_0^{\infty} \exp\left(-\frac{\Lambda}{2}\int_0^{\eta'} f(s)ds\right) d\eta'} \tag{7.3.40}$$

so that the surface mass flux is

$$\vec{j} = -D_f\varepsilon \frac{\partial\hat{c}(y)}{\partial y}\bigg|_{y=0} = -D_f c_s \varepsilon \frac{\partial\eta}{\partial y} \frac{dc(\eta)}{d\eta}\bigg|_{\eta=0} \tag{7.3.41}$$

where ε is the porosity of the medium.

In view of (7.3.20) and (7.3.40).

$$\vec{j} = D_f\varepsilon c_s \left(\frac{Ra}{xL}\right)^{1/2} \frac{1}{\int_0^{\infty} \exp\left(-\frac{\Lambda}{2}\int_0^{\eta'} f(s)ds\right) d\eta'} \tag{7.3.42}$$

The definite integral

$$I(\Lambda) = \int_0^{\infty} \exp\left(-\frac{\Lambda}{2}\int_0^{\eta'} f(s)ds\right) d\eta' \tag{7.3.43}$$

involves the function $f(\eta)$, i.e., the solution of (7.3.33) and the Lewis number parameter (7.3.28).

$$\Lambda = \frac{\alpha_e}{\varepsilon D_f} \tag{7.3.44}$$

We shall discuss the complete evaluation of $I(\Lambda)$ for arbitrary Λ values at a later time, but develop now the asymptotic form of this integral for large values of Λ which may arise due to small values of the diffusion coefficient in porous media. In this case the concentration boundary layer is very thin compared with the thermal layer, as sketched in

Fig. (7.3.2). One can then approximate $f(\eta)$ by the first term of its power series expansion, i.e.,

$$f(\eta) = \eta + O(\eta^2) \tag{7.3.45}$$

If one neglects terms of $O(\eta^2)$,

$$I(\Lambda) \simeq \int_0^\infty e^{-\frac{\Lambda}{4}\eta^2} d\eta \ ,$$

$$= \sqrt{\frac{\pi}{\Lambda}} \ , \text{ for } \Lambda \text{ large} \tag{7.3.46}$$

Thus (7.3.42) yields,

$$\vec{j} = D_f \varepsilon c_s \left(\frac{Ra}{xL}\frac{\Lambda}{\pi}\right)^{1/2} , \text{ for } \Lambda \text{ large} \tag{7.3.47}$$

If one expresses Ra by (7.3.24) one has in terms of the physical parameters

$$\vec{j} = D_f \varepsilon c_s \left(\frac{1}{\pi}\frac{k}{\mu}\frac{\rho_\infty g}{\varepsilon D_f} \ \beta(T_w - T_\infty) \ \frac{1}{x}\right)^{1/2} = \frac{D_f \varepsilon c_s}{\ell} \tag{7.3.48}$$

where the length ℓ is given by

$$\ell = \left(\frac{1}{\pi}\frac{k}{\mu}\frac{\rho_\infty g}{\varepsilon D_f} \ \beta(T_w - T_\infty) \ \frac{1}{x}\right)^{1/2} \tag{7.3.49}$$

The average rate of mass transfer per unit length of plate for a plate of length L is readily computed from equation (7.3.48).

References

1. M. J. Lippmann, et al, "Modeling Subsidence Due to Geothermal Fluid Production", ASCE Fall Convention and Exhibit, San Francisco, Calif., Oct. 1977.

2. G. E. Raines, et al, "Development of Reference Conditions for Geologic Repositories for Nuclear Waste in the USA", Material Research Society, Nov. 1980.

7.4 A Model for Leach and Diffusion Rates From Glass Bodies

Paul L. Chambré

Experimental evidence indicates that when a typical silica base glass is brought into contact with water two physical processes occur in the dissolution of the glass. One of these is an alkali ion transfer, such as for example, Na^+, across the glass-water interface which gives rise to a gel-like SiO_2 transition layer. The second process appears to be the corrosion of this layer resulting in the dissolution of the glass matrix. A number of theories have been proposed, differing in various detailed mechanistic ways, which attempt to explain qualitatively or quantitatively various aspects of experimental observations on glass dissolution. In the following, we develop a model which is based on only the two, generally accepted, experimental pieces of evidence. These are

i) The movement of the glass interface with a (regression) velocity v, which is initiated by

ii) The diffusion of an alkali ion across the glass-water interface.

Three simplifying assumptions will be made. The interface velocity is assumed to be constant in time. The support for this assumption is indirect. It will be shown in the following analysis that a constant regression velocity leads to the often observed experimental result (M4) that the fractional release of a particular nuclide f(t) follows the empirical formula

$$f(t) = c_1\sqrt{t} + c_2 t \qquad (7.4.1)$$

where c_1 and c_2 are constants. On the other hand there exists also some experimental evidence yielding a different time dependence for f(t)(M3). This has been interpreted by investigators to be due to a corrosion layer which is developing on the glass surface, gradually increasing the resistance

of mass transfer from the interface. In the analysis, the case of accretion, is also included and the f(t) function deduced. The remaining assumptions concern the nature of the diffusion mechanism of the alkali ion. We shall assume a constant diffusion coefficient for the ion in the bulk glass and the gel-like surface transition layer despite the fact that the diffusion coefficient is considerably larger in this layer (H2). Furthermore, we shall ignore the effect of the negative surface potential on the ion transfer. Such a potential is generated when glass is immersed in water. The effects of the latter two assumptions require future study.

The Analysis

The analysis applies to a body of planar, cylindrical and spherical shape. We take as the governing equation

$$\frac{\partial \bar{c}}{\partial t} = D \left\{ \frac{\partial^2 \bar{c}}{\partial r^2} + \frac{m}{r} \frac{\partial \bar{c}}{\partial r} \right\} - \lambda \bar{c} \qquad (7.4.2)$$

Here $\bar{c}(r,t)$ is the concentration of the nuclide, D the diffusion coefficient and λ the radioactive decay constant if the nuclide is radioactive. m describes the geometric character of the diffusion field. For the case of the sphere m = 2, for the cylinder (of infinite length) m = 1 and for the slab m = 0. r is the position variable within the region of interest, t the time and R(t) the position of the movable boundary which will be prescribed below. The initial nuclide concentration is given as c(r) so that

$$\bar{c}(r,0) = c(r), \quad 0 < r < R(0) \equiv a. \qquad (7.4.3)$$

At the surface of the solid

$$\bar{c} \left\{ R\ (t), t \right\} = 0, \quad t > 0 \qquad (7.4.4)$$

but if the surface concentration is instead $\bar{c}_s \neq 0$, it is always possible

to reduce this to the condition given by eq.(7.4.4) by taking the reference datum for the concentration at $\bar{c}_s$, provided $\lambda = 0$. In addition to the above conditions, one prescribes in case of the sphere and the cylinder that $\bar{c}\,(0,t)$ is bounded and in the case of the slab of thickness $2R(t)$ that $\partial\bar{c}\,(0,t)/\partial r$ vanishes for all times.

The equation for the moving boundary $R(t)$ is based on the simple hypothesis that

$$R(t) = a - vt, \quad o \leqslant t \leqslant {}^{a}/\,v \tag{7.4.5}$$

where a is the initial position and v the surface regression velocity. A regressive surface at time $T_L = {}^{a}/v$ the finite sized body has completely dissolved. This limits the time span for the solution. If there is accretion, we take v negative in the expression for $R(t)$ and consider $t \geqslant 0$. The equations(7.4.2) to (7.4.5) completely define the model.

The solution for the different geometric configurations (fig. 7.4.1a) is carried out below. It turns out that the solutions for the sphere, cylinder and slab are very similar. The case of the sphere is treated in detail, then the changes which need to be made in case of the slab are indicated and the final solution is given. These results are exact and are valid for any range of the parameters entering the problem. The cylinder is analyzed by an approximation method which is valid for the large values of the parameter (va/D) usually encountered in practice. By forming the product of the solutions for slabs of different or identical widths one obtains at once the solution to the case of a parallelopiped or cube, respectively. Similarly multiplication of the slab and (infinite) cylinder solutions yields the solution for a cylinder of finite length (fig. 7.4.1b). These results are consequences of some well known theorems and are valid for a time span in which the smallest initial dimension of the body has been reduced to naught by the leaching process.

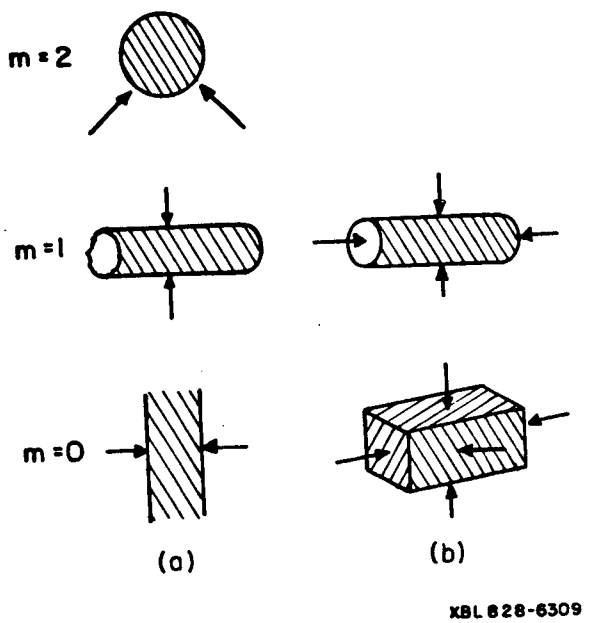

Fig. 7.4.1. Geometries of problems considered (arrows indicate direction of surface regression).

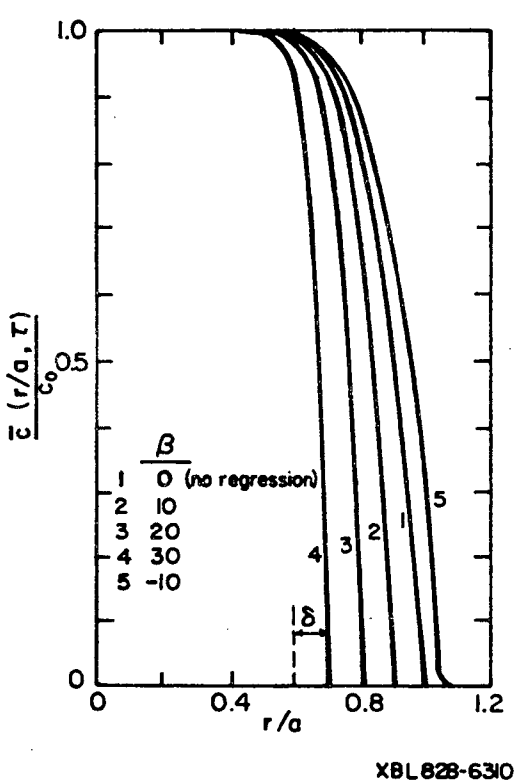

Fig. 7.4.2. Spatial distribution of the concentration inside sphere r = 0.01 for various rates of surface regression (λ=0).

The Sphere

Let

$$c(r,t) = \exp(\lambda t) r\bar{c}_{sp}(r,t) \tag{7.4.6}$$

then eqs. (7.4.2) to (7.4.5) reduce with m = 2 to

$$\frac{\partial c}{\partial t} = D\frac{\partial^2 c}{\partial r^2}, \quad 0 \leqslant r < a - vt, \quad 0 < t < a/|v| \tag{7.4.7}$$

$$c(r,0) = rc(r) \equiv g(r), \quad 0 \leqslant r \leqslant a, \tag{7.4.8}$$

$$c(a - vt,t) = 0 \quad 0 \leqslant t \leqslant a/|v| \tag{7.4.9}$$

and on account of the boundedness condition on $\bar{c}$ (0,t),

$$c(0,t) = 0, \quad 0 < t < a/|v| \tag{7.4.10}$$

Now the Kelvin function,

$$\frac{1}{2(\pi Dt)^{1/2}} \exp\left(-\frac{r^2}{4Dt}\right),$$

is a particular solution to eq. (7.4.7). By the super-position principle and the method of images one can construct a more general solution to eq. (7.4.7) which satisfies conditions (7.4.8) and (7.4.10) as a detailed verification shows.

This solution has the form,

$$c(r,t) = \frac{1}{2(\pi Dt)^{1/2}} \left\{ \int_0^a g(s)\, S(r,t;s)\, ds + \int_a^\infty h(s) S(r,t;s) ds \right\}, \tag{7.4.11}$$

$$0 \leqslant r \leqslant a - vt, \quad 0 \leqslant t \leqslant a/|v|$$

where the source function

$$S(r,t;s) = \exp\left[-\frac{(r-s)^2}{4Dt}\right] - \exp\left[-\frac{(r+s)^2}{4Dt}\right] \quad . \tag{7.4.12}$$

In eq. (7.4.11), g(s) is the initial concentration distribution and h(s) is an as yet unknown source density function which is determined by imposing the last remaining condition on the moving boundary, i.e., eq. (7.4.9),

$$\int_0^a g(s)S(a-vt,t;s)\,ds + \int_a^\infty h(s)S(a-vt,t;s)\,ds = 0. \tag{7.4.13}$$

Now the functions g(s) and h(s) are partly at our disposal. Since g(s) is prescribed only for $0 < s < a$, we analytically continue it in the following manner

$$g(s) = \begin{cases} 0, & |s| > a \\ -g(-s), & |s| < a\ . \end{cases} \tag{7.4.14}$$

Similarly h(s), which must be determined according to the solution (7.4.11) and the condition (7.4.13) in the span $a < s < \infty$, is chosen in the remaining part of the range as

$$h(s) = \begin{cases} h(s), & s > a \\ 0, & |s| < a \\ \text{arbitrary}, & s < -a. \end{cases} \tag{7.4.15}$$

With this choice one can now combine both integrals in eq. (7.4.13) by elementary transformations resulting in integrals with the same integration limits, i.e.,

$$\int_0^\infty \{h(s+a)\exp\left(-\frac{vs}{D}\right) - h(s-a) - g(s-a)\}\,.\exp\left(-\frac{s^2}{4Dt}\right)ds = 0. \tag{7.4.16}$$

The satisfaction of this condition requires that h(s) must obey the ordinary difference equation,

$$h(s+a)\exp(-vs/D) - h(s-a) = g(s-a). \tag{7.4.17}$$

The solution to this equation can be constructed in successive s spans of width 2a, utilizing the properties of the initial distribution g(s) and the continuation properties of h(s) with the result

$$h(s) = g(s-2na)\exp\left[nv(s-na)/D\right]$$

$$(2n-1)a < s < (2n+1)a, \quad n = 1,2,\ldots \tag{7.4.18}$$

Having found the unknown source distribution h(s), c(r,t) given by eq. (7.4.11) can be shown to satisfy all the conditions of the problem. There results, on returning to the original variables, after some minor simplifications

$$\bar{c}_{sp}(r,t) = \frac{\exp(-\lambda t)}{2r(\pi Dt)^{1/2}}\left\{\int_{-a}^{a} sc(s)\exp -\left[\frac{(r-s)^2}{4Dt}\right] ds + \right.$$

$$\left. + \sum_{n=1}^{\infty}\int_{-a}^{a} sc(s)\exp\left[nv(s+na)/D\right] S(r,t;s+2na)\, ds\right\},$$

$$0 \leqslant r \leqslant a-vt, \quad 0 \leqslant t \leqslant a/|v| \tag{7.4.19}$$

For bounded c(s), the series can be shown to converge for the indicated t range, i.e., for all times for which sphere material remains. It should be noted that, in view of eqs. (7.4.8) and (7.4.14), the initial distribution c(s) must be an even function about s = 0.

A case of practical interest is the one where the initial concentration is uniform throughout the sphere, i.e., $c(r) = c_0$ for $0 \leqslant r \leqslant a$. The

integration in eq. (7.4.19) then yields the following explicit result for the concentration in the interior of the sphere,

$$\hat{c}_{sp}(\tfrac{r}{a},\tau) = \frac{\bar{c}_{sp}(\frac{r}{a},\tau)}{c_o} = \frac{\exp\{(-\lambda a^2/D)\tau\}}{2(r/a)} \cdot$$

$$\cdot\{2(r/a) - (\mathrm{erfc}\ \varepsilon_1 - \mathrm{erfc}\ \varepsilon_2) - 2\tau^{1/2}\ (\mathrm{ierfc}\ \varepsilon_1 - \mathrm{ierfc}\ \varepsilon_2) -$$

$$- \sum_{n=1}^{\infty} \Big[(\mathrm{erfc}\ \theta_{21} + \mathrm{erfc}\ \theta_{11})\ \exp\ (-n\beta\delta_1) -$$

$$-(\mathrm{erfc}\ \theta_{22} + \mathrm{erfc}\ \theta_{12})\ \exp\ (-n\beta\delta_2) + \tag{7.4.20}$$

$$+ 2\tau^{1/2}\ (\mathrm{ierfc}\ \theta_{21} - \mathrm{ierfc}\ \theta_{11})\ \exp\ (-n\beta\delta_1) -$$

$$- 2\tau^{1/2}\ (\mathrm{ierfc}\ \theta_{22} - \mathrm{ierfc}\ \theta_{12})\ \exp\ (-n\beta\delta_2)\} ,$$

where

$$\theta_{ij} \quad \frac{\{2n(1-\beta\tau) + (-1)^i + (-1)^j\ (r/a)\}}{\left(2\tau^{1/2}\right)}$$

$$\delta_i \equiv n(1-\beta\tau) + (-1)^i(r/a), \tag{7.4.21}$$

$$\varepsilon_i \equiv \frac{\{1 + (-1)^i(r/a)\}}{\left(2\tau^{1/2}\right)} ,$$

and $\tau \equiv Dt/a^2$; $\beta \equiv va/D$, the interface Peclet number. (7.4.22)

erfc (z) and i^merfc (z) denote, respectively, the complementary error function and the m repeated integral error function which are tabulated in[4].

For $\beta = 0$, this reduces to

$$\frac{\bar{c}_{sp}(\frac{r}{a},\tau)}{c_o} = e^{-\lambda\frac{a^2}{D}\tau}\left\{1 - \frac{a}{r}\sum_{n=o}^{\infty}\left[\text{erfc}\,\frac{(2n+1)-r/a}{2\tau^{1/2}} - \right.\right. \tag{7.4.22a}$$

$$\left.\left. - \text{erfc}\,\frac{(2n+1) + r/a}{2\tau^{1/2}}\right]\right\}$$

The spatial distribution of the nuclide concentration given by eq. (7.4.20) is shown in fig. (7.4.2) for a specific value of the dimensionless time ($\tau = 0.01$) and for different values of the dimensionless regression parameter β. One observes as β increases that the regression of the interface steepens the concentration gradient compared to a stationary interface ($\beta = 0$). Fig. (7.4.2) also shows the effects of accretion. In contrast to the previous case the concentration profile is S-shaped and the surface mass flux shows a marked decrease which indicates a resistance to mass transfer.

A quantity of primary interest to the experimentalist is the fractional release of the radionuclide due to the combined effects of diffusion and interface movement. This may be obtained by integrating the concentration at any time t over the volume of the sphere, dividing the result by the initial amount of diffusant present and subtracting this quotient from unity. Thus for the case of an initially uniform concentration,

$$f(\tau) = 1 - Q(\tau)/Q_o, \tag{7.4.23}$$

where $Q(\tau) = \int_0^{(1-\beta\tau)a} 4\pi r^2 \bar{c}_{sp}(r/a,\tau)\, dr,$

$$Q_o = \frac{4}{3}\pi a^3 c_o\ . \tag{7.4.24}$$

$f(\tau)$ has been evaluated numerically with help of eq. (7.4.20) for $\lambda = 0$.

Fig.(7.4.3) shows the numerical results of the evaluation of eq.(7.4.23) for a number of regression Peclet numbers β and for a limited range of $0 < \tau < 2\times10^{-3}$. One observes that the fractional release is initially a linear function of $\tau^{1/2}$ and then it becomes quadratic in $\tau^{1/2}$. This is exactly the behavior observed in many laboratory leaching experiments as already stated in eq. (7.4.1). More extensive numerical evidence will be given in Section (7.6). To pressage this result, we will show here that eq. (7.4.23) is closely approximated by

$$f(t) = 6\left(\frac{Dt}{\pi a^2}\right)^{1/2} + \frac{3}{2}\left(\frac{vt}{a}\right) 0 \leqslant t \leqslant t^+ \leqslant 0.4T_L \qquad (7.4.25)$$

for both regression (v>o) and accretion (v<o).

The Slab

The system of eqs. (7.4.7) to (7.4.9) describes the diffusion process in a slab of half width (a-vt), with an initial concentration distribution $g(r) = c(r)$, in absence of radioactive decay. If the solid is exposed to regression over both faces, with the center of the slab located at $r = 0$, the boundary condition is replaced by the symmetry condition

$$\frac{\partial \bar{c}_{sL}(o,t)}{\partial r} = 0, \quad 0 \leqslant t \leqslant a/|v| \qquad (7.4.26)$$

In order to satisfy this relation, one chooses as the source function

$$S(r,t;s) = \exp\left[-\frac{(r-s)^2}{4Dt}\right] + \exp\left[-\frac{(r+s)^2}{4Dt}\right], \qquad (7.4.27)$$

instead of eq. (7.4.12). The analysis proceeds then along the same lines as

for the sphere. However, the function g(s) must now be defined as follows:

$$g(s) = \begin{cases} 0, & |s| > a \\ g(-s), & |s| < a. \end{cases} \tag{7.4.28}$$

The final result is

$$\bar{c}_{sL}(r,t) = \frac{\exp(-\lambda t)}{2(\pi Dt)^{1/2}} \int_{-a}^{a} c(s) \exp\left[-\frac{(r-s)^2}{4Dt}\right] ds$$

$$+ \sum_{n=1}^{\infty} (-1)^n \int_{-a}^{a} c(s) \exp\left[nv(s+na)/D\right] . S(r,t;s + 2na)\, ds\} \tag{7.4.29}$$

$$0 \leqslant |r| \leqslant (a-vt), \quad 0 \leqslant t \leqslant a/_{|v|}$$

For a bounded even function c(s) this result can be shown to converge to the solution of our problem. Again if the initial concentration is uniform throughout the slab one obtains with the shorthand notations introduced in eqs. (7.4.21) and (7.4.22) the following result

$$\hat{c}(\tfrac{r}{a},\tau) = \bar{c}_{sL}(r/a,\tau)/c_o = \tfrac{1}{2} \exp(-\lambda a^2\tau/D) \{(\mathrm{erf}\ \varepsilon_2 + \mathrm{erf}\ \varepsilon_1)$$

$$+ \sum_{n=1}^{\infty} (-1)^n \left[(\mathrm{erf}\ \theta_{21} - \mathrm{erf}\ \theta_{12}) \exp(-n\beta\delta_1) + \right. \tag{7.4.30}$$

$$\left. + (\mathrm{erf}\ \theta_{22} - \mathrm{erf}\ \theta_{12}) \exp(-n\beta\delta_2)\right]\} .$$

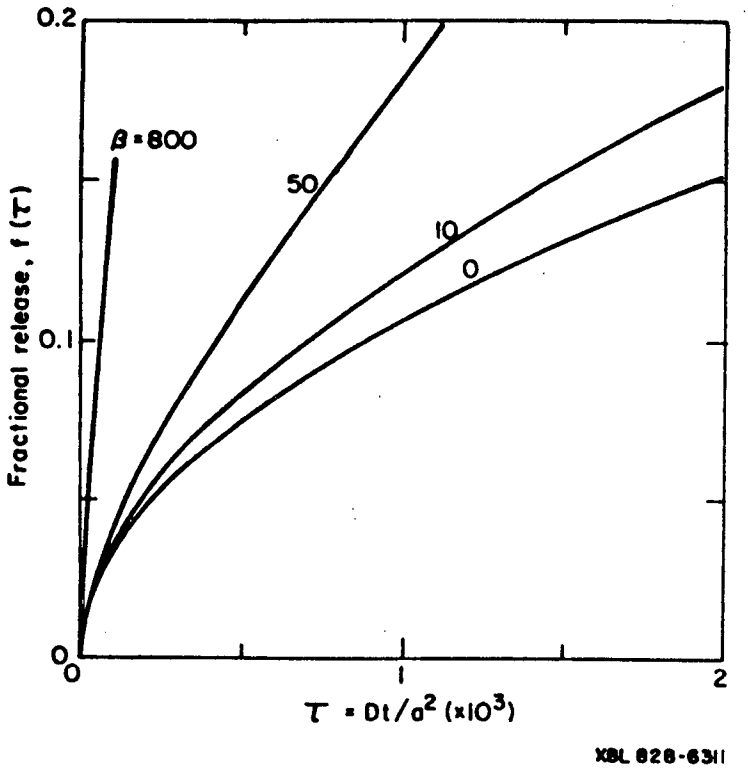

Fig. 7.4.3. Variation of fractional release from sphere (radius = a) with dimensionless time τ for different dimensionless regression speed.

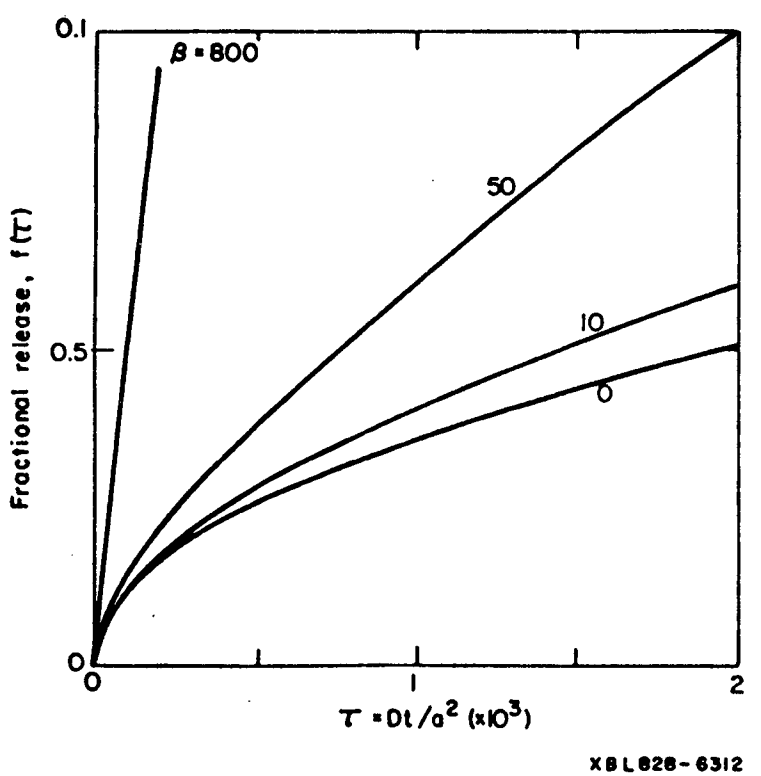

Fig. 7.4.4. Variation of fractional release from slab (initial width 2a) with dimensionless time τ for different dimensionless glass-water interface regression speed β.

For $\beta = 0$, this reduces to

$$\frac{\bar{c}_{sL}\left(\frac{r}{a},\tau\right)}{c_o} = \exp\left(\frac{-\lambda a^2}{D}\tau\right)\left\{1 - \sum_{n=0}^{\infty} (-1)^n \left[\operatorname{erfc} \frac{(2n+1) - \frac{r}{a}}{2\tau^{1/2}} + \operatorname{erfc} \frac{(2n+1) + \frac{r}{a}}{2\tau^{1/2}}\right]\right\} \tag{7.4.30a}$$

The total fractional release is given by eq.(7.4.23) with

$$Q(\tau) = 2 \int_0^{(1-\beta\tau)a} \bar{c}_{sL}(r/a,\tau)\, dr \tag{7.4.31}$$

$$Q_o = 2ac_o.$$

Performing the integration one obtains

$$f(\tau) = \beta\tau + \tau^{1/2}\left[\operatorname{ierfc}\left(\frac{\beta\tau^{1/2}}{2}\right) - \operatorname{ierfc}\left(\frac{2-\beta\tau}{2\tau^{1/2}}\right)\right] +$$

$$\sum_{n=1}^{\infty} \frac{(-1)^{n-1}}{2n\beta}\left\{\exp\left[n\beta(n-1)\right].\ (\operatorname{erf}\mu_{11} - \operatorname{erf}\mu_{12}) + \right. \tag{7.4.32}$$

$$\left. + \exp\left[n\beta(n+1)\right].\ (\operatorname{erf}\mu_{22} - \operatorname{erf}\mu_{21}) + \Omega_2(n) - \Omega_1(n)\right\}$$

where

$$\mu_{ij} \equiv \frac{2n + (-1)^i + (-1)^j\ (1-\beta\tau)}{2\tau^{1/2}}$$

$$\Omega_i(n) \equiv \exp\left\{-n\beta(1-\beta\tau)\left[n+(-1)^i\right]\right\}.\ \sum_{j=1}^{2} (-1)^j \operatorname{erfc}\left[\frac{(1-\beta\tau)\left[2n+(-1)^i\right]+(-1)^j}{2\tau^{1/2}}\right] \tag{7.4.33}$$

For $\beta=0$ this reduces to

$$f(\tau) = 2\tau^{1/2}\left[\frac{1}{\sqrt{\pi}} + 2\sum_{n=1}^{\infty} (-1)^n \operatorname{ierfc} \frac{n}{\tau^{1/2}}\right] \tag{7.4.34}$$

A numerical evaluation for $\lambda = 0$ is shown in Fig. 7.4.4 for some ranges in β and τ.

In section (7.6) we will give numerical evidence that eq. (7.4.32) can be closely approximated by

$$f(t) = 2\left(\frac{Dt}{\pi a^2}\right)^{1/2} + \frac{1}{2}\left(\frac{va}{D}\right)\frac{Dt}{a^2} \qquad (7.4.35)$$

The conclusions for the slab are thus quite comparable to those obtained for a sphere.

The Cylinder

In the case of the cylinder one can proceed in the same manner as above. Instead of the source function eq. (7.4.12) one utilizes the fundamental solution.

$$S(r,t;s) = \{s/(2Dt)\} \exp\left[-(r^2+s^2)/(4Dt)\right] . I_0\{rs/(2Dt)\} \qquad (7.4.36)$$

where $I_0(z)$ is the modified Bessel function of the first kind, zero order. However, this case leads to a rather complicated integral equation for the unknown source density $h(s)$ and for this reason the following approximate solution is recommended.

For large values of the parameter $\beta = va/D$ (about 200 or more) the interface regresses at such a rapid rate compared to temporal changes in the diffusion pattern that the latter is affected primarily in a very thin boundary layer of thickness δ close to the surface as the calculations show, see Fig. 2. Hence, in order to describe the rate of the diffusion of the ion through the interface, it is important to take

account of the steep concentration gradient close to the boundary. For this reason one introduces the transformation

$$c(r,t) = \exp(\lambda t) r^{1/2}\, \bar{c}_{cy}(r,t) \tag{7.4.37}$$

into eq.(7.4.2), where now m=1. There results

$$\frac{\partial c}{\partial t} = D\left(\frac{\partial^2 c}{\partial r^2} + \frac{c}{4r^2}\right) \tag{7.4.38}$$

Now close to the boundary where the diffusion effects are most prominent the two terms on the right hand side are of entirely different order of magnitudes, $\partial^2 c/\partial r^2 = O(1/\delta^2)$ and $c/4r^2 = O(1/r^2)$. Since δ is very small compared to r, the second term is dropped in favor of the first and there result the eqs. (7.4.6) to (7.4.10) with the initial distribution $g(r) = r^{1/2}\, c(r)$. Hence the approximate solution to the cylinder problem can be obtained by simply replacing the term sc(s) by $s^{1/2}c(s)$ on the right hand side of eq. (7.4.19). It is worthwhile to point out that if one merely drops the term $(1/r)\partial\bar{c}/\partial r$ in eq. (7.4.1) in favor of $\partial^2\bar{c}/\partial r^2$, one obtains a less accurate approximation to the solution than the one given above.

The exact analysis of the cylinder is planned for the future.

7.5. External Mass Loss Rate and Leach Time for a Glass Cylinder

7.5.1. Introduction

Two mathematical models for the rate of mass transport from a waste cylinder surrounded by groundwater in an infinite porous medium have been developed in sections (7.1) and (7.2). In the first model, the cylinder is approximated by a prolate spheroid and the rate of mass transfer of a species dissolved from the waste solid is assumed to be governed by the rate of molecular diffusion of the dissolved species into stagnant groundwater. This theory is illustrated by analyzing the steady-state mass transfer rate from the cylinder with the dissolved species having a constant concentration on the cylinder surface. The maximum value of this surface concentration is the solubility of the dissolved species in groundwater, and this saturation concentration at the surface is assumed in the illustration.

In the second model, the mass transfer of the dissolved species from the waste surface is due to both molecular diffusion and forced convection by the groundwater moving in D'Arcy's flow in the surrounding porous medium. Again, the theory is applied to the steady-state mass transfer with a constant saturation concentration of the diffusing specie on the cylinder surface. The waste cylinder is idealized as a cylinder of infinite length, and the groundwater is assumed to flow perpendicular to the cylinder axis. This allows one to obtain the rate of mass transfer from a unit length of the cylinder. Numerical calculations are made for a cylinder with the same radius as that of a cylindrical waste form with end effects accounted for.

Calculations are made for the rate of dissolution of silica, in amorphous form, from a borosilicate glass cylinder, and for the rate of

dissolution of low-solubility radioelements in the borosilicate glass, using the two models described above.

In Section 7.5.2, the steady-state mass transfer rate, mass transfer rate per unit length, and average surface mass flux of a species from a prolate spheroid and slender cylinder which is defined as a cylinder with a ratio of height to radius of 10 or greater are given. In Section 7.5.3, the leach times of the prolate spheroid and slender cylinder are derived, subject to the assumptions that the waste form consists of a single species and that the ratio of height to radius of the cylindrical waste-form is constant during the leaching process. In Section 7.5.4, the governing equations for obtaining the dimensions of the prolate spheroid approximating a cylindrical waste form are given. In Section 7.5.5 we present the dimensions of the cylindrical waste-form, calculated dimensions of the equivalent prolate spheroid, diffusivity of a species in a water-saturated porous medium, solubility of amorphous silica in water, and borosilicate glass density. In Section 7.5.6, a comparison between the dissolution rate and the leach time of different waste forms consisting only of amorphous silica are made. These sections deal primarily with the mass transport by molecular diffusion.

In Section 7.5.7, the steady-state mass transfer rate by molecular diffusion and convection are given. The mass transfer rate for a finite cylinder is derived subject to the assumption that the surface mass flux from the ends of the cylinder has the same value as the surface mass flux of the infinitely long cylinder. In Section 7.5.8 the leach time for the cylinder is derived. Section 7.5.9 contains data used for numerical evaluation of mass loss rate and leach time. In Section 7.5.10 a comparison is made between surface mass flux for diffusion and for the diffusion-convection model.

In Section 7.5.11, the diffusion and diffusion-convection models are applied to a silica-base glass cylinder containing low-solubility radioelements. Section 7.5.12 is the conclusion of the above analyses.

7.5.2. Dissolution Rate Due to Molecular Diffusion

At steady state the mass transfer rate per unit area (surface mass flux) is nonuniform for the prolate spheroid and depends on the position on the surface. The mass flux has a maximum at the poles and a minimum at the equatorial plane (see Fig. 7.1.1 in Section 7.1). The total rate of dissolution $\dot{m}_{ps}$ of a given species of effective surface concentration N_s is obtained by integration of the surface mass flux over the surface area of the prolate spheroid, and is given by (see Section 7.1)

$$\dot{m}_{ps} = \frac{4\pi\varepsilon\, D_f\, N_s\, f}{\log[\coth(\frac{\alpha_s}{2})]} \tag{7.5.1}$$

where:

$\dot{m}_{ps}$ = the total mass loss rate of the prolate spheroid, g/sec

D_f = molecular diffusivity of diffusing specie in water, cm^2/sec

ε = porosity

$N_s = c_s - c_\infty$ = effective surface concentration, g/cm^3

c_s = solubility limit in groundwater, g/cm^3

c_∞ = concentration in groundwater far from waste surface, g/cm^3

α_s = surface shape factor of the prolate spheroid defined in Section 7.1 by Eq.(7.1.4)

f = focal distance of the prolate spheroid, cm

For a slender cylinder, i.e., $L \geqslant 10r$, Eq.(7.5.1) simplifies to

$$\dot{m}_{sc} = \frac{2\pi\varepsilon\, D_f\, N_s\, L}{\log(\frac{L}{r})} \tag{7.5.2}$$

where:

$\dot{m}_{sc}$ = dissolution rate for a slender cylinder, g/sec

L = cylinder length, cm

r = cylinder radius, cm

From Eq.(7.5.1) the dissolution rate per unit length and the average dissolution rate per unit surface area of the prolate spheroid are given by Eqs.(7.5.3) and (7.5.4), respectively

$$\dot{m}^{\ell}_{ps} = \frac{2\pi\varepsilon\ D_f\ N_s}{\cosh(\alpha_s)\log[\coth(\frac{\alpha_s}{2})]} \tag{7.5.3}$$

$$\bar{j}_{ps} = \frac{2\varepsilon\ D_f\ N_s\ f}{b(b+\frac{a}{e}\sin^{-1}e)\log[\coth(\frac{\alpha_s}{2})]} \tag{7.5.4}$$

where:

$\dot{m}^{\ell}_{ps}$ = mass loss rate per unit length of the prolate spheroid, g/cm sec

$\bar{j}_{ps}$ = average surface mass flux of the prolate spheroid, g/cm^2 sec

e = f/a

a = semi-major axis of the prolate spheroid, cm

b = semi-minor axis of the prolate spheroid, cm

7.5.3. Leach Time Derivation

The leach time T is defined as the time interval between the beginning of dissolution and the completion of dissolution of the waste form. Assuming here a waste form consisting of a single species, the time-dependent waste form volume V(t) is given by

$$\frac{d}{dt}(\rho V(t)) = -\dot{m}(t) \tag{7.5.5}$$

where:

ρ = waste form density, g/cm^3

$V(t)$ = waste form volume at time t, cm^3

$\dot{m}(t)$ = mass-loss rate at time t, g/sec given by Eqs.(7.5.1) and (7.5.2).

The initial condition is $V(0) = V_0$, where V_0 is the initial volume of the waste form.

Here we assume that at any time t the dissolution rate can be approximated by the steady-state solutions, Eqs.(7.5.1) and (7.5.2), so that Eq.(7.5.5) can be solved for V(t). From definition of the leach time T we have that

$$V(T) = 0 \tag{7.5.6}$$

and leach time is obtained by solving Eq.(7.5.6) for T.

We have for the slender cylinder

$$V_{sc}(t) = \pi r^2(t)\, L(t) \tag{7.5.7}$$

and from (7.5.2)

$$\dot{m}_{sc} = \frac{2\pi\varepsilon\, D_f\, N_s\, L(t)}{\log\left[\frac{L(t)}{r(t)}\right]} \tag{7.5.8}$$

with the initial condition (I.C.) that

$r(0) = r_0$ initial radius, cm

$L(0) = L_0$ initial height, cm

Substituting Eqs.(7.5.7) and (7.5.8) into (7.5.5) yields

$$\frac{d}{dt}\left[\rho\, \pi\, r^2(t)\, L(t)\right] = -\frac{2\pi\varepsilon\, D_f\, N_s\, L(t)}{\log\left[\frac{L(t)}{r(t)}\right]} \tag{7.5.9}$$

with I.C.

$$r(0) = r_o$$

$$L(0) = L_o$$

To solve Eq.(7.5.9), it is necessary to have another relation between L(t) and r(t). We assume that the ratio of height to radius remains constant during the leaching process, i.e.,

$$L(t) = L_o \frac{r(t)}{r_o} \tag{7.5.10}$$

Substituting Eq.(7.5.10) into Eq.(7.5. 9) and solving for r(t) results in

$$r(t) = r_o \left[1 - \frac{4 \varepsilon D_f N_s t}{3 r_o^2 \rho \log(\frac{L_o}{r_o})} \right]^{1/2} \tag{7.5.11}$$

From the definition of leach time we have from (7.5.6-7) that $r(T_{sc}) = 0$, so that

$$T_{sc} = \frac{3 \rho r_o^2 \log\left[\frac{L_o}{r_o}\right]}{4 \varepsilon D_f N_s} \tag{7.5.12}$$

where:

T_{sc} = leach time for the slender cylinder, sec

In deriving the leach time of the prolate spheroid it is assumed that the ratio of the minor axis to the major axis is constant during the leaching process, resulting in the following equation (see Appendix A for details):

$$T_{ps} = \frac{\rho b_o^2 \cosh(\alpha_s) \log\left[\coth(\frac{\alpha_s}{2})\right]}{2 \varepsilon D_f N_s} \tag{7.5.13}$$

where:

T_{ps} = leach time for the prolate spheroid, sec

b_o = initial semi-minor axis of the prolate spheroid, cm

7.5.4. Approximating a Cylinder by a Prolate Spheroid

We assume that the prolate spheroid has the same volume and surface area as the cylindrical waste form. Thus, equating their volumes,

$$4 \frac{\pi}{3} a b^2 = \pi r^2 L \qquad (7.5.14)$$

and equating their surface areas

$$2 \pi b(b+\frac{a}{e} \sin^{-1} e) = 2 \pi r(r+L) \qquad (7.5.15)$$

Solution of Eqs.(7.5.14) and (7.5.15) for a and b defines the desired prolate spheroid. As is seen from the above equations, a closed-form mathematical solution for a or b cannot be obtained, so a numerical analysis is required.

7.5.5. Parameters of the Problem

The following table shows the physical characteristics of the waste form used in the numerical calculations:

Table 7.5.1. Physical characteristics of waste forms (R1)

Canister dimensions		Commercial high level waste	Defense high level waste
Inner diameter,	cm	30.5	59.1
Length,	cm	2.4×10^2 a/	2.4×10^2 a/
Surface area,	cm^2	2.446×10^4	5.005×10^4
Volume,	cm^3	1.75×10^6	6.58×10^6
Ratio L/r		15.7	8.1

a/ Assumed that 80% of waste canister is filled with waste glass.

The dimensions of the commercial high level waste form are used in numerical evaluation of the slender cylinder mass loss rate and leach time, listed in Table 7.5.4.

Table 7.5.2 is obtained by approximating the waste forms by a prolate spheroid using Eqs.(7.5.14) and (7.5.15), with the aid of a (computer) program described in Appendix C.

Table 7.5.2. Physical dimensions of prolate spheroid approximating cylindrical waste forms.

Waste Forms	a, cm	b, cm	c, cm	e	α_s
Defense high-level waste	158	31.5	155	0.980	0.202
Commercial high-level waste	145	16.9	144	0.993	0.117

The molecular diffusion coefficient of most nuclides in water-saturated porous media is usually lower than that in the unconfined water. The diffusivity of most species in water is between 1 to 5×10^{-5} cm^2/sec (W2). The molecular diffusion coefficient of silicon dioxide and other species in water is taken to be 1×10^{-5} cm^2/sec.

Table 7.5.3 shows the solubility of two forms of silicon dioxide, i.e., α quartz and amorphous silica, in water at a pressure of 0.1013 MPa, pH of 7.0, and at different temperatures. The solubility of silicon dioxide as a function of pressure and temperature is given (W1) in Appendix B.

Table 7.5.3. Solubility limit of silicon dioxide in water

	Temperature, °C	
	25°C	100°C
Alpha quartz, g/cm^3	4×10^{-6}	5×10^{-5}
Amorphous silica, g/cm^3	1.2×10^{-4}	4.1×10^{-4}

A surface concentration of 1.2×10^{-4} g/cm^3 and a density of 2.8 g/cm^3 are chosen for a pure amorphous silica cylinder. This density corresponds to that of typical borosilicate glass (T1),(M3).

7.5.6. Numerical Results for Dissolution Rate and Leach Time for a Pure Amorphous Silica Cylinder

Table 7.5.4 shows the calculated dissolution rates and leach times, using Eqs.(7.5.1), (7.5.2), (7.5.12), and (7.5.13) with the aid of a computer program (Appendix C). A porosity of 0.01 and the solubility of amorphous silica from Table 7.5.3 were used. The concentration of silicon dioxide in the groundwater far from the waste form is assumed zero.

Table 7.5.4. Mass loss rate and leach time for a pure amorphous silica in stagnant water at 25° C and porosity of 0.01.

	Mass loss rate, g/day	Leach time, yr
Slender cylinder	5.6×10^{-4}	3.54×10^{6}
Commercial high level waste	6.6×10^{-4}	3.03×10^{6}
Defense high level waste	8.8×10^{-4}	8.58×10^{6}

All three waste forms yield similar results. There is reasonable agreement of mass loss rate and leach time between a prolate spheroid approximating the commercial high level waste form and the slender cylinder. Thus, Eqs.(7.5.2) and (7.5.12), derived for the mass loss rate and leach time of the slender cylinder respectively, can be used.

7.5.7. Dissolution Rate Due to Molecular Diffusion and Groundwater Motion

The mass loss rate per unit length of an infinite cylinder with groundwater flow normal to its axis is given by (see Section 7.2)

$$\dot{m}_{\infty}^{\ell} = \frac{8}{\sqrt{\pi}} D_f \, \varepsilon \, N_s \, (Pe)^{1/2} \text{ , valid for } Pe \geq 4 \qquad (7.5.16)$$

where:

$\dot{m}_{\infty}^{\ell}$ = mass loss rate per unit length of cylinder, g/cm sec

$Pe = Ur/D_f$, Peclet number

U = groundwater pore velocity, cm/sec

From Eq.(7.5.1), the mass loss rate per unit surface area of the cylinder is obtained

$$\bar{j}_c = \frac{8}{\pi^{3/2}} \varepsilon N_s \left(\frac{U D_f}{r}\right)^{1/2} \quad , Pe \geq 4 \qquad (7.5.17)$$

where:

$\bar{j}_c = \frac{\dot{m}^{\ell}_{\infty}}{2\pi r}$ = mass loss per unit surface area of the cylinder, g/cm^2 sec

From this, one obtains the dissolution rate for a cylinder of length L, subject to the assumption that the mass flux from the ends of the cylinder has the same value as the surface mass flux from the cylindrical surface. The result is

$$\dot{m}_c = \frac{8}{\sqrt{\pi}} D_f \varepsilon N_s (r+L) (Pe)^{1/2} \quad , Pe \geq 4 \qquad (7.5.18)$$

where $\dot{m}_c$ = dissolution rate from cylinder, g/sec

7.5.8. Leach Time for a Cylinder, Diffusion and Convection

As a result of dissolution, the radius decreases with time as does the Peclet number. The leach time T is defined as the time interval from the beginning of the steady-state dissolution of an infinitely long cylinder until the cylinder has completely dissolved. For simplicity it is assumed that Eq.(7.5.16) is also valid for Peclet numbers less than four. The following expression for the leach time is obtained (see Appendix A for derivation).

$$T_c = \frac{\pi^{3/2} \rho r_o^2}{6 \varepsilon D_f N_s Pe_o^{1/2}} \quad , Pe_o \equiv \frac{U r_o}{D_f} \qquad (7.5.19)$$

where:

T_c = leach time for the cylinder located in flowing groundwater, sec

r_o = initial radius of the cylinder, cm

7.5.9. Parameters of the Problem

Groundwater pore velocities of 10, 5, and 1 m/yr are assumed. The radius of the cylinder is 15.2 cm, which is the same as that of a commercial high level waste glass cylinder. The cylinder consists of silicon dioxide. The surface concentration of silicon dioxide is 1.2×10^{-4} g/cm^3 and the concentration of silicon dioxide in the groundwater far from the cylinder is assumed to be zero. The diffusivity of SiO_2 in groundwater is taken to be 1×10^{-5} cm^2/sec. The porosity of the medium is 0.01.

7.5.10. Numerical Results for Surface Mass Flux

In Table 7.5.5 are presented the calculated average surface mass fluxes for diffusion and convection in flowing groundwater (Eq. 7.5.17) and for diffusion in stagnant groundwater (Eq. 7.5.4), using the computer program described in Appendix C. A porosity of 0.01 is chosen.

Table 7.5.6 Average surface mass flux of silicon dioxide g/cm^2 day for the diffusion and diffusion-convection models, porosity = 0.01, $N_s = 1.2 \times 10^{-4}$ g/cm^3, $D_f = 1 \times 10^{-5}$ cm^2/sec, r = 15.2 cm, and L = 2.4 m.

	Groundwater pore velocity, m/yr			
	10	5	1	0[a]
Surface mass flux, g/cm^2 day	3.5×10^{-7}	2.5×10^{-7}	1.1×10^{-7}	2.7×10^{-8}

a/Molecular diffusion model, Eq.(7.5.4)

For the pure amorphous silica cylinder (r = 15.2 cm) emplaced in a medium with porosity of 0.01 and groundwater pore velocity of 10 m/yr, from Eq.(7.5.19), we obtain $T_c = 2.3 \times 10^5$ yr. The proper value may be less, if an accurate solution for Pe< 4 were available. Such an analysis is presently being completed. For example, from Eq.(A.29), we find that after 1.7×10^5 years the cylinder radius has decreased from the initial value of 15.2 cm to 1.2 cm when the Peclet number becomes four.

7.5.11. Solubility Limited Dissolution of Silica and Low-Solubility Radioelements in a Silica-Base Glass Cylinder

In the previous sections two mathematical models of dissolution from a cylinder with only one diffusing component were considered. In this section, a silica-base glass cylinder containing additional low solubility components, such as various radioelements, is considered.

The time-dependent fractional dissolution rate of component j is defined as

$$\dot{f}_j\ (t) = \dot{m}_j\ (t)/\ M_j\ (t) \qquad (7.5.20)$$

where:

$\dot{f}_j$ (t) = fractional dissolution of component j at time t, 1/sec

$\dot{m}_j$ (t) = dissolution rate of component j at time t given by Eq.(7.5.1) for molecular diffusion and Eq.(7.5.18) for the molecular diffusion-convection models, g/sec

M_j (t) = V_j (t) n_j (t) = mass of j at time t in glass, g

V_j (t) = volume of undissolved waste at time t, cm^3

n_j (t) = density of j in undissolved solid waste at time t, g/cm^3

Substituting the $\dot{m}_j$ (t) given by Eqs.(7.5.1) and (7.5.18) into (7.5.20) yields

$$\dot{f}_j(t) = \frac{N_{s,j}}{n_j(t)} \cdot \left\{ \begin{array}{ll} \dfrac{3\varepsilon\ D_f^{\,j}\ e}{b^2\ \log[\coth(\frac{\alpha_s}{2})]}, & \text{molecular diffusion} \\[2ex] \dfrac{8\varepsilon\ D_f^{\,j}\ (Pe^j)^{1/2}\ (1+\frac{r}{L})}{\pi^{3/2}\ r^2}, & \text{molecular diffusion-convection} \\ & Pe^j \equiv \dfrac{Ur}{D_f^j} \geq 4 \end{array} \right\}$$

$$, 0 \leq t \leq T$$

(7.5.21)

where:

$N_{s,j}$ = difference between the concentration of j in the groundwater on the waste surface and concentration of j in groundwater far from waste surface, g/cm^3

D_f^j = diffusion coefficient of specie j in groundwater, cm^2/sec

T = leach time given by Eq.(7.5.13) and Eq.(7.5.19), sec

In the above equation it is assumed that the ratio of the major axis to the minor axis of the prolate spheroid is constant during the leaching process. In Eq.(7.5.21) r and b are functions of time, with functional forms given by Eqs.(A.29) and (A.10), respectively.

To apply Eq.(7.5.21), it is assumed that the rate of bulk dissolution of the solid waste is controlled by dissolution of the silica matrix, i.e., the preferential release of a waste-component by diffusion in solid is neglected. As the silica matrix dissolves, all the components in the silica matrix are released congruently from the solid but are not necessarily dissolved. If the solubility of an individual waste component is so low that its fractional dissolution rate is less than that of the waste matrix, then precipitates of the low-solubility component will form. It is assumed that the precipitates remain on the waste surface and slowly dissolve at a rate given by the rate of mass transfer of the low-solubility species into the surrounding liquid, with the concentration of the low-solubility species in the liquid adjacent to the waste surface given by the solubility of that species in groundwater. The possibility of forming colloids or other non-dissolved suspended particulates within the groundwater is neglected.

These assumptions can be written as

$$\dot{f}_j(t) = \text{Min}\ (\dot{f}_{silica}\ (t),\ \dot{f}_j\ (t)) \quad j = 1,2,..,N \qquad (7.5.22)$$

where:

Min (X,Y) = minimum value of X or Y

For numerical demonstration we consider a borosilicate waste glass with r = 15.2 cm and L = 2.40 m emplaced in a porous medium with a porosity of 0.01 and groundwater pore velocity of 1 m/yr. The concentration of each of the components in the groundwater far from waste cylinder is assumed zero. The molecular diffusion coefficient in groundwater is assumed to be 1×10^{-5} cm^2/sec for all the diffusing components. The initial inventories and solubilities of constituents in groundwater and the corresponding calculated fractional release rates are given in Table 7.5.7. Table 7.5.8 shows the calculated fractional release rate of the constituents from the above waste glass in absence of groundwater flow. For this case the prolate spheroid has the same volume and surface area as the waste cylinder.

Table 7.5.8 also shows the experimental results of fractional release rate for some radionuclides(M1). The experimental results are adjusted for the surface area of the waste cylinder on the assumption that the release rate is proportional to surface area exposed. Comparison between these calculated values indicate that in the repository conditions dissolution of the low-solubility radionuclides is controlled by the concentration boundary layer and not by the kinetics inside the glass matrix.

7.5.12. Conclusion

Two solubility-limited dissolution models were developed in Sections 7.1 and 7.2. The models permit one to calculate the steady-state dissolution rate of a diffusing species from a cylinder which is embedded in a water saturated porous medium. In one model the mass loss is due to molecular diffusion only, while in the other it is governed by molecular diffusion and groundwater convection.

The models are applied to an amorphous silica cylinder embedded in a medium with porosity of 0.01. The cylinder radius of 15.2 cm and height of 2.4 m are used, which are dimensions of a commercial high level waste

glass cylinder. For the diffusion model an average surface mass flux of 2.7×10^{-8} g/cm^2 day and leach time of 3×10^6 yr are calculated.

The models are applied to a borosilicate high level waste glass. The fractional release rates of some low-solubility components are calculated. The numerical results indicate that if the solubility of these constituents is low enough, and their initial inventories high enough, they will not initially dissolve congruently with the waste matrix. Comparison of fractional release rates due to diffusion and those due to diffusion-convection indicates that the groundwater pore velocity of 1 m/yr causes a four fold increase in dissolution rate. This indicates a narrow range for dissolution rates obtained by the two models.

Comparison between calculated fractional release rate and experimental values indicates that for low-solubility glass components the dissolution rate may be controlled by concentration boundary layer, porosity of the medium, and groundwater pore velocity and not by kinetics inside the glass matrix or solid-liquid interactions. Therefore, interior cracks of the waste solid, devitrification, and other mechanisms that could increase the rate of solid-liquid interaction would not be expected to affect the solubility-limited dissolution rate, unless they have some affect on the solubilities. If the solubility is sufficiently large, then the kinetics of interaction between the solid waste and water may be dominant.

Table 7.5.7 Calculated fractional release rates for borosilicate glass waste in flowing groundwater.

Waste cylinder: r = 0.152 m, L = 2.40 m, fission-product and actinide oxides from 460 kg of uranium fuel. Groundwater pore velocity of 1 m/yr.

Constituent	Initial species concentration in the waste, g/cm^3	Solubility, g/cm^3	Fractional Dissolution rate, yr^{-1}
SiO_2	1.6 a/	1.2×10^{-4} c/	3.4×10^{-6}
Tc	1.92×10^{-3} b/	3×10^{-9} d/	7×10^{-8}
U	1.22×10^{-2} b/	2×10^{-9} d/	8×10^{-9}
Np	1.92×10^{-3} b/	2.4×10^{-11} d/	5.7×10^{-10}
Pu	1.15×10^{-4} b/	1×10^{-9} d/	4×10^{-7}
Am	3.56×10^{-4} b/	1.8×10^{-12} d/	2.3×10^{-10}

a/ Reference (M2).

b/ Assumed 0.5% U and Pu and all fission products and actinides (B1).

c/ For amorphous SiO_2 (S1).

d/ Reference (K1).

Table 7.5.8 Calculated fractional dissolution rates for borosilicate glass waste in stagnant groundwater.

Waste cylinder: r = 0.152 m, L = 2.40 m, fission-product and actinide oxides from 460 kg of uranium fuel.

Constituent	Initial specie concentration in the waste, g/cm^3	Solubility, g/cm^3	Fractional dissolution rate, yr^{-1}	
			Calculated	Observed a/
SiO_2	1.6 b/	1.2×10^{-4} d/	8.7×10^{-7}	1.6×10^{-3}
Tc	1.92×10^{-3} c/	3.0×10^{-9} e/	1.8×10^{-8}	--
U	1.22×10^{-2} c/	2.0×10^{-9} e/	1.9×10^{-9}	1.5×10^{-6}
Np	1.92×10^{-3} c/	2.4×10^{-11} e/	1.5×10^{-10}	6.6×10^{-4}
Pu	1.15×10^{-4} c/	1.0×10^{-9} e/	1.0×10^{-7}	2.6×10^{-5}
Am	3.56×10^{-4} c/	1.8×10^{-12} e/	5.8×10^{-11}	2.7×10^{-6}

a/ Reference (M1).

b/ Reference (M2).

c/ Assumed 0.5% U and Pu and all the fission products and actinides (B1).

d/ For amorphous SiO_2.

e/ Reference (K1).

7.5.13 Nomenclature

a	Semi-major axis of the prolate spheroid cm
b	Semi-minor axis of the prolate spheroid cm
b_o	Initial semi-minor axis of the prolate spheroid cm
c_s	Solubility limit in groundwater g/cm^3
c_∞	Concentration in groundwater far away from waste surface g/cm^3
D_f	Molecular diffusivity in water cm^2/sec
D_f^j	Molecular diffusivity of component j in water cm^2/sec
e	Eccentricity of prolate spheroid
f	Focal distance of the prolate spheroid
$\dot{f}_j(t)$	Fractional dissolution rate of component j at time t sec^{-1}
$\bar{j}_c$	Average surface mass flux of infinitely long cylinder in flowing groundwater g/cm^2sec
$\bar{j}_{ps}$	Average surface mass flux of the prolate spheroid g/cm^2 sec
L	Cylinder height cm
L_o	Initial cylinder height cm
$L(t)$	Cylinder height at time t after dissolution begins cm
$\dot{m}(t)$	Dissolution rate at time t g/sec
$\dot{m}_j(t)$	Dissolution rate of component j at time t g/sec
$\dot{m}_{ps}$	Total dissolution rate of the prolate spheroid g/sec
$\dot{m}_p^L$	Dissolution rate per unit length of the prolate spheroid g/cm sec
$\dot{m}_{sc}$	Dissolution rate for a slender cylinder g/sec
$\dot{m}_c$	Dissolution rate from a cylinder in flowing groundwater
$\dot{m}_c^\ell$	Dissolution rate per unit length of infinitely long cylinder in flowing groundwater g/cm sec
$M_j(t)$	Mass of j at time t in the waste glass g
$n_j(t)$	Density of j in undissolved waste at time t g/cm^3
N_s	Difference between concentration in the liquid adjacent to waste surface and concentration in the groundwater far away from waste surface g/cm^3

$N_{s,j}$ Difference between concentration of component j in liquid adjacent to the waste surface and concentration in the groundwater far away from waste surface g/cm^3

r Cylinder radius cm

$r(t)$ Cylinder radius at time t after dissolution begins cm

r_o Initial cylinder radius cm

T Leach time (sec)

T_{ps} Leach time for prolate spheroid sec

T_{sc} Leach time for slender cylinder sec

T_c Leach time for the infinitely long cylinder in flowing groundwater sec

U Groundwater pore velocity cm/sec

$V_j(t)$ Volume of undissolved waste at time t cm^3

$Pe \equiv \frac{Ur}{D_f}$ Peclet number

$Pe_o \equiv \frac{Ur_o}{D_f}$

$Pe^j \equiv \frac{Ur}{D_f^j}$

<u>Greek letters</u>

ρ = waste form density g/cm^3

ε = porosity

$\alpha_s = \cosh^{-1}(\frac{1}{e})$ Surface shape factor of prolate spheroid Defined by Eq.(7.1.4)

7.6 Calculations of Dissolution of a Glass Matrix by Internal Molecular Diffusion and Surface Regression

P. L. Chambré and S. J. Zavoshy

1. Introduction

In this paper we consider the dissolution of a glass matrix containing sodium oxide. It is experimentally observed that sodium molecular diffusion and ion-exchange at the glass-water interface depletes the glass matrix of sodium ion. Further, the glass matrix is dissolved by water. This matrix dissolution is viewed as regression of dissolved glass-water interface. The fractional release of sodium from the glass has a form of $c_1 t^{1/2} + c_2 t$, where c_1 and c_2 are two constants (H1,M3). A dissolution model that yields a fractional release which is initially parabolic (proportional to $t^{1/2}$), and then becomes linear function of time (proportional to t), is developed in section 7.4.

A mathematical dissolution model is developed based upon these two observed phenomena, i.e., internal molecular diffusion and glass surface regression. It is assumed that the loss of the diffusing ion from the interior of the glass due to molecular diffusion will lessen the integrity of the glass matrix. Furthermore, it is assumed that the glass-water interface has a constant velocity during the dissolution process. The regression speed is positive for the case of a regressive glass-water interface, zero for stationary interface, and negative for the progressive interface. The concentration inside the glass and fractional release of the diffusant from the glass are obtained for a sphere and slab of finite width.

For numerical evaluation a ternary sodium-borosilicate glass is considered. Sodium is the diffusing nuclide. The concentration of sodium

at the glass-water interface is chosen to be zero. The radius and half width of the slab are equal to the radius of a spent fuel canister. A range of regression speeds from -9.7×10^{-13} to 3.9×10^{-11} cm/sec is chosen. The normalized concentration, surface mass flux, and fractional release of sodium are evaluated.

2. Governing equations for the normalized concentration, surface mass flux, and fractional release.

Case 1. Finite slab

The following equation defines the normalized concentration of the diffusing specie in the slab of width 2a

$$c^n_{sL}(x,t) = N^s + N^o \hat{c}_{sL}(x,t) \tag{7.6.1}$$

where:

$c^n_{sL}(x,t)$ = normalized concentration of diffusing specie in the slab

$\hat{c}_{sL}(x,t)$ = normalized concentration of the stable diffusing specie in the slab with zero concentration on the boundary (see Eq. (7.4.30) in section 7.4 with λ=o)

$N^s = \frac{c_s}{c_o}$

$N^o = (c_o - c_s) / c_o$

c_s = surface concentration of the diffusing specie, g/cm^3

c_o = initial bulk density of diffusing specie in the glass, g/cm^3

x = position from center of slab, cm

t = time, sec

The fractional release is obtained by the following equation:

$$f_{sL}(t) = 1 - N^s (1-vt/a) - N^o \int_0^{1-\beta\tau} \hat{c}_{sL}(y,t)\, d\, y \tag{7.6.2}$$

where:

$f_{sL}(t)$ = fractional release of diffusing specie at time t from the finite slab

$\beta = va/D$

a = initial half width of finite slab, cm

D = molecular diffusion coefficient of diffusing specie in the glass matrix, cm^2/sec

$\tau = Dt/a^2$

v = regression speed, cm/sec

An asymptotic form for $f_{sL}(t)$ is obtained which is

$$f_{sL}(t) = \frac{2}{\sqrt{\pi}} N^o (D/a^2)^{1/2} t^{1/2} + vt/2d \qquad (7.6.3)$$

The surface mass flux is given by

$$j_{sL} = - D (c_o - c_s) \frac{\partial \hat{c}_{sL}}{\partial x} \Big|_{a-vt} + v c_s \qquad (7.6.4)$$

where j_{sL} is the surface mass loss of diffusing specie from the finite slab, g/cm^2 sec.

<u>Case 2</u>. Sphere.

The normalized concentration of the diffusing specie in the sphere is given by

$$c^n_{sp}(r,t) = N^s + N^o \hat{c}_{sp}(r,t) \qquad (7.6.5)$$

where:

$c^n_{sp}(r,t)$ = normalized concentration of the diffusing specie in the sphere

$\hat{c}_{sp}(r,t)$ = normalized concentration of stable diffusing specie in the sphere with zero concentration at the boundary (see Eq. (7.4.20) in section 7.4 with λ=o)

r = radial position from center of sphere, cm

From Eq. (7.6.5) we obtain the surface mass flux, i.e.,

$$j_{sp} = -D\,(c_o - c_s)\,\frac{\partial \hat{c}_{sp}}{\partial r}\Big|_{R-vt} + v\,c_s \qquad (7.6.6)$$

where j_{sp} is the surface mass loss of diffusing specie from sphere, g/cm^2 sec

The fractional release is obtained by

$$f_{sp}(t) = 1 - N^s\,(1-vt/R)^3 - 3\,N^o \int_0^{1-\beta\tau} \hat{c}_{sp}(y,t)\,y^2 dy \qquad (7.6.7)$$

where:

$f_{sp}(t)$ = the fractional release of diffusing specie from sphere at time t

$\beta = vR/D$

R = initial radius of sphere, cm

An asymptotic form of $f_{sp}(t)$ for early period of dissolution is

$$f_{sp}(t) = \frac{6N^o}{\sqrt{\pi}}\,(D/R^2)^{1/2} + 3\,(vt/2R)\,(1+N^s) \qquad (7.6.8)$$

and as the total dissolution time is approached the following asymptotic relation is obtained

$$f_{sp}(t) = 1 - (1 - vt/R)^3 \qquad (7.6.9)$$

This is due to time dependency of surface area of the sphere.

3. Parameters of the problem

The values of a and R were chosen to be 17.8 cm, equal to the radius of a spent fuel canister. The glass density is taken to be 2.8 g/cm^3. Table 7.6.1 gives the value of molecular diffusion coefficient of sodium in a ternary sodium-borosilicate glass at 100° and 200°C. Table 7.6.1 was obtained by applying the following equation (F1)

$$D(T) = D_o \mathrm{Exp}(-\,Q/RT) \qquad (7.6.10)$$

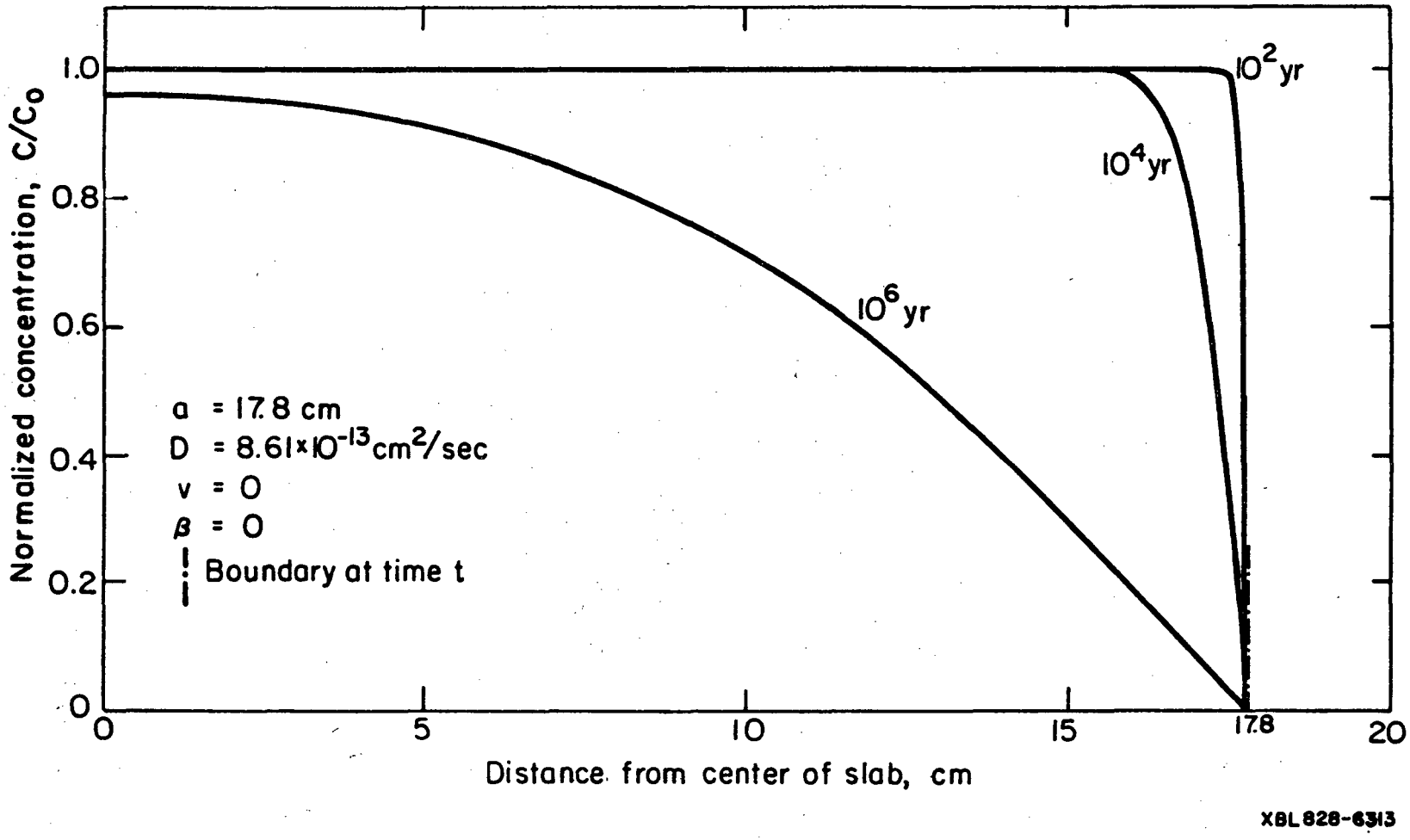

Fig. 7.6.1. Variation of Na normalized concentration in the slab (initial width 2a) with position at different times after glass dissolution begins.

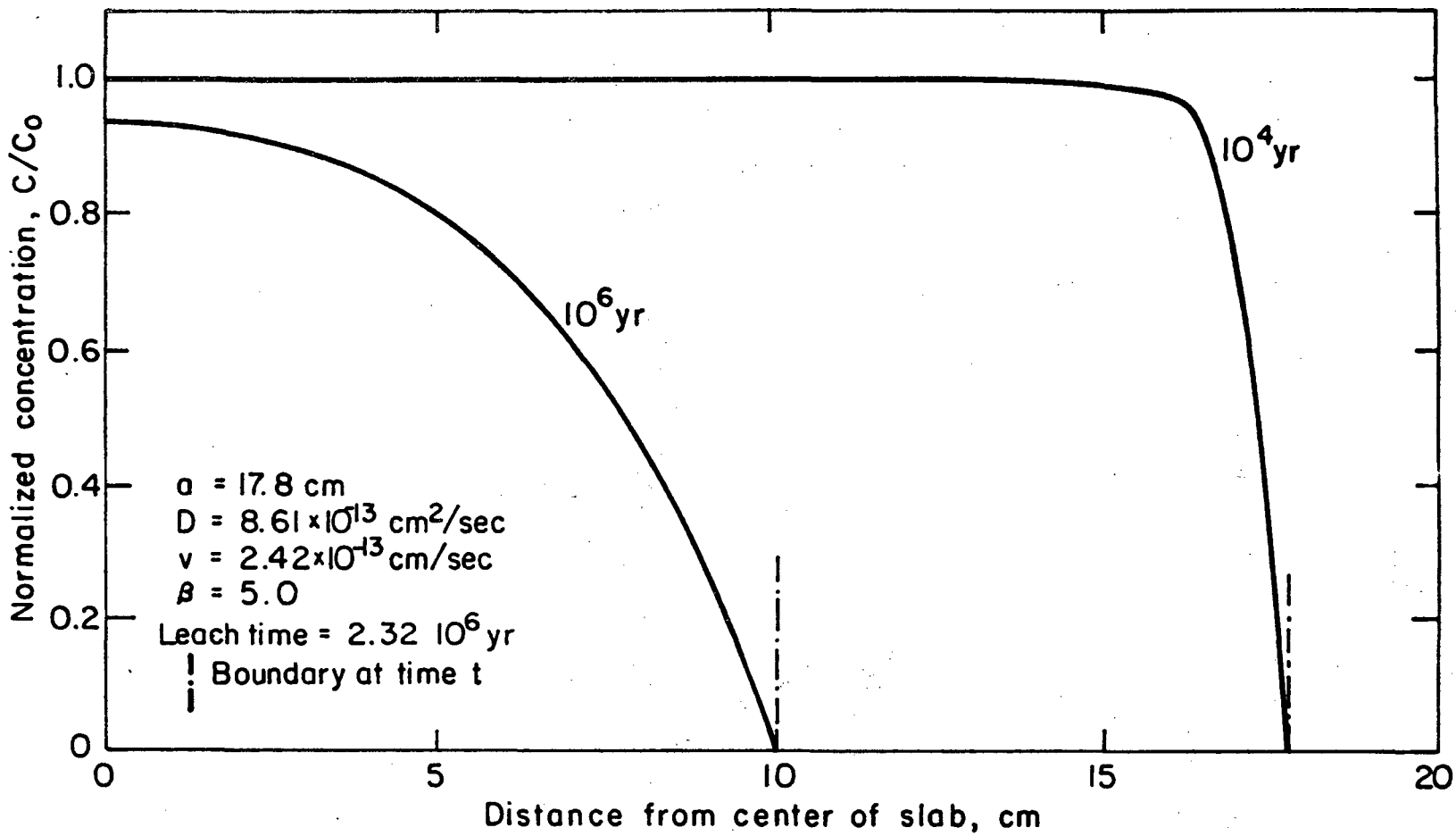

XBL 828-6314

Fig. 7.6.2. Variation of Na normalized concentration in the slab (initial width 2a) with position at different times after glass dissolution begins.

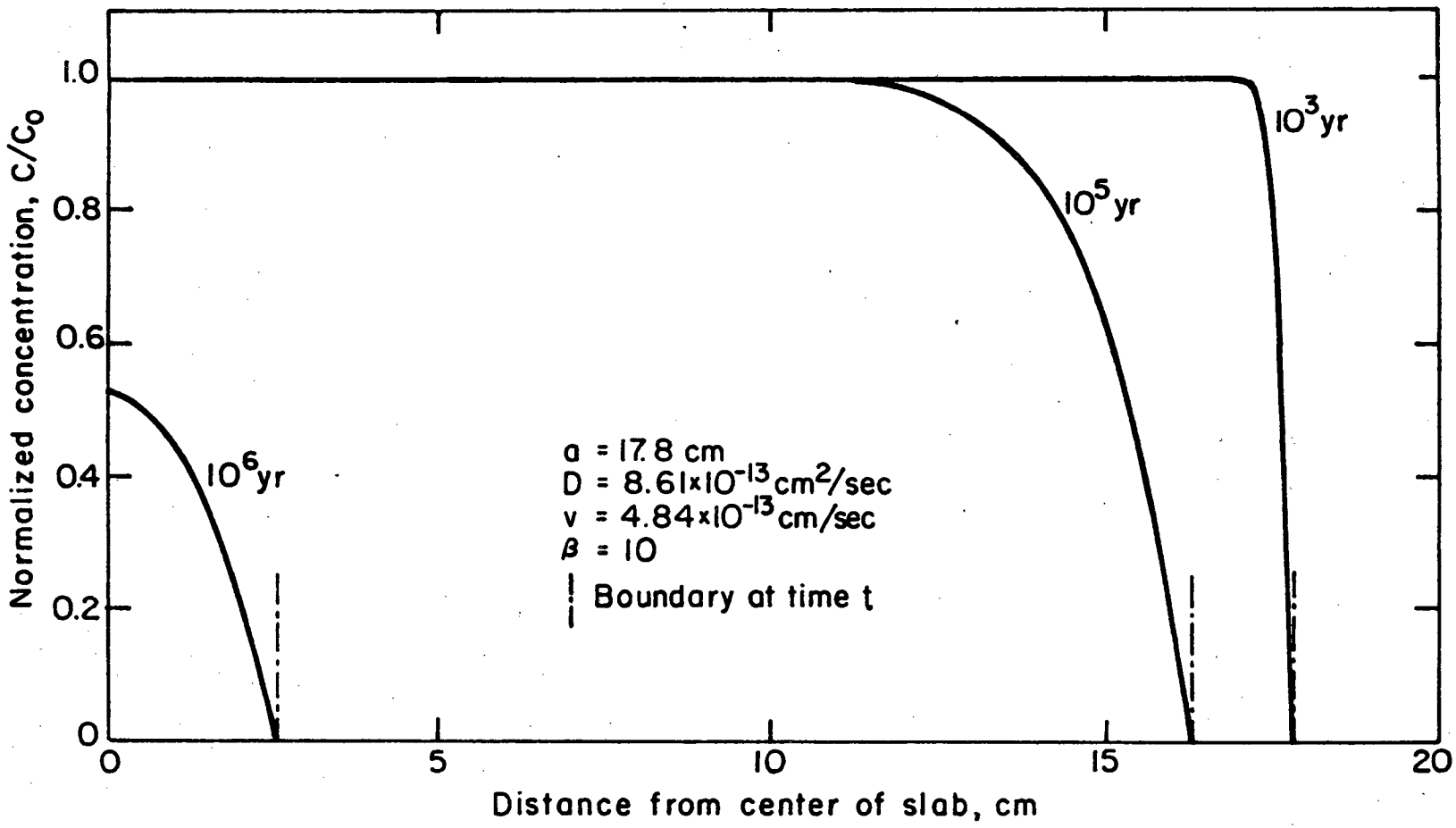

XBL 828-6315

Fig. 7.6.3. Variation of Na normalized concentration in the slab (initial width 2a) with position at different times after glass dissolution begins.

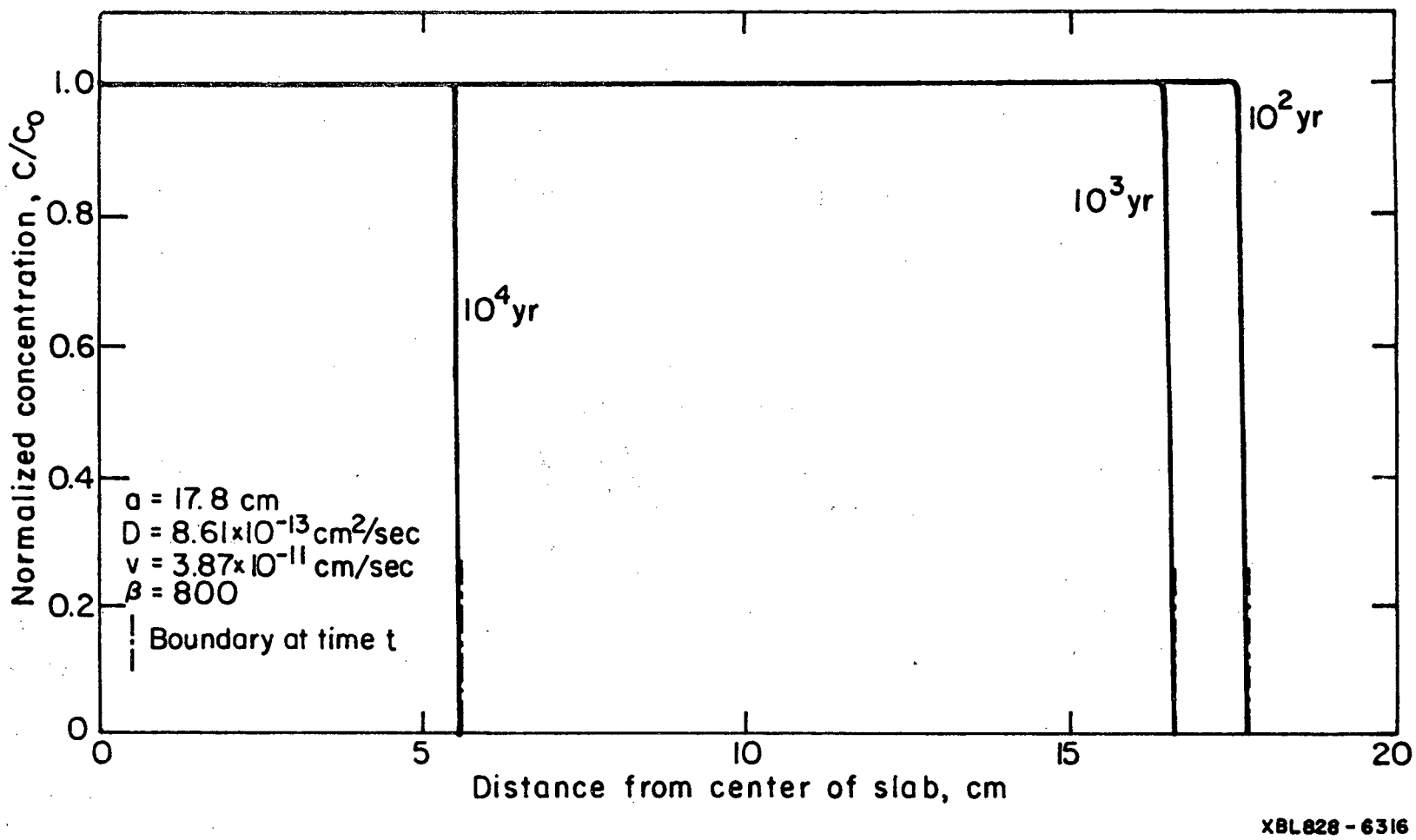

Fig. 7.6.4. Variation of Na normalized concentration in the slab (initial width 2a) with position at different times after glass dissolution begins.

where:

$D(T)$ = sodium diffusion coefficient at temperature T, cm^2/sec

D_o = frequency factor, cm^2/s

Q = activation energy, Kcal/mole

R = gas constant = 1.99×10^{-3} Kcal/mole °K

T = temperature in degrees Kelvin, °K

Table 7.6.1. Na self-diffusion in ternary Na_2O-B_2O_3-SiO_2 glasses (F1)

Na_2O/B_2O_3 mole%	$D_o(cm^2/s)$ a/	Q(Kcal/mole) a/	$D_{100}(cm^2/s)$ b/	$D_{200}(cm^2/s)$ c/
31.3/6.25	5.01×10^{-6}	11.5	9.36×10^{-13}	2.84×10^{-11}
30.9/9.10	6.31×10^{-6}	11.7	9.00×10^{-13}	2.52×10^{-11}
28.6/14.3	3.98×10^{-5}	13.1	8.61×10^{-13}	3.59×10^{-11}
32.3/3.22	5.01×10^{-4}	13.4	7.24×10^{-12}	3.29×10^{-10}
31.7/4.76	1.21×10^{-4}	13.0	3.00×10^{-12}	1.22×10^{-10}

a/ For temperature range of 100° to 250°C.

b/ At 100°C.

c/ At 200°C.

For numerical evaluation a ternary sodium-borosilicate glass at 100°C with the composition 28.6 Na_2O/14.3 B_2O_3 mole % was considered. From Table 7.6.1 we obtain $D=D_{100} = 8.61 \times 10^{-13}$ cm^2/s. The surface concentration is taken to be zero.

Values of β = -20, -10, -5, 0, 5, 10, 50, and 800 were chosen. Value of β = 800 corresponds to $v = 3.3 \times 10^{-6}$ cm/day.

4. Numerical results and discussion

The numerical results are obtained with the aid of four computer

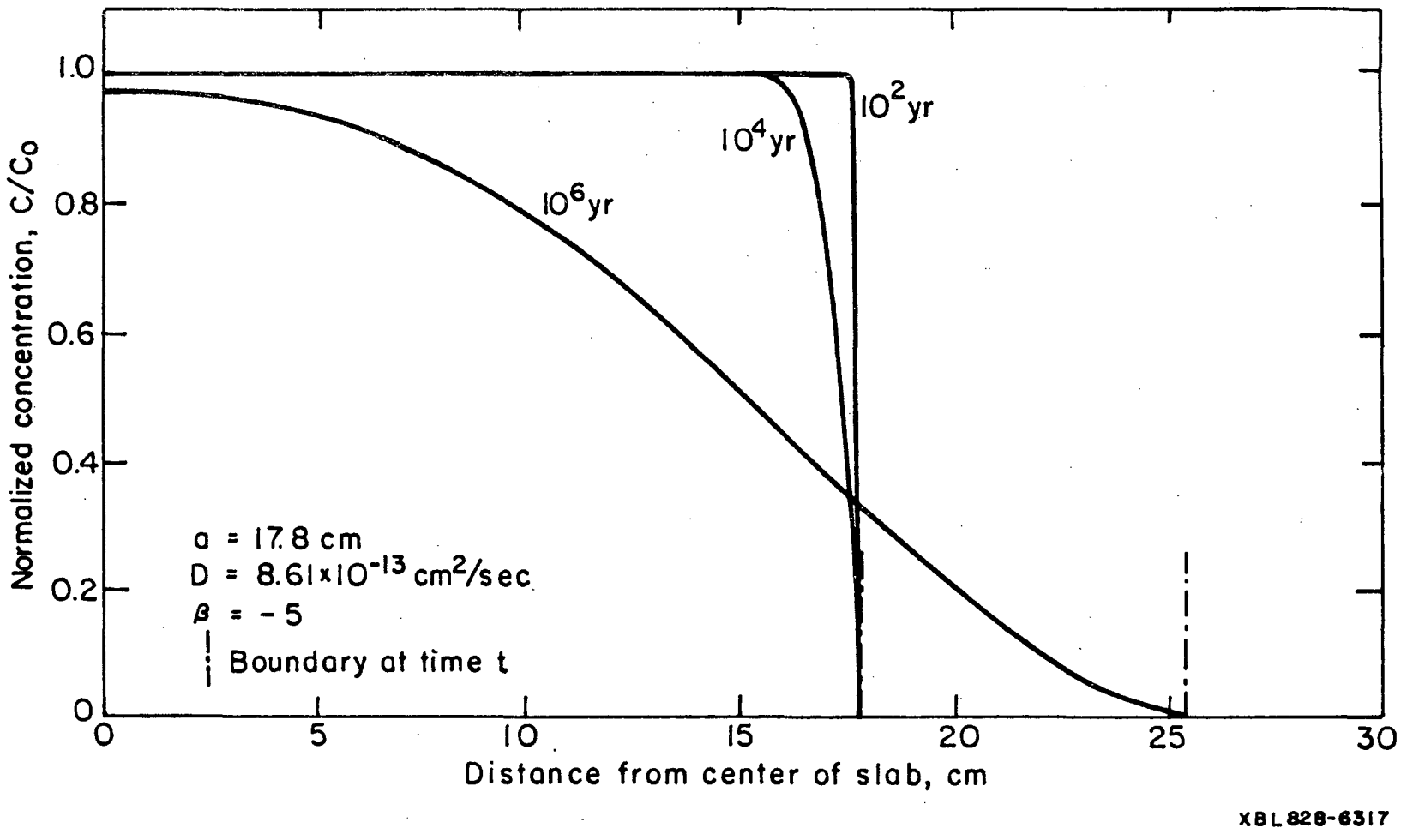

Fig. 7.6.5. Variation of Na normalized concentration in the slab (initial width 2a) with position at different times after glass dissolution begins.

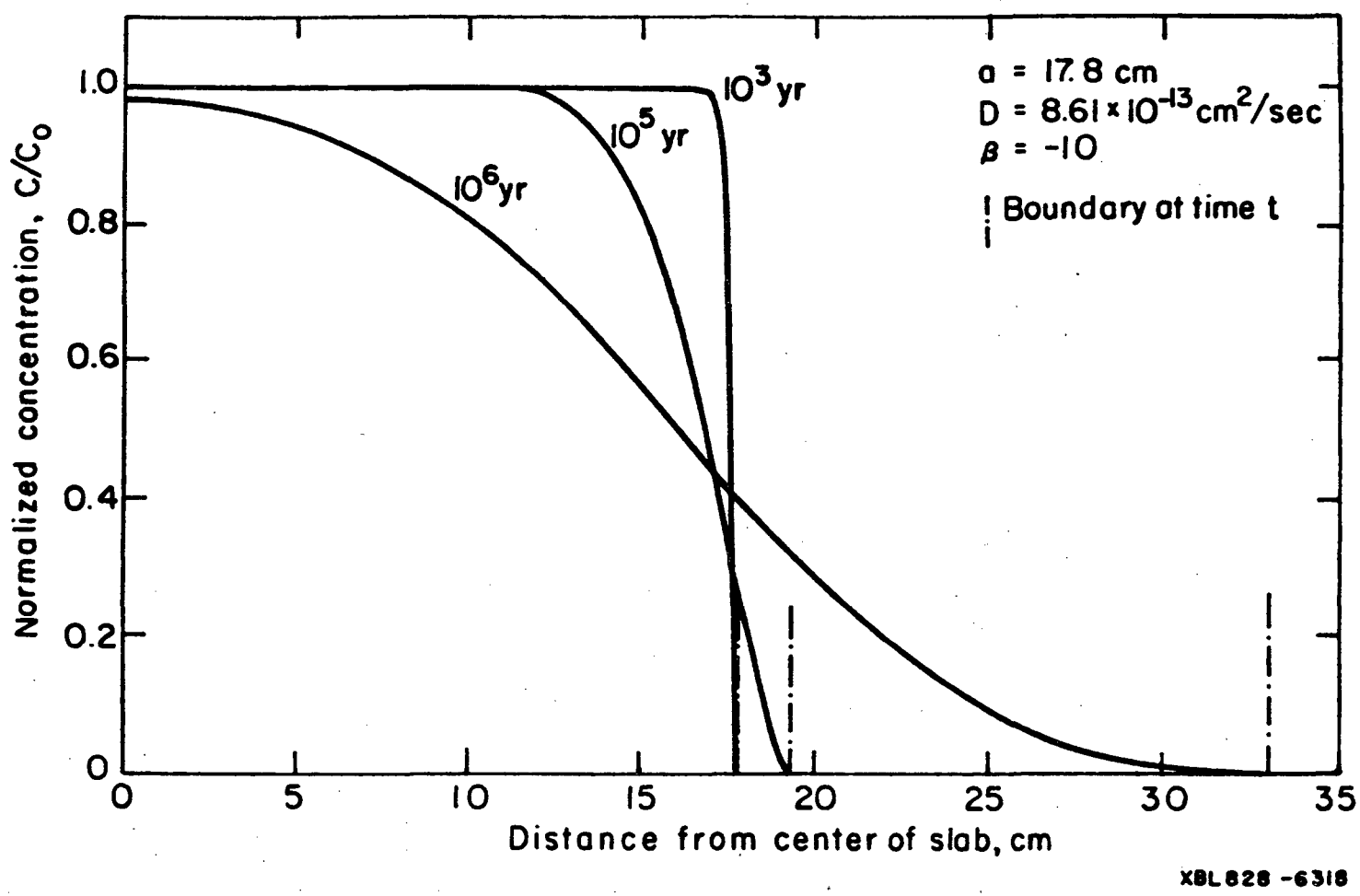

Fig. 7.6.6. Variation of Na normalized concentration in the slab (initial width 2a) with position at different times after glass dissolution begins.

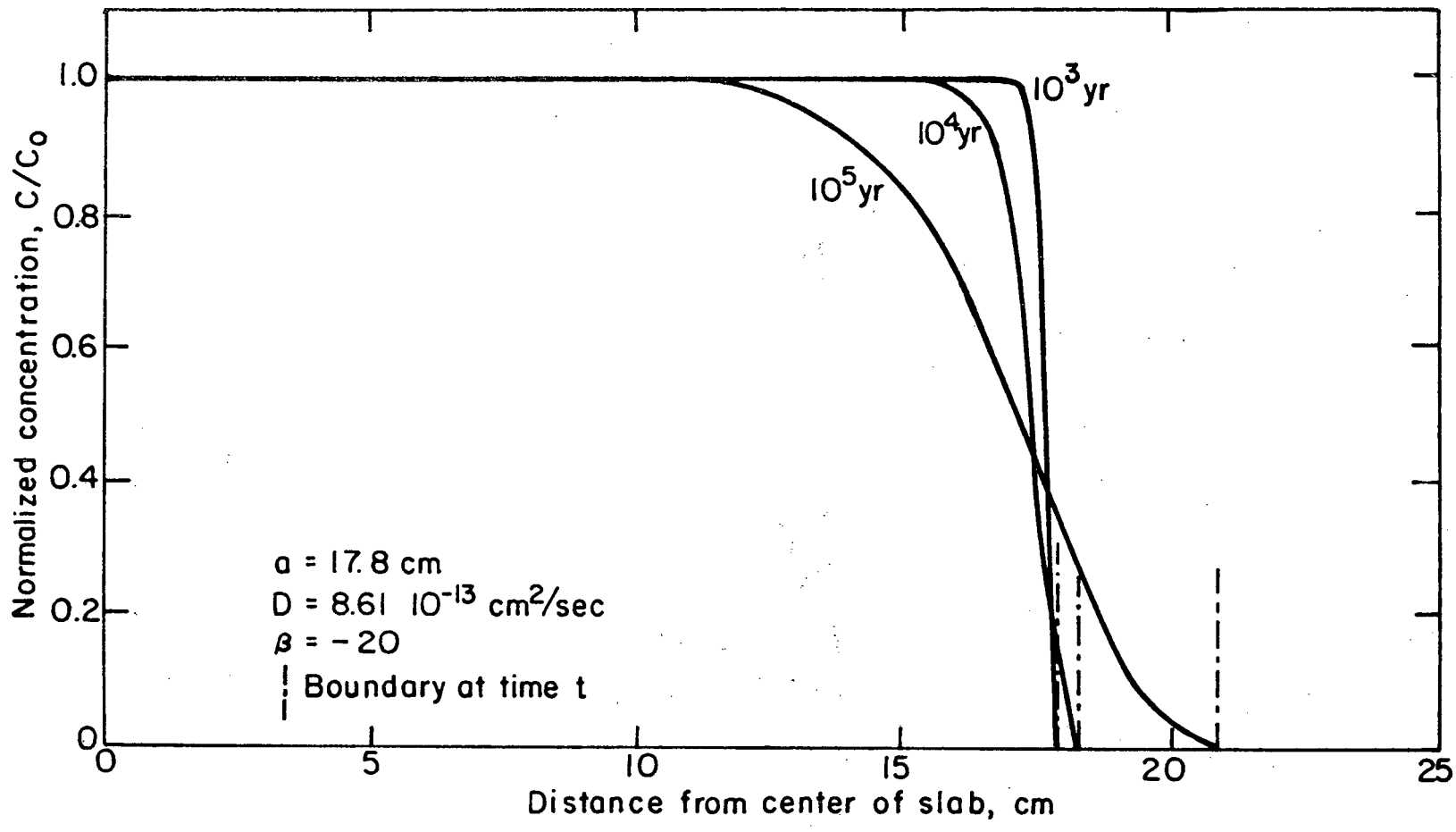

XBL828-6319

Fig. 7.6.7. Variation of Na normalized concentration in the slab (initial width 2a) with position at different times after glass dissolution begins.

programs (see Appendix A for the program details). The cut off time for calculations is the leach time T_L. This is defined as

$$T_L = | L/v | \quad , v \neq 0 \tag{7.6.11}$$

where:

T_L = leach time, sec

L = initial characteristic length of the problem, cm (half width of the finite slab or sphere radius).

The value of T_L corresponds to total dissolution of the glass matrix if $v > 0$, and doubling of L if $v < 0$. The surface mass flux was obtained by numerical differentiation of Eqs. (7.6.4) and (7.6.6).

Figs. 7.6.1 - 7.6.7 show the normalized concentration vs. half width of the finite slab, for β = 0, 5, 10, 800, -5, -10, and -20 respectively. For $v > 0$, increase in v, (β) will result in steepening of the concentration profile at the glass-water interface. This effect can be best seen in Fig.7.6.4, where β = 800. Also, the absolute value of the concentration gradient at the interface is increased as v increases. For negative values of v, the normalized concentration profile becomes S-shaped, see Fig. 7.6.5.

Fig.7.6.8 shows the variation of the normalized surface mass flux of the finite slab with time ($\tau = Dt/a$) for different values of β, (v). At the early period of glass dissolution the normalized surface mass flux is proportional to $t^{-1/2}$ and is independent of the regression velocity. This indicates the diffusion-controlled mass loss. For β = 800, after approximately 100 years, a constant surface mass flux of 2.4×10^{-6} g sodium/cm^2 day is obtained.

Fig.7.6.9 shows the variation of the fractional release with time for

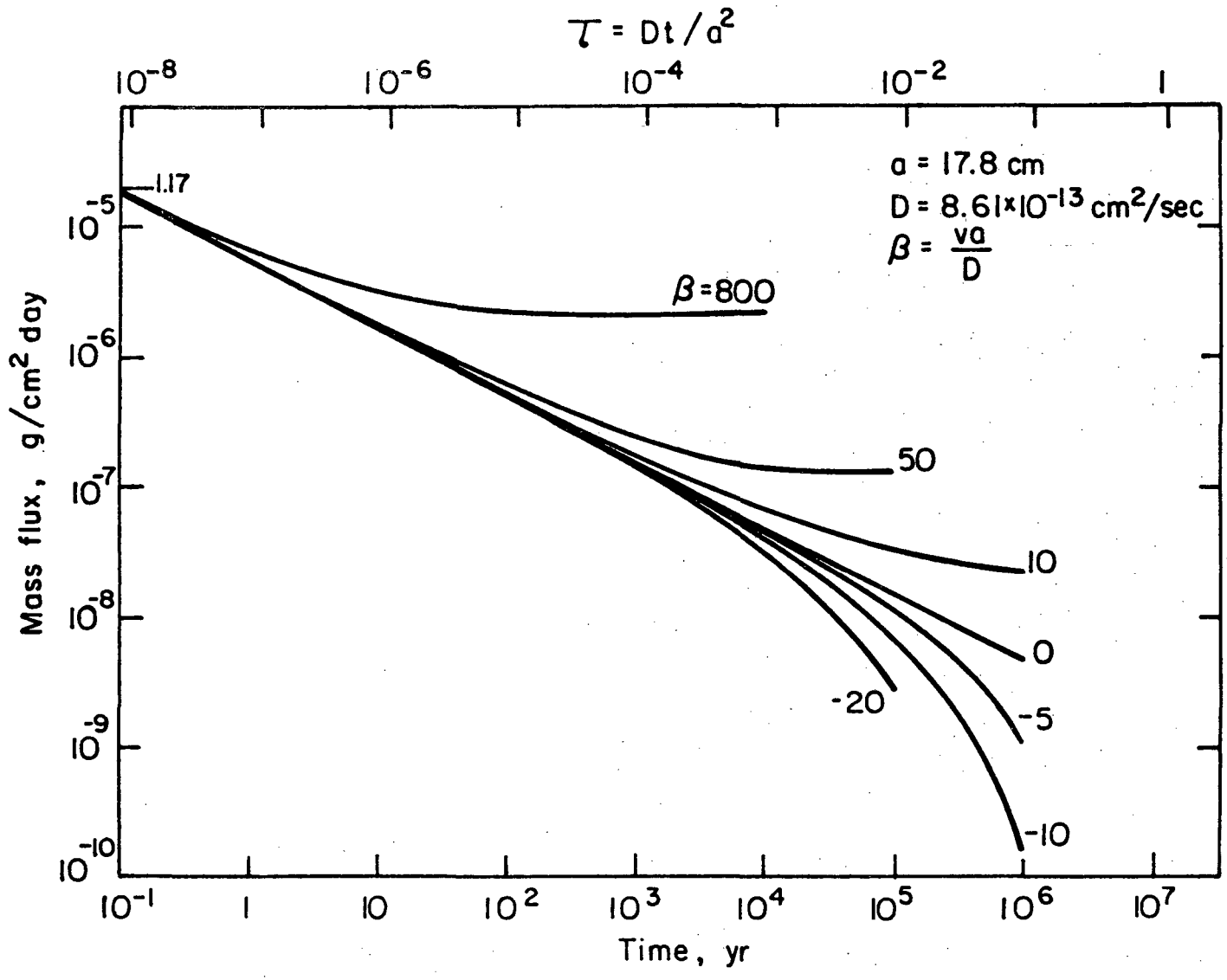

Fig. 7.6.8. Variation of Na surface mass flux from slab (initial width 2a) with time for different β (glass-water interface regression speed).

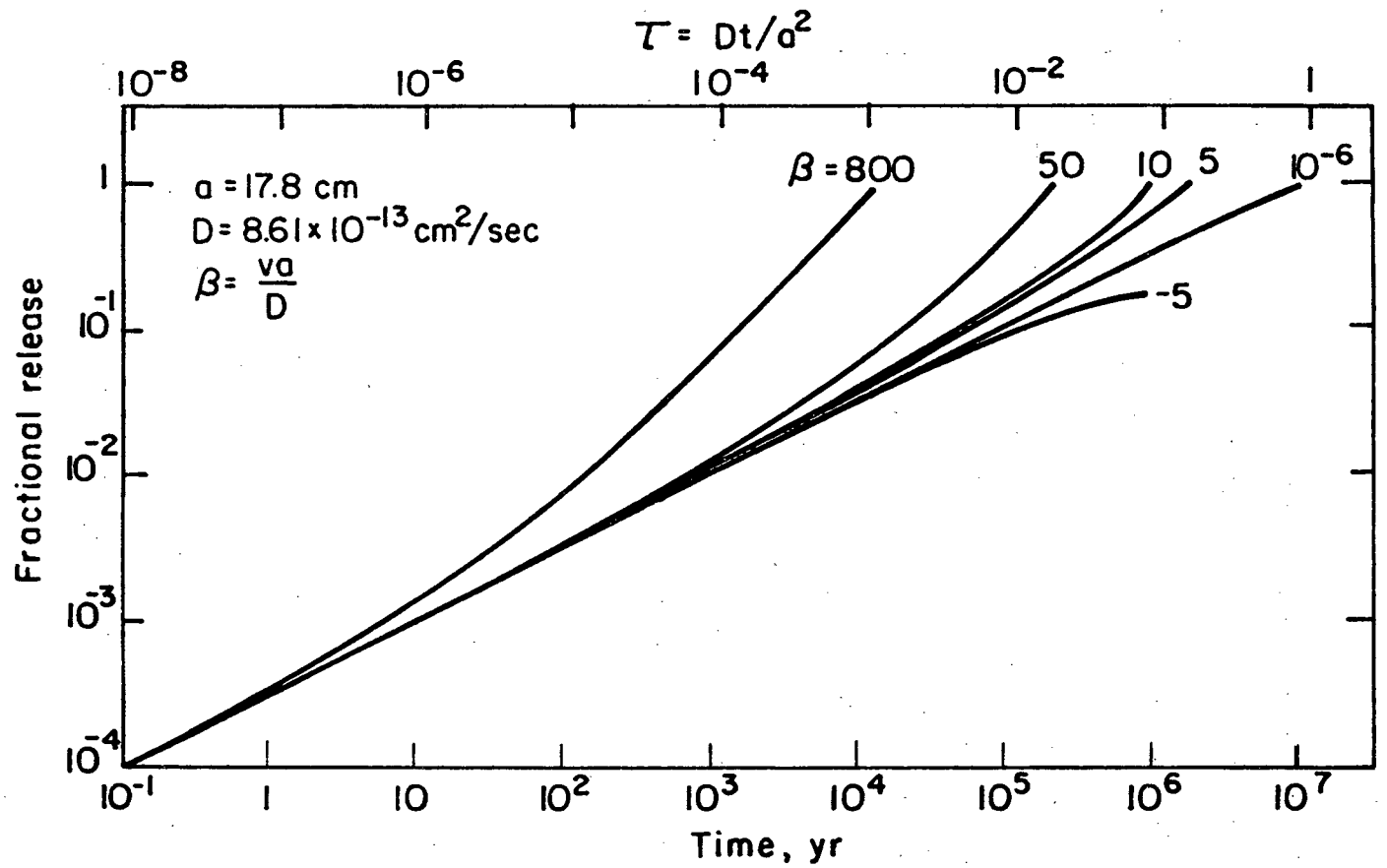

XBL 828-6321

Fig. 7.6.9. Variation of Na fractional release from slab (initial width 2a) with time (τ) for different glass water interface regression speed (β).

different values of v. Fractional release has a behavior of the form $c_1 t^{1/2} + c_2 t$, where c_1 and c_2 are two constants, see Eq. (7.6.6) for values of c_1 and c_2.

Figs. 7.6.10 - 7.6.13 apply to the sphere and show the normalized concentration vs. radius of sphere for β = 0, 10, -5, and -10 respectively. Comparison with Figs. 7.6.1, 3, 5 and 6 indicates that sodium depletion is faster for the sphere than for the slab. The plot obtained for β = 800 is identical to Fig. 7.6.7, thus it is not reproduced.

Fig. 7.6.14 shows the variation of the normalized surface mass flux of the sphere with time (τ) for different values of β, (v). As leach time is approached there is a drop in surface mass flux due to depletion of sodium inside the sphere.

Fractional release for the sphere case is obtained by way of numerical integration of the normalized concentration. Fig. 7.6.15 shows the variation of fractional release with time (τ) for different values of β, (v).

5. Conclusion

A glass dissolution model based upon two observed phenomena, i.e., internal molecular diffusion and glass surface regression, is developed. An asymptotic equation is obtained for fractional dissolution of diffusant from the glass. The asymptotic equation has a form of $c_1 t^{1/2} + c_2 t$ where c_1 and c_2 are a function of molecular diffusion coefficient and regression speed. The experimental results of fractional dissolution of component 'i' is of the form $C_1 t^{1/2} + C_2 t$, where C_1 and C_2 are two constants which depend on the diffusing component. Values of C_1 and C_2 are obtained from glass dissolution experiment. By fitting Eq. (7.6.3) or (7.6.8) to the

experimentally observed f(t) we can obtain the internal molecular diffusion coefficient of component 'i' and the glass-water regression speed. This is presently under study.

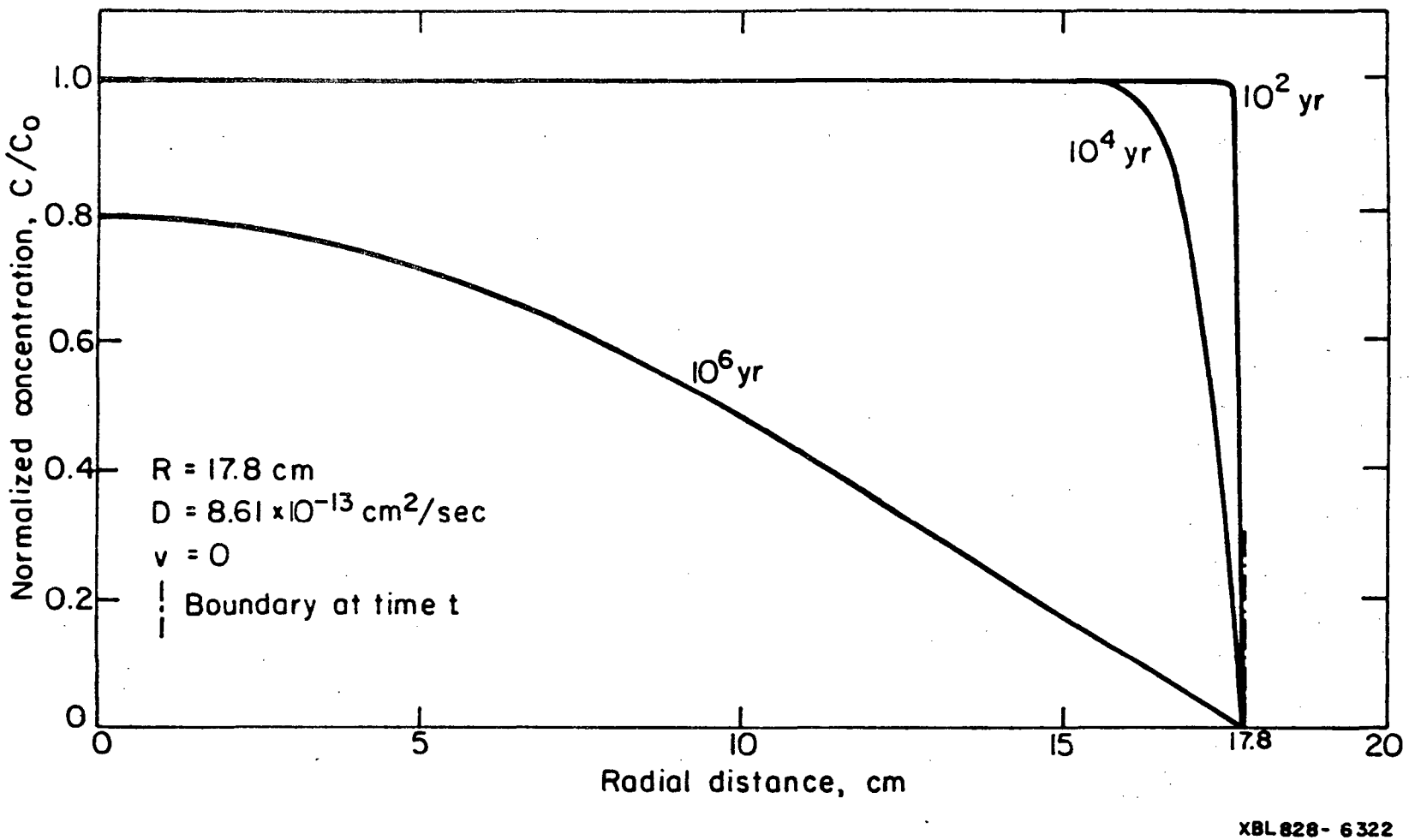

Fig. 7.6.10. Variation of Na normalized concentration in the sphere with radial position at different times after glass dissolution begins.

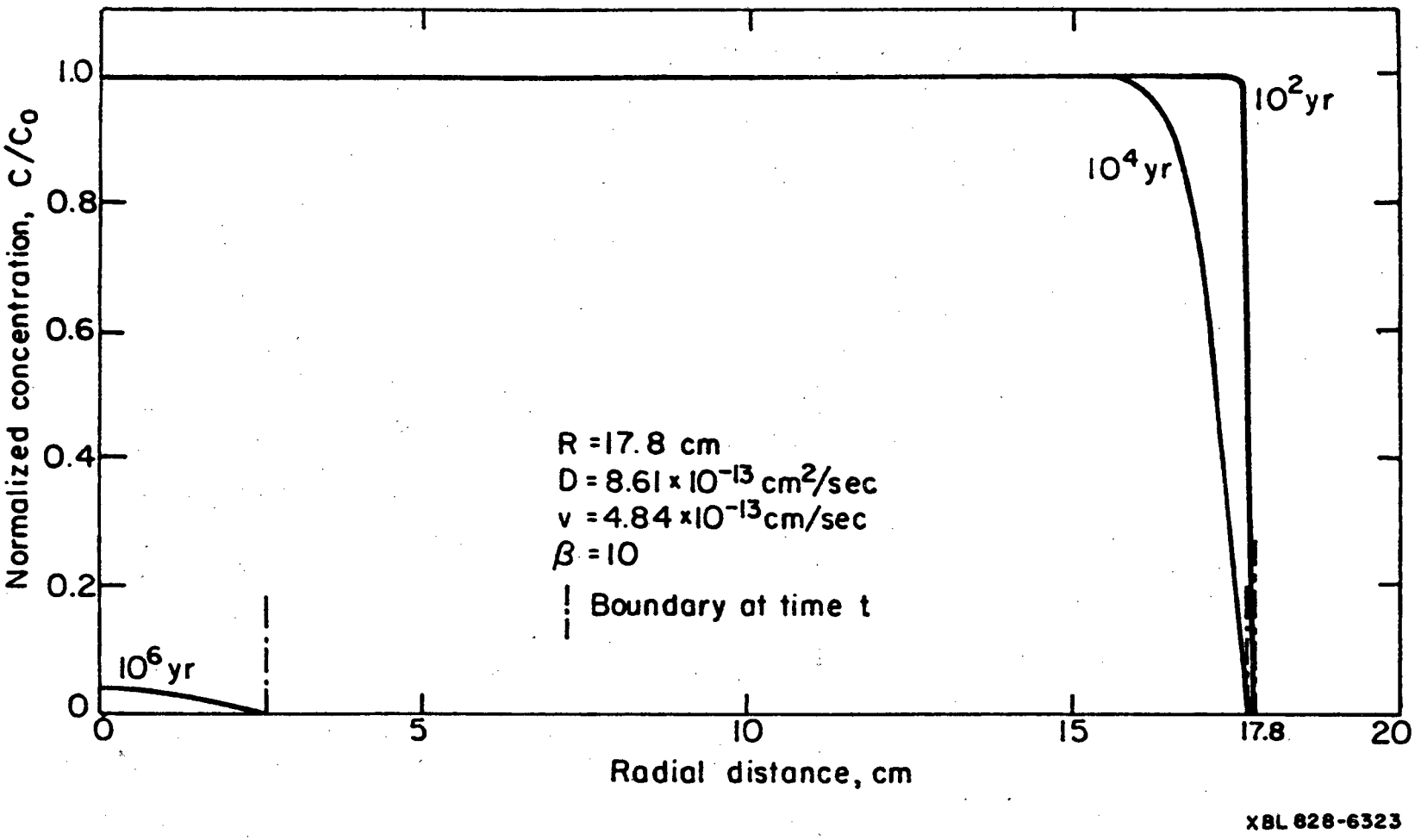

Fig. 7.6.11. Variation of Na normalized concentration in the sphere with radial position at different times after glass dissolution begins.

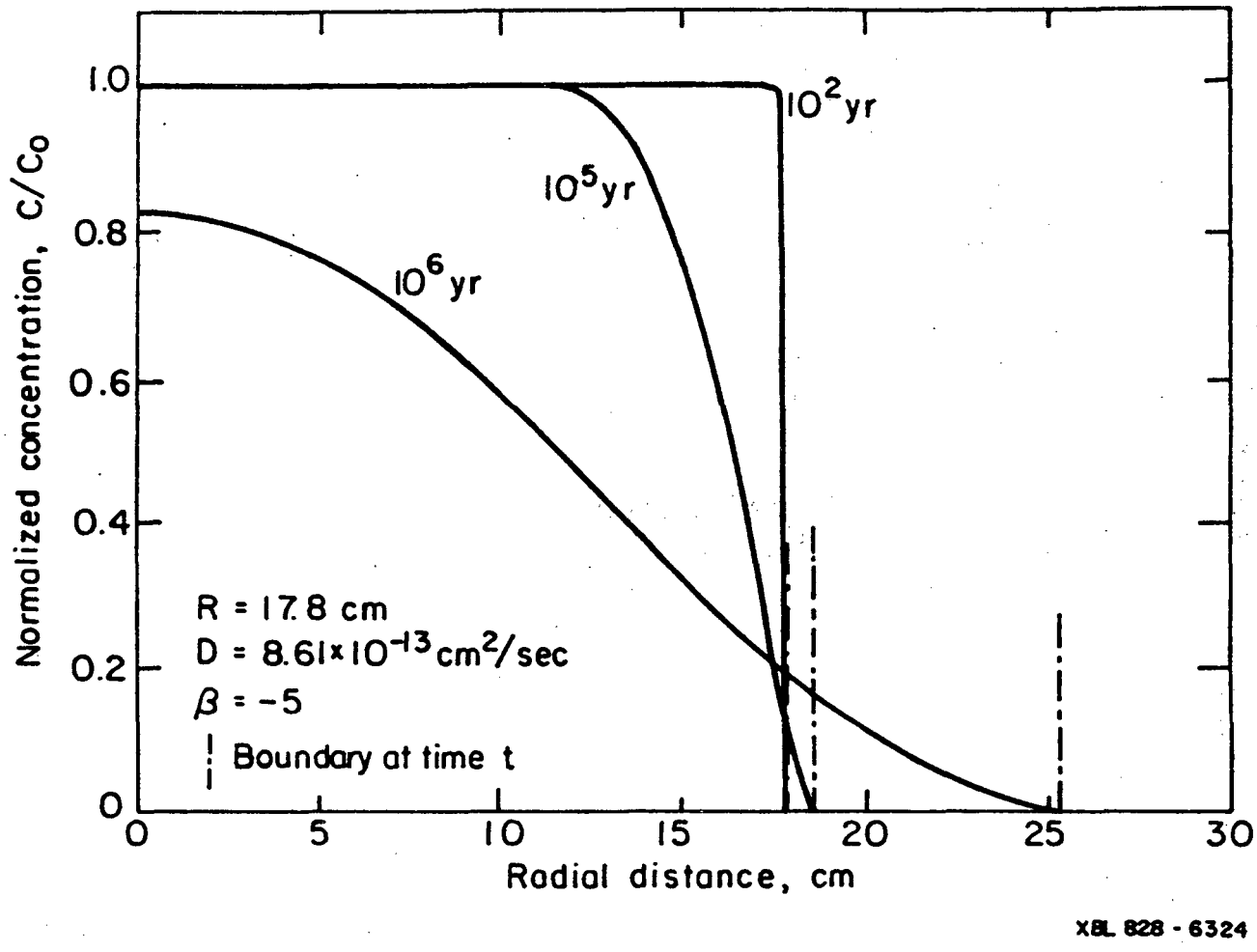

Fig. 7.6.12. Variation of Na normalized concentration in the sphere with radial position at different times after glass dissolution begins.

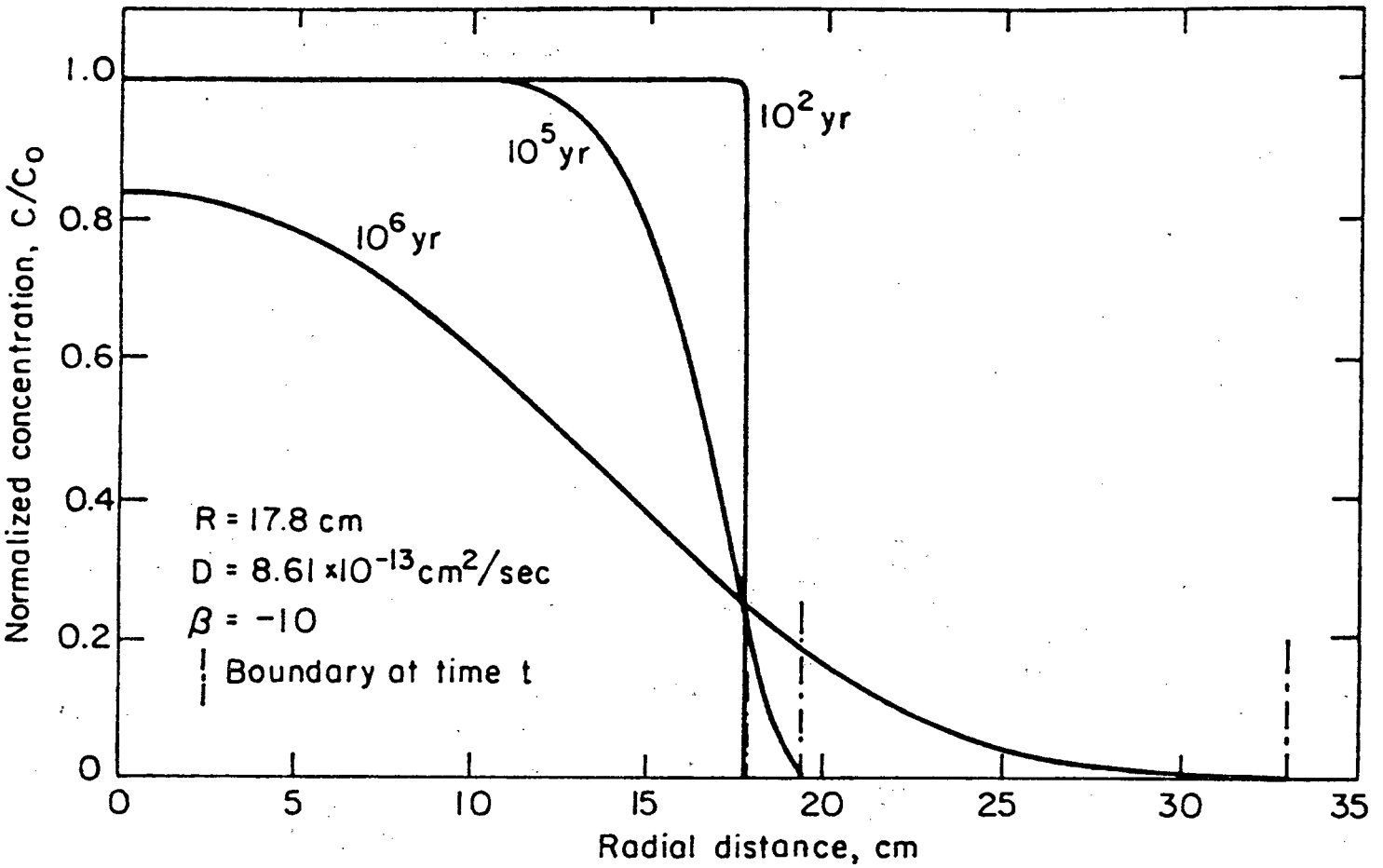

XBL 828-6325

Fig. 7.6.13. Normalized Na concentration in the sphere as a function of radial position at different times after glass dissolution begins.

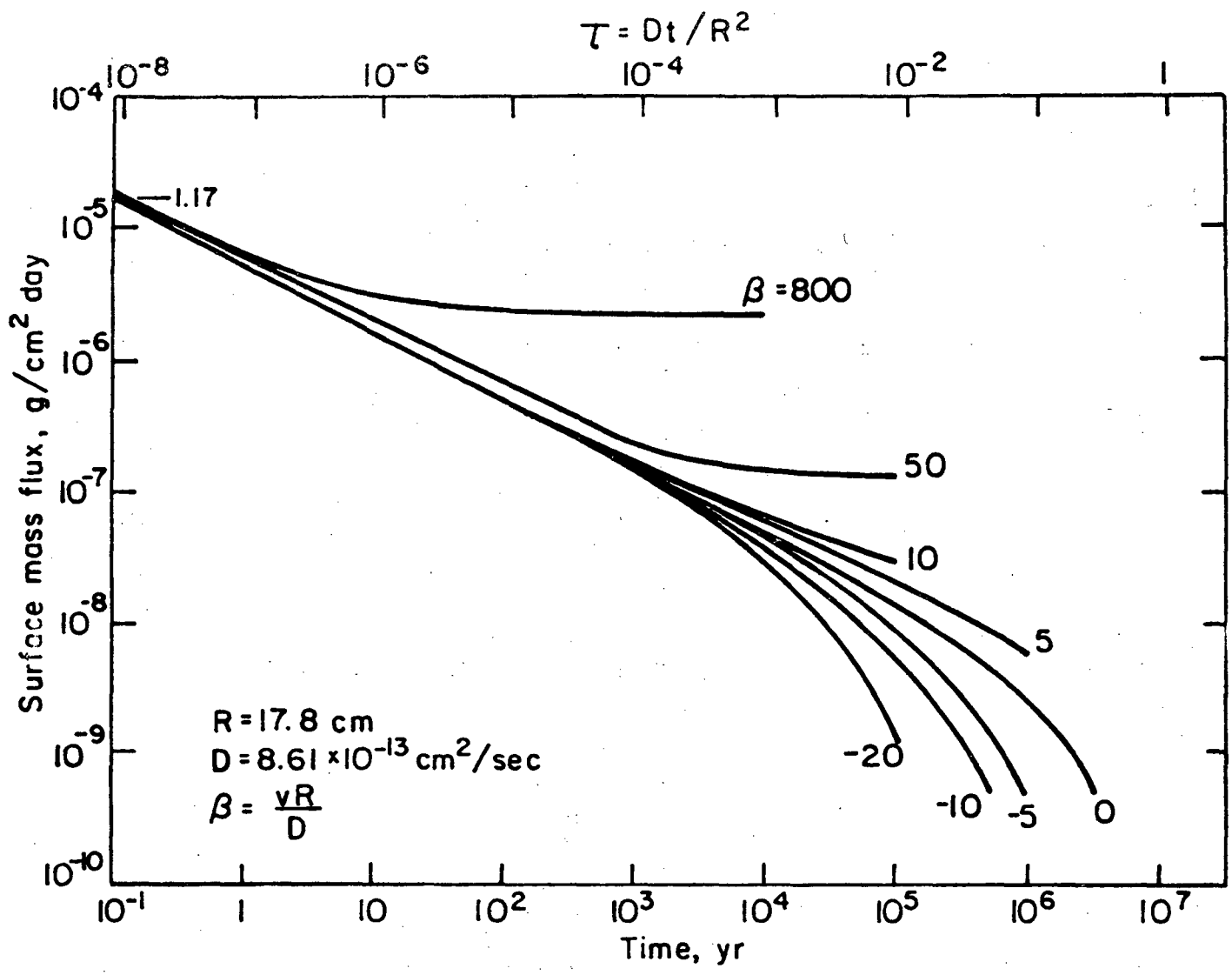

XBL 828-6326

Fig. 7.6.14. Variation of surface mass flux of Na from sphere with time (τ) for different values of β.

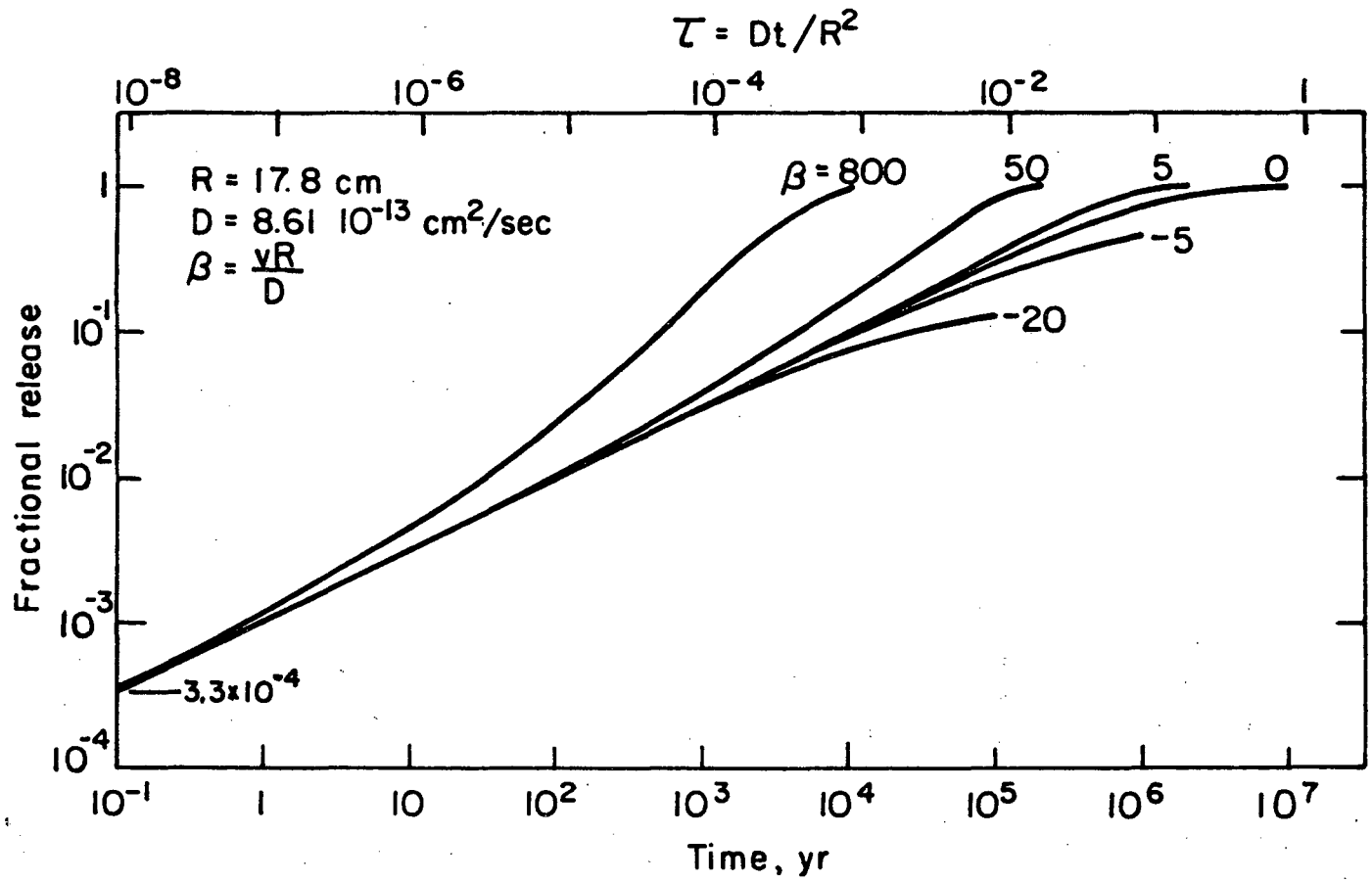

XBL828-6329

Fig. 7.6.15. Fractional release of Na from sphere against time (τ) for different values of β.

7.7 Literature References

B1. M. Benedict, T. H. Pigford, H. Levi, "Nuclear Chemical Engineering", 2nd Ed., Chapter 8, pp 369, McGraw-Hill Book Co., 1981.

B2. Blasius, 1908, Z. Math. Phys. 561.

F1. G. H. Frischat, Ionic Diffusion in Oxide Glasses, Trans. Tech. Publications, Ohio, U.S.A., 1975.

H1. Heimerl, et al, 'Research on Glasses for Fission Product Fixation', Hahn-Meitner Institut, HMI-B109, Sept. 1971.

H2. L. Holland, "The Properties of Glass Surfaces", John Wiley and Sons, Inc., New York, 1964.

K1. Krauskopf, K. K., Private communication, March 1, 1982.

K2. F. Kreith, "Principles of Heat Transfer", 2nd Ed., pp 404, International Textbook Co., 1966.

L1. W. Lobrich, VDI-Forsch.-Heft No. 322, 1929.

M1. McVay, G. L., Bradley, D. J., and Kricher, J. F., "Elemental Release from Glass and Spent Fuel", in press in, "Advances in the Science and Technology of Management of High-Level Nuclear Waste", 1982.

M2. G. L. McVay, Private communication, 1982.

M3. Mendel, et al, 'A State-of-the-Art Review of Materials Properties of Nuclear Waste Forms', PNL-3802, April 1981.

M4. W. F. Merrit, "High-Level Waste Glass: Field Leach Test", Nuclear Technology, Vol. 32, 88, Jan. 1977.

R1. G. E. Raines, L. D. Rickertsen, H. C. Caliborne, J. L. McElroy, and R. W. Lynch, 'Development of Reference Condition for Geological Repositories for Nuclear Waste in the U.S.A.', Proc. Mtg. Material Research Societies, Boston, 1980.

S1. Seidell, A., 'Solubilities Inorganic and Metal-Organic Compound' 4th Ed., Vol. 2, pp 1452, American Chemical Soc., Washington, DC, 1965.

T1. Tymochowicz, S., 'A Collection of Results and Methods on the Leachability of Solidified High Level Radioactive Waste', Hahn-Meitner Institut, HMI-B241, April 1977.

W1. Walther, J. V. and Helgson, H. C., 'Calculation of the Thermodynamic Properties of Aqueous Silica and Solubility of Quartz and Its Polymorphs at High Pressures and Temperatures', American J. of Science, V277 (1977).

W2. Weast, R. C., Astle, M. J., Handbook of Chemistry and Physics, 61st Ed., pp F-62, CRC Press, 1980-1981.

LAWRENCE BERKELEY LABORATORY
TECHNICAL INFORMATION DEPARTMENT
UNIVERSITY OF CALIFORNIA
BERKELEY, CALIFORNIA 94720